CFD MODELS FOR ANALYSIS AND DESIGN OF CHEMICAL REACTORS

Rodney O. Fox*

Department of Chemical Engineering, Iowa State University, Ames, IA 50011-2230, USA

I. Introduction

The field of chemical reaction engineering (CRE) is intimately and uniquely connected with the design and scale-up of chemical reacting systems. To achieve the latter, two essential elements must be combined. First, a detailed knowledge of the possible chemical transformations that can occur in the system is required. This information is represented in the form of chemical kinetic schemes, kinetic rate parameters, and thermodynamic databases. In recent years, considerable progress has been made in this area using computational chemistry and carefully

*Corresponding author. Tel: +1 515 294 9104; Fax: +1 515 294 2689. E-mail: rofox@iastate.edu

Advances in Chemical Engineering, vol. 31
ISSN 0065-2377
DOI 10.1016/S0065-2377(06)31004-6

controlled experiments to isolate the chemical kinetics in the absence of transport effects. The second essential element is detailed knowledge of the transport phenomena in chemical reacting systems. Indeed, because commercial chemical reactors are almost always operated in a regime where mass and energy transport affect or even control the product distribution from the system, understanding the coupling between transport processes and chemical reactions is an essential step in the design and scale-up of chemical reacting systems.

From its beginning, the "holy grail" of CRE has been a computational model that is capable of predicting reactor performance based on the fundamental molecular-scale parameters describing the chemical kinetics and the transport coefficients. In principle, the latter can be measured experimentally in small-scale laboratory experiments (or estimated using computational chemistry). The chemical reaction engineer then incorporates this information into a computational model to predict the behavior of the plant-scale reactor. By avoiding the need for pilot-scale experiments, this "experiment-free" scale-up approach should result in more rapid process development at much lower cost. Admittedly, while CRE has made considerable progress toward this goal, much work remains to be accomplished. Nevertheless, due to the tremendous expansion in computing power over the last 30 years, computational models used in CRE can now account for much more detail than was previously thought possible. This trend is unlikely to abate, and thus, to remain relevant to industry, chemical reaction engineers of the future must become adept at employing detailed flow models for chemical reacting systems.

For example, over the past 15 years computational fluid dynamics (CFD) has become an important tool in CRE for understanding the coupling between transport processes and chemical reactions. The definition of "CFD" has in the process expanded from its original emphasis on fluid dynamics (i.e., momentum transport) to include mass and energy transport, as well as detailed chemical reactions. One might argue that it would, therefore, be more accurate to refer to the field as "computational transport phenomena." On the other hand, because CFD models rarely resolve all of the relevant scales (as described below), one might also argue that "computational chemical reaction engineering" is a more accurate description. However, both of these names are perhaps too broad and lose the essential focus on the fact that CFD always includes a description of momentum transport in the fluid phase(s). Thus, the original name continues to be used to designate all computational approaches that solve for the spatial distribution of the *velocity*, concentration, and temperature fields. CFD models have also been developed for multiphase systems, and commercial CFD codes now offer a wide range of options for modeling chemical reactors.

Despite the many advances, the users of CFD codes must keep in mind that the underlying transport equations are based on *models*, which may or may not be valid for a particular application. This fact often escapes the minds of newcomers to the field who are typically overwhelmed by the numerical issues associated with convergence, grid-independence, and post-processing. Even

many CFD experts tend to avoid the issue by working exclusively in an application area where acceptably accurate models are already available. Unfortunately (at least for industrial users!), the application of CFD to chemical reactor analysis introduces new modeling challenges with each new reactor type. In the simplest case of laminar flow with fully resolved concentration and temperature fields, the models have a strong fundamental basis that typically involves *molecular-scale* transport coefficients. These CFD models are based on the so-called *microscopic balance* equations that are taught to undergraduate students in chemical engineering courses on transport phenomena. The extension of the microscopic balance equations to multiphase flow systems is also well understood, but brings with it a wide range of new flow phenomena in even the simplest cases.

In reality, most of the applications in CRE for which CFD is used cannot be treated using the microscopic balance equations alone. Instead, CFD models are introduced to describe the effects of unresolved phenomena on the resolved quantities. These models introduce *phenomenological* transport coefficients, much like the ones developed in CRE models for chemical reactors. In fact, in many cases, spatial transport is dominated by *convection* and the molecular-scale spatial transport can be neglected. Nevertheless, just as in ''classical'' CRE models for interphase mass/energy transport, the molecular-scale transport coefficients appear in the dimensionless numbers used to formulate the phenomenological coefficients. Indeed, because the accuracy of CFD predictions are strongly dependent on the accuracy of these so-called *subgrid-scale* (SGS) models, the modeling skills developed in CRE over its long history are a crucial component in the development of CFD for chemical reactor design and analysis. In fact, it would not be pretentious to claim that, due to their considerable abilities to deal with the coupling between chemical reactions and transport phenomena, chemical reaction engineers are uniquely qualified to develop the SGS models needed for CFD modeling of chemical reacting systems.

In the remainder of this work we review the current status of CFD models for chemical reacting systems. In some cases (e.g., single-phase reacting flow) the current models are fully predictive in the limits of high and low Reynolds numbers, and quite accurate in the transition region between these limits. In other cases (e.g., multiphase reacting flow), the predictive abilities of current CFD models are, in general, limited. Nevertheless, for particular multiphase reactors (e.g., gas–solid reacting flow), powerful models exist and are making their way into commercial CFD codes. The goal of the presentation will not be to describe every model in detail, but rather to indicate the current status of models for treating reacting flows and to point out areas where further research is needed. The reader interested in a deeper understanding of the particular aspects a model will be pointed to the appropriate research literature for further reading. Moreover, consistent with our desire to use CFD for chemical reactor analysis and design, we will not discuss models whose primary purpose is to describe nonreacting flows. For single-phase reactors, excellent descriptions of

such models are available in the literature. Likewise, CFD models for multiphase flows are described by other authors in this issue.

The organization of the material is as follows. In Section II we provide a general introduction to CFD models for chemical reacting systems, and to the critical modeling issues that arise in their development and application. In Section III we describe the current state of the art in CFD models for single-phase reacting flows. In Section IV we extend the discussion of single-phase reacting flows to include systems that produce fine particles that follow the continuous-phase flow. In these systems, the principal novelty is the inclusion of a population balance model for the particulate phase. In Section V, we describe the current state of the art in CFD models for multiphase reacting flows. Because this last area is the least developed, but most rapidly advancing, we will limit our discussion to CFD models that can potentially be used to describe plant-scale reactors (i.e., multifluid models and related mean-field descriptions). Even for these models, we will not cover the details on how momentum exchange is treated between phases. Rather, we will focus our attention on factors that affect directly the chemical reactions. Finally, in Section VI conclusions are drawn concerning the current status of CFD models for chemical reactor analysis, and an attempt is made to point out the research directions where progress can be expected in the near future.

II. Computational Fluid Dynamics for Reacting Systems

In this Section we give an overview of the formulation of CFD models for reacting systems, with particular emphasis on systems requiring SGS models. For the reader to understand the procedure followed to create a CFD model for a chemical reactor, we cover first the basic formulation. Then, because the SGS models are often needed due to the flow being turbulent, we next review the principal length and time scales present in turbulent transport. We then give examples of SGS phenomena and their corresponding models in turbulent reacting flows. Finally, we end the section with a brief discussion of the types of reactor systems that can currently be treated using CFD.

A. Basic Formulation of CFD Models

When applying CFD to model a chemical reactor, we are interested in knowing how the basic quantities (density, velocity, concentrations, etc.) vary with the spatial location in the reactor at a given time instant. The starting point for developing a CFD model is the *microscopic balance* equation, described in detail in standard textbooks on transport phenomena (Bird *et al.*, 2002). Letting Φ denote a quantity of interest, the general form of its microscopic balance

equation is

$$\frac{\partial \Phi}{\partial t} + \nabla \cdot (\mathbf{U}\Phi) + \nabla \cdot \left(\mathbf{J}_\phi\right) = S_\phi \tag{1}$$

where $\mathbf{U}$ is the convective velocity, $\mathbf{J}_\phi$ is a molecular-scale model for the diffusive flux, and $\boldsymbol{S}_\phi$ is a molecular-scale source term. Typical examples of quantities of interest are fluid density ρ, species mass fractions ρY_α, and the fluid momentum $\rho\mathbf{U}$. Likewise, for multiphase systems similar quantities are of interest, but for each individual phase present in the reactor. The generalized source term S_ϕ will then include mass/momentum/heat-transfer between phases. For complex fluids (e.g., non-Newtonian flows), molecular-scale models for $\mathbf{J}_\phi$ and S_ϕ can be quite complicated and can lead to numerical difficulties, requiring specially developed CFD solvers.

As mentioned in Section I.A, CFD codes were originally developed to solve for the fluid momentum for Newtonian fluids, for which the right-hand side of Eq. (1) is well understood (Bird *et al.*, 2002). However, even for such fluids, it is not possible to accurately solve the microscopic balance equation for Reynolds numbers commonly observed in chemical reactors. It is thus necessary to distinguish between *direct-numerical simulations* (DNS) and CFD models using phenomenological descriptions of the turbulence. The two most widely used CFD approaches for describing turbulent flow are large-eddy simulations (LES) and Reynolds-averaged Navier–Stokes (RANS) models (Pope, 2000). In both approaches, it is no longer possible to solve Eq. (1) directly for Φ due to the enormous computational cost. Instead, Eq. (1) is filtered (LES) or ensemble-averaged (RANS), yielding

$$\frac{\partial \tilde{\Phi}}{\partial t} + \nabla \cdot (\tilde{\mathbf{U}}\tilde{\Phi}) + \nabla \cdot (\widetilde{\mathbf{u}\phi}) + \nabla \cdot \left(\mathbf{J}_\phi\right) = \tilde{S}_\phi \tag{2}$$

This transport equation cannot be solved directly because it involves several unclosed terms. The SGS flux $\widetilde{\mathbf{u}\phi}$ represents the spatial transport of Φ by the unresolved velocity fluctuations. Models for this term can generally be written in the form of a generalized transport equation:

$$\frac{\partial \tilde{\Phi}}{\partial t} + \nabla \cdot (\tilde{\mathbf{U}}\tilde{\Phi}) + \nabla \cdot \left(\tilde{\mathbf{J}}_\phi + \tilde{\mathbf{J}}_{\mathrm{T}\phi}\right) = \tilde{S}_\phi + \tilde{S}_{\mathrm{T}\phi} \tag{3}$$

where the SGS diffusive flux is denoted by $\tilde{\mathbf{J}}_{\mathrm{T}\phi}$ and SGS source term by $\tilde{S}_{\mathrm{T}\phi}$. To distinguish this expression from Eq. (1), we will refer to Eq. (3) as the *CFD transport* equation. Thus, only in the (rare) case of DNS will the CFD transport equation correspond to the microscopic balance equation.

In chemical reacting systems, the Reynolds number of the flow is not the only source of computational challenges. Indeed, even for laminar reacting flows the chemical source term can be extremely stiff and tightly coupled to the diffusive transport terms. Averaging, as done above to treat turbulent flows, does not

alleviate this difficulty. Thus, turbulent reacting flows offer many difficult challenges and require specialized models to describe the coupling between molecular diffusion and chemical reactions (Fox, 2003). We will look at some of the more widely applicable models in Section III.

Keeping in mind the discussion leading to Eq. (3), the formulation of a CFD model for a chemical reactor can be broken down into the following broad steps:

(i) First we must identify the set of state variables needed to completely describe the reactor. Typical examples are

$$\tilde{\boldsymbol{\Phi}} \in \left[\tilde{\rho},\ \tilde{\rho}\tilde{\mathbf{U}},\ \tilde{\rho}\tilde{\boldsymbol{Y}}_\alpha,\ \tilde{\rho}\tilde{T},\ \tilde{\rho}\tilde{\phi}_\beta\right]$$

where, in addition to the quantities introduced earlier, $\tilde{T}$ is the fluid temperature and $\widetilde{\phi}_\beta$ is a set of scalar quantities. The latter are introduced to define, for example, the closure for the chemical source term (Fox, 2003) and the turbulence model (Pope, 2000). Note that the identification of the state variables is analogous to what is done in "classical" CRE models. Thus, chemical reaction engineers are generally well acquainted with the methodology needed to complete this step. The only new quantity that does not appear in "lumped" CRE models is the fluid velocity. However, chemical engineers are typically introduced to momentum balances in courses on transport phenomena, and thus understand its significance.

(ii) The next and arguably the most difficult step is to find closures for the CFD transport equation, expressed in terms of the state variables. For example, in turbulent flows the diffusive-flux terms can often be modeled successfully as gradient-diffusion terms:

$$\tilde{\mathbf{J}}_\phi + \tilde{\mathbf{J}}_{\mathrm{T}\phi} = -\left(D_\phi + D_{\mathrm{T}\phi}\right)\boldsymbol{\nabla}\tilde{\Phi} \tag{4}$$

where D_ϕ is a molecular-diffusion coefficient and $D_{\mathrm{T}\phi}$ is a turbulent-diffusion coefficient. In high-Reynolds-number flows, D_ϕ is negligible compared to $D_{\mathrm{T}\phi}$. Note that in general $D_{\mathrm{T}\phi}$ will depend on the scalar quantities $\widetilde{\phi}_\beta$ appearing in the turbulence model. Closure of the source terms in Eq. (3) is much more difficult, and requires fundamental knowledge about how the *local* flow field interacts with the quantity of interest (e.g., how the local turbulence level affects the rates of diffusive mixing and chemical reactions at the subgrid scale). Nevertheless, the final closures must be expressed as follows in terms of the state variables:

$$\tilde{S}_\phi\left(\tilde{\rho},\ \tilde{\mathbf{U}},\ \tilde{\boldsymbol{Y}}_\alpha,\ \tilde{T},\ \tilde{\phi}_\beta\right) \quad \text{and} \quad \tilde{S}_{T\phi}\left(\tilde{\rho},\ \tilde{\mathbf{U}},\ \tilde{\boldsymbol{Y}}_\alpha,\ \tilde{T},\ \tilde{\phi}_\beta\right)$$

Note that these closures describe SGS phenomena and hence are essentially *local* in space (i.e., interior to a computational grid cell). For this reason, it is

often possible to use DNS of *statistically homogeneous* systems (i.e., for which the [filtered] state variables $\tilde{\Phi}$ do not depend on $\boldsymbol{x}$) to develop closure models for $\tilde{S}_\phi$ and $\tilde{S}_{T\phi}$. This procedure has been widely used in single-phase turbulence modeling (Pope, 2000; Fox, 2003), and more recently in multiphase flow systems (e.g., Bunner and Tryggvason, 2003; Nguyen and Ladd, 2005). For the latter, the generalized source terms include mass/momentum/heat-transfer between phases, and as discussed in Section V the closure models involve dimensionless parameters such as the particle Reynolds number.

(iii) The coupled system of CFD transport equations now appears as follows in closed form:

$$\frac{\partial \tilde{\Phi}}{\partial t} + \boldsymbol{\nabla} \cdot (\tilde{\mathbf{U}} \tilde{\Phi}) = \boldsymbol{\nabla} \cdot \left(D_\phi + D_{\mathrm{T}\phi}\right) \boldsymbol{\nabla} \tilde{\Phi} + \tilde{S}_\phi + \tilde{S}_{T\phi} \tag{5}$$

and the remaining task is to find a suitable numerical algorithm to solve them. Fortunately, CFD experts have developed powerful and robust algorithms for solving equations in the form of Eq. (5), and these are now available in commercial CFD codes. Thus, from the perspective of the chemical reaction engineer working in industry, the efficient application of CFD to chemical reactor analysis and design will inevitably involve the use of a commercial CFD code. The next step in the CFD model formulation will thus be to introduce the closure models developed in the previous step into the CFD code. This is facilitated in most commercial CFD codes by the availability of so-called "user-defined scalars." In many cases, the basic turbulence and multiphase models will already be available in a commercial code. The chemical reaction engineer will thus only need to add the specialized closure models (in terms of $\tilde{\phi}_\beta$) needed to describe the state variables in a particular application.

(iv) Once the CFD model equations have been implemented in the code, the next step is to create a computational grid to capture the specific geometry of the chemical reactor. The qualities of the grid strongly affect the accuracy and the speed of convergence of the numerical algorithm. Thus, for complex reactor geometries, it may make sense to hire a specialist in grid generator to carry out this step.

(v) The remaining steps involve solving the CFD model and postprocessing of the results. The latter is greatly facilitated by the built-in functions available in most commercial CFD codes. It is at this point that reactor analysis and design actually come into full play. By experimenting with variations in the operating conditions and reactor geometry, the CFD model can be used to enhance product selectivity and reactor performance.

When applying the steps outlines above, the prudent engineer will start by modeling an existing reactor for which plant-scale data are available for validation of the CFD results. If the agreement is poor, usually this will be due to

inadequate choices for the state variables and/or closure models. Nevertheless, one should also examine the computational results to see if there are numerical errors leading, for example, to inconsistencies in the mass, species, or energy balances. Getting acceptable agreement may take several iterations of changes in the closures. For many cases, this process can be facilitated by breaking it down into independent steps (e.g., flow-field predictions can be validated before adding the chemistry). After reasonable agreement between the model and data is obtained, the CFD model can be safely used to explore alternative design scenarios.

B. Length and Time Scales in Turbulent Flows

As mentioned before in Eq. (3), the most common source of SGS phenomena is turbulence due to the Reynolds number of the flow. It is thus important to understand what the principal length and time scales in turbulent flow are, and how they depend on Reynolds number. In a CFD code, a turbulence model will provide the *local* values of the turbulent kinetic energy k and the turbulent dissipation rate ε. These quantities, combined with the kinematic viscosity of the fluid ν, define the length and time scales given in Table I. Moreover, they define the local turbulent Reynolds number Re_L also given in the table.

The integral scale of a turbulent flow characterizes the largest and most energetic flow structures. In a CFD simulation, the local grid size will be proportional to the integral length scale L_u. Likewise, the characteristic lifetime of the largest eddies is proportional to the integral time scale τ_u. The Kolmogorov scale characterizes the smallest flow structures and is resolved by neither LES nor RANS simulations (only in DNS). Note that the ratios of the length and time scales are as follows:

$$\frac{L_\mathrm{u}}{\eta} = \mathrm{Re}_\mathrm{L}^{3/4} \quad \text{and} \quad \frac{\tau_\mathrm{u}}{\tau_\eta} = \mathrm{Re}_\mathrm{L}^{1/2} \tag{6}$$

Thus, as the local turbulent Reynolds number increases, the separation between the scales will increase. As a general rule, Re_L will be proportional to the

TABLE I

The principal length and time scales, and Reynolds numbers characterizing a turbulent flow defined in terms of the turbulent kinetic energy k, and turbulent dissipation rate ε, and the kinematic viscosity ν

Quantity	Integral scale	Kolmogorov scale
Length	$L_\mathrm{u} = k^{3/2}/\varepsilon$	$\eta = (\nu^3/\varepsilon)^{1/4}$
Time	$\tau_\mathrm{u} = k/\varepsilon$	$\tau_\eta = (\nu/\varepsilon)^{1/2}$
Reynolds number	$\mathrm{Re}_\mathrm{L} = k^2/\varepsilon\nu$	$\mathrm{Re}_\eta = 1$

macroscopic Reynolds number for the flow (i.e., Re defined in terms of a characteristic flow velocity and length scale.)

In general, for a fixed-flow geometry, the integral length scale will remain approximately constant (e.g., in a turbulent jet the integral length scale is proportional to the jet diameter). Likewise, the integral scale velocity, defined by L_u/τ_u, will be proportional to the characteristic velocity of the flow (e.g., the jet velocity). Thus, as the Reynolds number increases (e.g., to enhance turbulent mixing), η, τ_u, and τ_η will all decrease. In the CFD simulation, the grid will remain approximately the same and the time step must decrease to follow τ_u. This implies that at high Reynolds numbers less and less of the small-scale flow structures are captured by the CFD simulation.

To estimate the amount of turbulent kinetic energy lost when filtering at a given grid size, it is useful to introduce a normalized model energy spectrum (Pope, 2000) as follows:

$$E_u(\kappa) = C\kappa^{-5/3} f_L(\kappa) f_\eta(\kappa) \tag{7}$$

where κ is the dimensionless wavenumber (inverse length), and the Kolmogorov constant is $C = 1.61$ (based on the most recent DNS (Watanabe and Gotoh, 2004)). The nondimensional cut-off functions are defined by

$$f_L(\kappa) \equiv \left(\frac{\kappa}{(\kappa^2 + c_L)^{1/2}} \right)^{5/3+p_0} \tag{8}$$

and

$$f_\eta(\kappa) \equiv \exp\left[-\beta \left([\kappa^4/\mathrm{Re}_L^3 + c_\eta^4]^{1/4} - c_\eta \right) \right] \tag{9}$$

wherein $p_0 = 2$ and $\beta = 5.2$. The parameters c_L and c_η are found by applying two integral constraints as follows:

$$1 = \int_0^\infty E_u(\kappa)\, \mathrm{d}\kappa \tag{10}$$

and

$$\mathrm{Re}_L = \int_0^\infty 2\kappa^2 E_u(\kappa) \mathrm{d}\kappa \tag{11}$$

Note that the final form of the energy spectrum depends only on the local turbulent Reynolds number. As an example, spectra found with different Re_L are shown in Fig. 1.

In the normalized energy spectrum, $\kappa = 1$ corresponds to the inverse of the local integral length scale and $\kappa = \mathrm{Re}_L^{3/4}$ to the inverse of the local Kolmogorov length scale. The range of wavenumbers in Fig. 1 over which the slope is $-5/3$ is

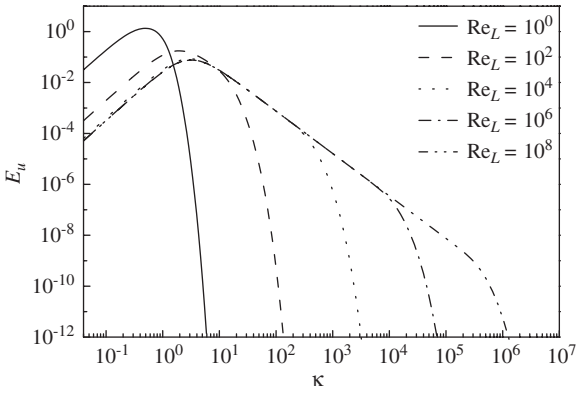

FIG. 1. The normalized model turbulent energy spectrum for a range of Reynolds numbers.

called the *inertial range*. Thus, for the flow to be considered turbulent (as opposed to transitional flow), $\mathrm{Re_L}$ must be larger than approximately 20. In contrast, high-Reynolds-number turbulence (i.e., with a significant inertial range) does not begin until $\mathrm{Re_L}$ is larger than 450. In RANS turbulence models designed for low-Reynolds-number turbulent flows, the model parameters are functions of $\mathrm{Re_L}$, and as the local turbulent Reynolds number approaches zero, the microscopic balance equation (Eq. 1) is recovered. In contrast, in LES turbulence models the filter size is typically fixed at some Reynolds-number-independent wavenumber $\kappa_c > 10$. Thus, the fraction of turbulent kinetic energy captured by LES can be found from

$$f_c = \int_0^{\kappa_c} E_u(\kappa)\mathrm{d}\kappa \tag{12}$$

and varies from $f_c = 1$ for small $\mathrm{Re_L}$ up to a constant value less than one for very large $\mathrm{Re_L}$ (Pope, 2000).

In the discussion above, we have considered only the velocity field in a turbulent flow. What about the length and time scales for turbulent mixing of a scalar field? The general answer to this question is discussed in detail in Fox (2003). Here, we will only consider the simplest case where the scalar field ϕ is inert and initially nonpremixed with a scalar integral length scale L_ϕ that is approximately equal to L_u. If we denote the molecular diffusivity of the scalar by Γ, we can use the kinematic viscosity to define a dimensionless number in the following way:

$$\mathrm{Sc} \equiv \frac{\nu}{\Gamma} \tag{13}$$

called the Schmidt number. In gases, typical values of the Schmidt number are near unity, while in liquids values near 1,000 are quite common. The Schmidt

number and the Kolmogorov length scale can be used to define the Batchelor length scale as follows:

$$\lambda_B \equiv \mathrm{Sc}^{-1/2}\eta = \mathrm{Sc}^{-1/2}\mathrm{Re}_L^{-3/4}L_u \tag{14}$$

which is the length scale where molecular diffusion occurs. In a nonpremixed turbulent flow seen under magnification (e.g., using planar laser-induced fluorescence), the smallest observable structures over which concentration gradients are seen have characteristic size λ_B. Note that for large Sc, the Batchelor scale can be very small even at low Reynolds numbers.

The degree of local mixing in a RANS simulation is measured by the scalar variance $\langle\phi'^2\rangle$, which ranges from zero for complete mixing (i.e., $\phi = \langle\phi\rangle$ is uniform at the SGS) up to $(\phi_{\max} - \langle\phi\rangle)(\langle\phi\rangle - \phi_{\min})$ where $\langle\phi\rangle$ is the mean concentration and $\phi_{\max}$ and $\phi_{\min}$ are the maximum and minimum values, respectively. The rate of local mixing is controlled by the scalar dissipation rate ε_ϕ (Fox, 2003). The scalar time scale analogous to the turbulence integral time scale is (Fox, 2003) as follows:

$$\tau_\phi \equiv \frac{2\langle\phi'^2\rangle}{\varepsilon_\phi} \tag{15}$$

In a RANS simulation of scalar mixing, a model for ε_ϕ must be supplied to compute $\langle\phi'^2\rangle$. In fully developed turbulence, τ_ϕ can be related to τ_u by considering the scalar energy spectrum, as first done by Corrsin (1964).

To determine how the scalar time scale defined in Eq. (15) is related to the turbulence integral time scale given in Table I, we can introduce a normalized model scalar energy spectrum (Fox, 2003) as follows:

$$E_\phi(\kappa) = C_{OC}\mathrm{Re}_L^{(3\beta(\kappa)-5)/4}\kappa^{-\beta(\kappa)}f_L(\kappa)f_B(\kappa) \tag{16}$$

where the scaling exponent is defined by

$$\beta(\kappa) \equiv 1 + \frac{2}{3}\left[7 - 6f_D(\kappa)\right]f_\eta(\kappa) \tag{17}$$

and Obukhov–Corrsin constant is $C_{OC} = 0.67$–0.68 (Sreenivasan, 1996; Watanabe, and Gotoh, 2004; Yeung *et al.*, 2005). In the model spectrum, the diffusive-scale cut-off function is defined by

$$f_D(\kappa) \equiv \left(1 + c_D\mathrm{Sc}^{-d(\kappa)/2}\kappa/\mathrm{Re}_L^{3/4}\right)\exp\left(-c_D\mathrm{Sc}^{-d(\kappa)/2}\kappa/\mathrm{Re}_L^{3/4}\right) \tag{18}$$

with $c_D = 2.59$, and the diffusive exponent is

$$d(\kappa) \equiv \frac{1}{2} + \frac{1}{4}f_\eta(\kappa) \tag{19}$$

The Batchelor-scale cut-off function is defined by

$$f_{\mathrm{B}}(\kappa) \equiv \left(1 + c_{\mathrm{d}}\mathrm{Sc}^{-d(\kappa)}\kappa/\mathrm{Re}_{\mathrm{L}}^{3/4}\right)\exp\left(-c_{\mathrm{d}}\mathrm{Sc}^{-d(\kappa)}\kappa/\mathrm{Re}_{\mathrm{L}}^{3/4}\right) \tag{20}$$

wherein the scalar-dissipation constant c_{d} is found by applying an integral constraint as follows:

$$\mathrm{Re}_{\mathrm{L}}\mathrm{Sc} = \int_0^\infty 2\kappa^2 E_\phi(\kappa)\mathrm{d}\kappa \tag{21}$$

Note that the scalar-dissipation constant computed from Eq. (21) depends only on Re_{L} and Sc.

In Fig. 2, the normalized model scalar energy spectrum is plotted for a fixed Reynolds number ($\mathrm{Re}_{\mathrm{L}} = 10^4$) and a range of Schmidt numbers. In Fig. 3, it is shown for $\mathrm{Sc} = 1000$ and a range of Reynolds numbers. The reader interested in the meaning of the different slopes observed in the scalar spectrum can consult Fox (2003). By definition, the ratio of the time scales is equal to the area under the normalized scalar energy spectrum as follows:

$$\frac{\tau_\phi}{2\tau_{\mathrm{u}}} = \int_0^\infty E_\phi(\kappa)\mathrm{d}\kappa \tag{22}$$

Thus, from Figs. 2 and 3 we can conclude that the time-scale ratio will depend on Re_{L} and Sc.

In the literature on turbulent mixing, the mechanical-to-scalar time-scale ratio is defined by

$$R \equiv \frac{2\tau_{\mathrm{u}}}{\tau_\phi} \tag{23}$$

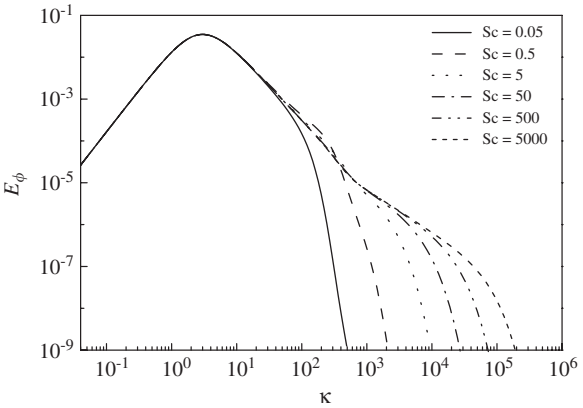

FIG. 2. Normalized model scalar energy spectra for a range of Schmidt numbers and $\mathrm{Re}_{\mathrm{L}} = 10^4$.

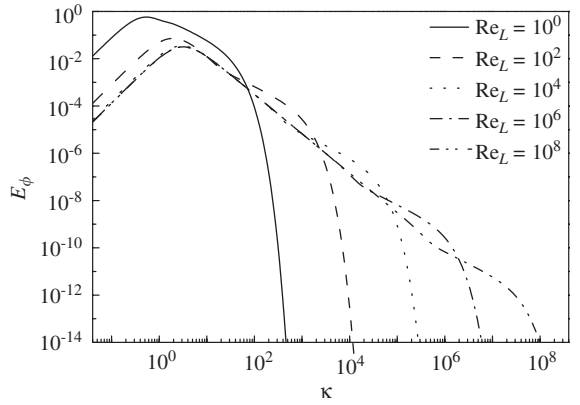

FIG. 3. Normalized model scalar energy spectra for a range of Reynolds numbers and $Sc = 10^3$.

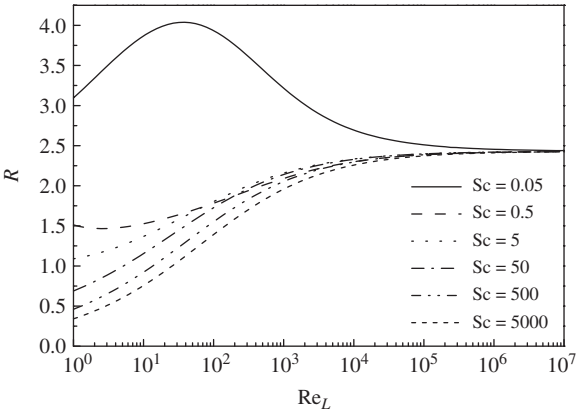

FIG. 4. Mechanical-to-scalar time-scale ratio found from the normalized model scalar energy spectra.

and is plotted based on Eq. (16) for a range of Schmidt numbers as a function of Reynolds number in Fig. 4. Note that for very large Reynolds numbers, R is independent of Sc and approaches a constant value of $R = C/C_{OC} = 2.37$, i.e., the ratio of the Kolmogorov and the Obukhov–Corrsin constants. In contrast, for Re_L less than 10^6, R is strongly dependent on both the Reynolds and Schmidt numbers. The dependence on Reynolds number is especially significant for Schmidt numbers far from unity. For example, liquid-phase reactors used for material processing (Mahajan and Kirwan, 1993, 1996; Johnson and Prud'homme, 2003a,b) have high Schmidt numbers and operate at low to moderate Reynolds numbers (Liu and Fox, 2006). In a CFD simulation, τ_u can be found from the turbulence model and τ_ϕ from the data in Fig. 4. Thus, the curves in Fig. 4 define a SGS model for τ_ϕ parameterized in terms of Re_L and Sc.

We will revisit this topic in Section III when discussing CFD models for mixing-sensitive reactions. Note that while the discussion above applies to RANS turbulence models, the method can be extended to LES by integrating over the SGS wavenumbers (i.e., starting at κ_c).

In summary, we have seen that the principal length and time scales in a single-phase turbulent flow depend on the local turbulent Reynolds number Re_L. In a CFD code, standard turbulence models will provide the local values of k and ε. Given the fluid viscosity, it will thus be possible to compute the local turbulent Reynolds number and related integral-scale quantities such as L_u and τ_u. Using the model energy spectra, we have also shown how the scalar mixing time τ_ϕ depends on the Schmidt number and local turbulent Reynolds number. In principle, a similar analysis could be carried out for multiphase turbulent flows to understand the scaling laws for the length and time scales and their dependence on the relevant dimensionless numbers. Unfortunately, DNS of multiphase flow is still in its infancy and experimental measurements of energy spectra are difficult to obtain. Nevertheless, we can expect significant progress in our understanding of turbulent multiphase flows using DNS for particular systems (e.g., gas–solid flows) in the coming years.

C. Models for SubGrid Scale Phenomena

As noted earlier, in most applications of CFD to chemical reactor design and analysis the CFD transport equation (Eq. 3) will require SGS closures. (Here we use "subgrid scale" to refer to LES and RANS models for terms not fully resolved by the computational grid.) Thus, one of the principal tasks of a chemical reaction engineer is to develop the SGS models that accurately describe the chemistry and physics occuring at the unresolved scales of the flow. As discussed above, for a single-phase turbulent flow, the unresolved scales are those smaller than the integral length and time scales (L_u and τ_u, respectively). Obviously, the SGS models will be highly dependent on the type of flow under consideration (e.g., single-phase vs. multiphase, nonreacting vs. reacting, etc.), and a complete listing of all such models would be lengthy and uninformative to the general reader. Thus, instead of giving general examples, in this section we will demonstrate how the SGS model is developed for a particular example (single-phase turbulent mixing). In the subsequent sections we will extend this model to reacting scalars of various types. Readers interested in more details on the models can consult Fox (2003).

One of the first questions that arises when considering a chemical reactor is "Can the reactor be considered perfectly mixed?". In CRE, this question implies at least two physical situations:

1. The reactor is **perfectly macromixed** if the mean concentration at every point in the reactor is equal to the volume average.
2. The reactor is **perfectly micromixed** if the instantaneous, local concentration at every point in the reactor is equal to the local mean concentration.

The "classical" CRE model for a perfectly macromixed reactor is the continuous stirred tank reactor (CSTR). Thus, to fix our ideas, let us consider a stirred tank with two inlet streams and one outlet stream. The CFD model for this system would compute the flow field inside of the stirred tank given the inlet flow velocities and concentrations, the geometry of the reactor (including baffles and impellers), and the angular velocity of the stirrer. For liquid-phase flow with uniform density, the CFD model for the flow field can be developed independently from the mixing model. For simplicity, we will consider this case. Nevertheless, the SGS models are easily extendable to flows with variable density.

Following the steps for formulation of a CFD model introduced earlier, we begin by determining the set of state variables needed to describe the flow. Because the density is constant and we are only interested in the mixing properties of the flow, we can replace the chemical species and temperature by a single inert scalar field $\xi(\mathbf{x}, t)$, known as the mixture fraction (Fox, 2003). If we take $\xi = 0$ everywhere in the reactor at time $t = 0$ and set $\xi = 1$ in the first inlet stream, then the value of $\xi(\mathbf{x}, t)$ tells us what fraction of the fluid located at point $\boldsymbol{x}$ at time t originated at the first inlet stream. If we denote the inlet volumetric flow rates by q_1 and q_2, respectively, for the two inlets, at steady state the volume-average mixture fraction in the reactor will be

$$\bar{\xi} \equiv \frac{q_1}{q_1 + q_2} \tag{24}$$

Thus, the reactor will be perfectly mixed if and only if $\xi = \bar{\xi}$ at every spatial location in the reactor. As noted earlier, unless we conduct a DNS, we will not compute the instantaneous mixture fraction in the CFD simulation. Instead, if we use a RANS model, we will compute the ensemble- or Reynolds-average mixture fraction, denoted by $\langle\xi\rangle$. Thus, the first state variable needed to describe macromixing in this system is $\langle\xi\rangle$. If the system is perfectly macromixed, $\langle\xi\rangle = \bar{\xi}$ at every point in the reactor. The second state variable will be used to describe the degree of local micromixing, and is the mixture-fraction variance $\langle\xi'^2\rangle$. When the variance is zero, the fluid is perfectly micromixed so that $\xi = \langle\xi\rangle$. The maximum value of the variance at any point in the reactor is $\langle\xi\rangle(1 - \langle\xi\rangle)$, and varies from zero in the feed streams to a maximum of 1/4 when $\langle\xi\rangle = 1/2$.

At this point, we should clarify an all-to-common misconception in the chemical-engineering literature concerning the meaning of "Reynolds average." Unfortunately, many textbooks and journal articles still define it as a time average or a volume average over an interval that "is not too long, but not too short." This definition confuses methods for *estimating* the expected value from experimental data for a single realization (i.e., time and volume averages), which are statistics, with the underlying expected values with respect to all possible realizations. In general, a statistic will be different every time it is computed, while an expected value is constant at a given point in space and time. Thus, when deriving closures for expected values such as $\langle\xi\rangle$ and $\langle\xi'^2\rangle$, we start with a general transport theory based on the joint probability density function (PDF)

as described in Pope (2000) and Fox (2003). Space or time averages only come into the picture when we must validate the predictions of the CFD model against experimental data. For example, if the flow is *statistically stationary*, then the time average of $\xi(\mathbf{x}, t)$ can be used to estimate $\langle\xi\rangle(\mathbf{x})$. (Note that by definition of "statistically stationary" the expected values will not depend on time.) Likewise, if the flow is *statistically homogeneous*, then the volume average of $\xi(\mathbf{x}, t)$ can be used to estimate $\langle\xi\rangle(t)$. In chemical reactors, the flow is almost never homogeneous (if it were, CFD would not be needed). Nevertheless, one still finds authors who confuse micromixing, rigorously defined in terms of the variance $\langle\xi'^2\rangle$, with deviations of the mean $\langle\xi\rangle$ from its volume-average. In reality, such fluctuations correspond to poor macromixing and are a mathematical artifact caused by "lumping" inhomogeneous flow into a homogeneous model (e.g., by modeling laminar flow in a tubular reactor using a plug-flow model). Finally, we should note that identical statistical concepts can be used to derive CFD models for scalar mixing in low-Reynolds-number chaotic flows encountered in high-viscosity mixing. The principal difficulty in these flows is finding *general* state variables to describe the length and time scales of the flow.

The remaining state variables in our CFD model for turbulent mixing are needed to describe the flow field in the reactor. In a RANS model for turbulent flow, the mean velocity $\langle\mathbf{U}\rangle$ appears in the Reynolds-average momentum balances. The latter is closed by providing a turbulence model for the Reynolds stresses (Pope, 2000). If a turbulent-viscosity-based model is used, two state variables are introduced to describe the local turbulent integral time scale and length scale (see Table I). Common choices are the turbulent kinetic energy k, and the turbulent dissipation rate, ε. The set of state variables used to described turbulent mixing in the reactor are thus

$$\tilde{\Phi} \in \left[\langle\mathbf{U}\rangle,\ k,\ \varepsilon,\ \langle\xi\rangle,\ \langle\xi'^2\rangle\right]$$

Note that when solving the CFD transport equations, the mean velocity and turbulence state variables can be found independently from the mixture-fraction state variables. Likewise, when validating the CFD model predictions, the velocity and turbulence predictions can be measured in separate experiments (e.g., using particle-image velocimetry [PIV]) from the scalar field (e.g., using planar laser-induced fluorescence [PLIF]).

Now that the state variables have been determined, we can go to steps (ii) and (iii), which involve finding closed CFD transport equations. The derivation of the RANS equations is described in detail in Fox (2003), and will not be repeated here. Instead, we will simply give the CFD transport equations and discuss the closures appearing in the equations. The five transport equations are

$$\frac{\partial\rho\langle\mathbf{U}\rangle}{\partial t} + \boldsymbol{\nabla}\cdot(\rho\langle\mathbf{U}\rangle\langle\mathbf{U}\rangle) = \boldsymbol{\nabla}\cdot\left(\mu+\mu_{\mathrm{T}}\right)\boldsymbol{\nabla}\langle\mathbf{U}\rangle - \boldsymbol{\nabla}p + \rho\mathbf{g} \tag{25}$$

$$\frac{\partial \rho k}{\partial t} + \nabla \cdot (\rho \langle \mathbf{U} \rangle k) = \nabla \cdot \left(\mu + \mu_{\mathrm{T}}/\sigma_k\right) \nabla k + P_k - \rho\varepsilon \tag{26}$$

$$\frac{\partial \rho \varepsilon}{\partial t} + \nabla \cdot (\rho \langle \mathbf{U} \rangle \varepsilon) = \nabla \cdot \left(\mu + \mu_{\mathrm{T}}/\sigma_\varepsilon\right) \nabla \varepsilon + \frac{\varepsilon}{k}(C_{\varepsilon 1} P_k - C_{\varepsilon 2} \rho \varepsilon) \tag{27}$$

$$\frac{\partial \rho \langle \xi \rangle}{\partial t} + \nabla \cdot (\rho \langle \mathbf{U} \rangle \langle \xi \rangle) = \nabla \cdot (D + D_{\mathrm{T}}) \nabla \langle \xi \rangle \tag{28}$$

and

$$\frac{\partial \rho \langle \xi'^2 \rangle}{\partial t} + \nabla \cdot \left(\rho \langle \mathbf{U} \rangle \langle \xi'^2 \rangle\right) = \nabla \cdot (D + D_{\mathrm{T}}/\sigma_\xi) \nabla \langle \xi'^2 \rangle + 2 D_{\mathrm{T}} |\nabla \langle \xi \rangle|^2 - \rho \varepsilon_\xi \tag{29}$$

Note that although the density is constant, we have included it in the transport equations to be consistent with the formulation used in commercial CFD codes.

The left-hand sides of Eqs. (25)–(29) have the same form as Eq. (5) and represent accumulation and convection. The terms on the right-hand side can be divided into spatial transport due to "diffusion" and source terms. The diffusion terms have a molecular component (i.e., μ and D), and turbulent components. We should note here that the turbulence models used in Eqs. (26) and (27) do not contain corrections for low Reynolds numbers and, hence, the molecular-diffusion components will be negligible when the model is applied to high-Reynolds-number flows. The turbulent viscosity is defined using a closure such as

$$\mu_{\mathrm{T}} = \rho C_\mu k^2/\varepsilon \tag{30}$$

The turbulent diffusivity is defined by introducing a so-called "turbulent" Schmidt number $\mathrm{Sc_T}$:

$$D_{\mathrm{T}} = \mu_{\mathrm{T}}/\mathrm{Sc_T} \tag{31}$$

which should not be confused with the molecular Schmidt number Sc. Like the other diffusion-model constants (i.e., σ_κ, σ_ε, and σ_ξ), $\mathrm{Sc_T}$ has been determined using canonical turbulent mixing experiments (see Pope (2000) and Fox (2003) for details). We should note, however, that these "constants" must sometimes be adjusted for noncanonical flows.

The source terms on the right-hand sides of Eqs. (25)–(29) are defined as follows. In the momentum balance, $\mathbf{g}$ represents gravity and p is the modified pressure. The latter is found by forcing the mean velocity field to be solenoidal ($\nabla \cdot \langle \mathbf{U} \rangle = 0$). In the turbulent-kinetic-energy equation (Eq. 26), P_k is the source term due to mean shear and the final term is dissipation. In the dissipation equation (Eq. 27), the source terms are closures developed on the basis of the form of the turbulent energy spectrum (Pope, 2000). Finally, the source terms

for the mixture-fraction variance (Eq. 29) are due to production by mean mixture-fraction gradients and dissipation by micromixing. As written, Eq. (29) is not yet closed: we need to add a model for the mixture-fraction dissipation rate ε_ξ. Using Eq. (23), the latter can be modeled by

$$\varepsilon_\xi = R\frac{\varepsilon}{k}\langle\xi'^2\rangle \tag{32}$$

where R depends on $\mathrm{Re_L}$ and Sc as shown in Fig. 4. The CFD model for turbulent mixing is now complete, and can be solved to investigate the degree of macro- and micromixing in a chemical reactor.

The next step in the CFD model formulation involves adding Eqs. (25)–(29) to a CFD code. For this particular example, this step is facilitated in some commercial CFD codes that have the model already included in the standard release of the code. The final step is to solve the model and to compare with experimental data when available. In this step, it may be useful to define new variables during postprocessing to quantify the degree of mixing, mixing zones or the characteristic times for macro- and micromixing. See Liu and Fox (2006) for examples of how this can be done using output from a CFD mixing model.

The CFD model developed above is an example of a ''moment closure.'' Unfortunately, when applied to reacting scalars such as those considered in Section III, moment closures for the chemical source term are not usually accurate (Fox, 2003). An alternative approach that yields the same moments can be formulated in terms of a presumed PDF method (Fox, 1998). Here we will consider only the simplest version of a multi-environment micromixing model. Readers interested in further details on other versions of the model can consult Wang and Fox (2004).

The basis idea behind multi-environment models is that the mixture fraction at any location in the reactor can be approximated by a distribution function in the form of a sum of delta functions as follows:

$$f_\xi(\zeta;\mathbf{x},t) = \sum_{n=1}^{N} p_n(\mathbf{x},t)\delta(\zeta - \xi_n(\mathbf{x},t)) \tag{33}$$

where p_n is the mass fraction of environment n, and ξ_n the mixture fraction in environment n. Using the definition of mixture-fraction moments, we have

$$\langle\xi\rangle = \sum_{n=1}^{N} p_n\xi_n \tag{34}$$

and

$$\langle\xi'^2\rangle = \sum_{n=1}^{N} p_n\xi_n^2 - \langle\xi\rangle^2 \tag{35}$$

In other words, if we know p_n and ξ_n at every point in the reactor, then we can compute up to $2N-1$ independent mixture-fraction moments.

The simplest model of this type is the two-environment model ($N = 2$) for which the independent state variables in the CFD model are

$$\tilde{\Phi} \in \left[\langle \mathbf{U} \rangle, \kappa, \varepsilon, p_1, \xi_1, \xi_2\right]$$

In theory, this model can be used to fix up to three moments of the mixture fraction (e.g., $\langle \xi \rangle$, $\langle \xi^2 \rangle$, and $\langle \xi^3 \rangle$). In practice, we want to choose the CFD transport equations such that the moments computed from Eqs. (34) and (35) are exactly the same as those found by solving Eqs. (28) and (29). An elegant mathematical procedure for forcing the moments to agree is the direct quadrature method of moments (DQMOM), and is described in detail in Fox (2003). For the two-environment model, the transport equations are

$$\frac{\partial \rho p_1}{\partial t} + \boldsymbol{\nabla} \cdot \left(\rho \langle \mathbf{U} \rangle p_1\right) = \boldsymbol{\nabla} \cdot (D + D_{\mathrm{T}}) \boldsymbol{\nabla} p_1 \tag{36}$$

$$\frac{\partial \rho p_1 \xi_1}{\partial t} + \boldsymbol{\nabla} \cdot \left(\rho \langle \mathbf{U} \rangle p_1 \xi_1\right) = \boldsymbol{\nabla} \cdot (D + D_{\mathrm{T}}) \boldsymbol{\nabla} p_1 \xi_1 + \rho \gamma p_1 p_2 (\xi_2 - \xi_1) + \frac{D_{\mathrm{T}}}{\xi_1 - \xi_2} \left(p_1 \left|\boldsymbol{\nabla} \xi_1\right|^2 + p_2 \left|\boldsymbol{\nabla} \xi_2\right|^2\right) \tag{37}$$

and

$$\frac{\partial \rho p_2 \xi_2}{\partial t} + \boldsymbol{\nabla} \cdot \left(\rho \langle \mathbf{U} \rangle p_2 \xi_2\right) = \boldsymbol{\nabla} \cdot (D + D_{\mathrm{T}}) \boldsymbol{\nabla} p_2 \xi_2 + \rho \gamma p_1 p_2 (\xi_1 - \xi_2) + \frac{D_{\mathrm{T}}}{\xi_2 - \xi_1} \left(p_1 \left|\boldsymbol{\nabla} \xi_1\right|^2 + p_2 \left|\boldsymbol{\nabla} \xi_2\right|^2\right) \tag{38}$$

where $p_2 = 1 - p_1$. Summing together Eqs. (37) and (38) and using Eq. (34), the reader can easily show that Eq. (28) is recovered. With a little algebra (Fox, 2003), one can also show using all three equations and Eq. (34) that Eq. (29) will be recovered if we let the micromixing parameter be

$$\gamma = \frac{R\varepsilon}{2k} \tag{39}$$

Although we will not do so here, with a little more work one can use Eqs. (36)–(38) to find the transport equation for $\langle \xi^3 \rangle$. The two-environment model thus provides an extra piece of information that can be compared to experimental data.

The next step would be to implement the CFD transport equation for the state variables in a CFD code. This is a little more difficult for the two-environment model (due to the gradient terms on the right-hand sides of Eqs. 37 and 38) than for the moment closure. Nevertheless, if done correctly both models will

predict exactly the same values for the mean and variance of the mixture fraction. (See Wang and Fox (2004) and Liu and Fox (2006) for specific examples.) The real advantage of the two-environment model comes when dealing with reacting scalars. Unlike the moment method, multi-environment models can easily be extended to multiple reacting scalars with virtually no changes in the model formulation and, more importantly and surprisingly, are often nearly as accurate as more sophisticated closures (Wang and Fox, 2004). We will look at examples of how this is done in Sections III and IV.

In summary, we have presented two different SGS models for single-phase turbulent mixing of an inert scalar. The goal of this presentation was not to show the reader the specific details of how models are derived and tested, but rather to show how a rather complicated physical process can be modeled by adding additional scalars to a CFD model in the form of Eq. (5). Once the equations are in this form, they can be solved in a commercial CFD code for arbitrarily complex reactor geometries. The primary task faced when developing a CFD model for a new reacting system is to develop closures in terms of an appropriate set of state variables. For chemical reaction engineers, the usual starting point will be an existing CFD model for the fluid phase(s), which has been developed and (hopefully!) validated by experts in fluid dynamics. Given such a model for momentum transport, the chemical reaction engineer can focus on the significant task of describing *local* mass/heat-transfer and chemical reactions. Thus, the availability of accurate models for momentum transport is the baseline requirement when faced with a new reactor system, and essentially determines which systems are amenable to CFD.

D. Reactor Systems Amenable to CFD

It would be difficult to construct an exhaustive list of reactor systems that can be treated to some degree using CFD. However, we can give a partial list with a few examples to illustrate the technical issues. First, the simplest systems to treat with CFD are laminar-flow reactors for which the microscopic transport equation can be solved directly (i.e., no SGS modeling is required.) For such reactors, it is possible to use detailed chemical kinetics in complex flow geometries involving heat and mass-transfer and catalytic surfaces. Nevertheless, even for laminar systems computational difficulties can arise, for example, when the working with liquid systems wherein the Schmidt (Prandtl) number is much larger than unity. For such cases the scalar field will require a much finer grid than the velocity field to fully resolve all of the chemistry and physics (i.e., reaction-diffusion layers). One might therefore consider using a micromixing model for the scalar fields to describe the molecular mixing below the grid resolution of the velocity field. In principle, such a model would have the same form as those used for turbulent reacting flows (see Section III), but with a micromixing rate (or local scalar dissipation rate) found from the local strain-rate tensor of the velocity field.

Finally, we can also mention that laminar-flow systems with non-Newtonian fluids often require special numerical algorithms that are usually not available in CFD codes designed mainly for turbulent flows.

Turbulent single-phase flow reactors can also be treated quite accurately with current CFD technology. The key issues in this case are the SGS models and the modeling of heat/mass transfer and reactions at flow boundaries. These issues arise in the CFD transport equation due to the inability to resolve the smallest scales of the flow or boundary layers. For turbulent reacting flows, it is now possible to handle relatively complex chemistry. Nevertheless, due to the computational cost, the total number of chemical species that can be transported by a CFD code for a large computational grid is on the order of 10–100. Furthermore, due to numerical stiffness of many kinetic schemes, simply adding a large number of scalar equations coupled through the chemical source terms leads to unrealistically long computing times. It is thus still very much of interest to find "smart" methods for reducing the number of transported scalars needed to describe complex chemistry. Several useful methods have been proposed to do this (e.g., using the quasi steady state for free radicals (Kolhapure *et al.*, 2005), but methods based on tabulation in terms of a set of "progress variables" (e.g., Fiorina *et al.*, 2005) appear to be promising for complex gas-phase reaction systems. Difficult complications arise, however, if the chemical reactor has multiple inlets or recycled product streams. Such reactors cannot be classified as either nonpremixed or premixed (which are the types that can be most easily handled using tabulation), and the number of degrees of freedom in scalar phase space is large enough that it is very difficult to determine a priori an appropriate set of progress variables to describe the flow. It, thus, may be necessary to carry a large number of scalar fields to describe such reactors, but one can still use tabulation schemes (Raman *et al.*, 2004) to handle the numerical stiffness of the chemical source term.

Multiphase reactor systems offer many challenges to CFD modelers. In terms of complexity, fluid–solid systems are more amenable to CFD modeling than gas–liquid systems. Nevertheless, progress has been made in both fields. For fluid–solid systems, we can distinguish (see Section IV) between reactor systems with fine particles that follow exactly the fluid and systems with solid-particle velocities different than the fluid's velocity. In the first case, the solids can be treated as a scalar field advected by the (single-phase) fluid. In the second case, the solid phase must have its own momentum equation that is coupled to the momentum equation for the fluid. The momentum equation for the solid phase requires many modeling assumptions to describe all possible flow regimes. From the point of view of the fluid dynamics, in general, dilute fluid–solid systems (e.g., circulating fluidized beds), dominated by fluid-phase turbulence, are easier to deal with than dense systems (e.g., bubbling fluidized beds). However, the addition of chemical species and reactions is challenging in both cases. In theory, a general CFD code for fluid–solid flows must account for homogeneous reactions occuring in the fluid (or solid) phase and heterogeneous reactions occuring at the interface between phases. Given that the solid phase is very often a complex

porous material with microchannels that cannot be resolved by the CFD code, it will be necessary to develop subgrid-scale models to describe mass/heat transfer to the particle surface and through the pores. Indeed, in many cases, the solid-phase and surface reactions will be mass-transfer limited and the overall conversion predicted by the CFD code will be determined by the model used to describe mass/heat transfer between the fluid and solid phases. Additional complications arise for fluid–solid systems when the solid particles change in size due, for example, to surface growth, breakage, or agglomeration. It is then necessary to include a description of the particle size distribution (Fan *et al.*, 2004). Finally, we should note that although turbulence models have made considerable progress for dilute gas–solid systems (Minier and Peirano, 2001), the same cannot be said for dense systems. As a result, CFD simulations of bubbling fluidized beds are usually done without turbulence models (see Section V) and require relatively fine computational grids to capture integral-scale properties of the flow (e.g., total pressure drop). The high computational cost of such models makes them intractable for analyzing plant-scale fluidized-bed reactors.

From the perspective of CFD, the most difficult reactor systems are gas–liquid and liquid–liquid flows. Using the denser phase as the reference phase, such systems range from dilute (e.g., liquid sprays) to dense (e.g., bubbly flow). From the point of view of the fluid dynamics, these systems are challenging because the interface between the phases is deformed by (and deforms) the flow. A completely general CFD model would need to keep track of the fluid velocity in each phase and the location and velocity of the interface. Although it is possible to use this approach for specific model problems, it is intractable for actual reactor systems where a less-detailed approach must be applied. For example, continuum model can be used that describes gas and liquid as interpenetrating fluids. However, it is then necessary to introduce models for momentum, mass, and energy exchange between the phases that describe the unresolved processes occuring at the phase interphase. Unlike in fluid–solid flows where the interfaces are rigid, in gas–liquid flows the interface can change due to the fluid dynamics and chemical/physical processes occuring at the interface. Moreover, under industrial conditions where the volume fraction of the gas phase is often very high, turbulence and bubble coalescence and breakage must be accounted for in the CFD model (Sanyal *et al.*, 2005). Unfortunately, it is very difficult to validate (and thus to improve) multiphase turbulence models using modern laser-based measurement techniques. CFD models for gas–liquid chemical reactors remain, therefore, the least developed and should be applied with caution for reactor design and analysis.

III. Mixing-Dependent, Single-Phase Reactions

CFD models for single-phase chemical reactors are by far the most advanced and widely used in industry. The number of different chemical reactors that can be

modeled by CFD is very broad and ranges for laminar flow reactors with detailed gas-phase chemistry coupled with catalytic-surface chemistry to complex turbulent hydrocarbon flames. For many of the more complicated flow configurations, specialized CFD codes have been developed to take advantage of the particular characteristics of the flow. Thus, we will not attempt to describe the entire range of flow phenomena that can be predicted using CFD in any detail. For turbulent reacting flows, a recent monograph (Fox, 2003) covering specific SGS models with abundant references to the literature is recommended as a starting point for anyone wanting to know more about the subject. Here, we will confine our attention to a few specific examples of single-phase turbulent reacting flows to give the reader a general idea of the key modeling issues in the context of CFD.

The topics in this section are arranged in the order of the computational difficulty faced when treating the chemical source term. For completeness, we should note that the simplest case, which simply neglects SGS fluctuations of the scalar fields, will not be discussed for two reasons. First, its implementation in a CFD code is trivial (at least for cases where it is accurate!) and it is the usual default model in a commercial CFD code. Second, since it is accurate in the limit where the reaction rates are slow compared to the flow time scales, CFD is often not required to understand how to scale up chemical reactors with slow chemistry. The discussion here will thus proceed in the opposite direction: starting with very fast chemistry and progressing toward so-called finite-rate chemistry. As discussed in Fox (2003), the speed of the reactions is taken with respect to the resolved scales of the fluid flow. Thus, in a DNS, the smallest characteristic time scale is the Kolmogorov time scale τ_η (see Table I), and a fast reaction occurs on time scales shorter than τ_η. In contrast, in RANS simulations the flow time scale is given by the local integral time scale τ_u. In comparison, for a "classical" CRE model the flow time scale is the residence time, which is typically much larger than τ_u. Therefore, we can conclude that CFD models will start to have utility for reactor analysis whenever the reaction time scales are smaller than the residence time of the reactor.

Before looking at specific SGS models, we should highlight highly exothermic chemical reactions (e.g., combustion). The CFD models for these systems are complicated by the fact that the reaction rates change dramatically across the flow domain depending on the local temperature. Thus, these systems can behave as not only nonreacting flows under ambient conditions but also infinitely fast reactions once ignited. For this reason, combustion models for premixed and nonpremixed systems are usually formulated very differently (Peters, 2000; Poinsot and Veynante, 2001; Veynante and Vervisch, 2002). In contrast, if we consider fast, nearly isothermal reactions in the liquid phase the range of behaviors is more limited in terms of the observed reaction rates. For example, it does not make sense to discuss CFD models for a *premixed* acid–base reaction, because once mixed the reaction occurs instantaneously. For this reason, liquid-phase reactions that are sensitive to mixing are almost always operated under nonpremixed conditions. We will thus limit our attention to these cases in the following discussion.

A. Acid–Base and Equilibrium Chemistry

Acid–base reactions are the archetypical instantaneous reactions. If we let A denote the acid concentration and B the base concentration, the chemical source term for both the acid and base can be expressed as

$$S(A, B) = -kAB \tag{40}$$

where the rate constant k is extremely large. In essence, acid and base cannot coexist at the same spatial location so that either $A = 0$ when $B > 0$, or $B = 0$ when $A > 0$. These zones with excess acid or base are separated by stoichiometric surfaces whereon $A = B = 0$. In a CFD simulation of an acid–base reaction it makes no sense to try to solve the problem directly using the chemical source term. Indeed, even if k were only moderately large, including the source term will lead (at best) to very slow convergence.

To overcome this difficulty, we can introduce a new variable ξ defined in terms of a linear combination of A and B such that the chemical source term for ξ is null. Consider an acid–base reaction of the form

$$\mathrm{A} + r\mathrm{B} \rightarrow \mathrm{P} \tag{41}$$

The microscopic transport equations for A and B are, respectively,

$$\frac{\partial \mathrm{A}}{\partial t} + \mathbf{U} \cdot \boldsymbol{\nabla} \mathrm{A} = \boldsymbol{\nabla} \cdot \Gamma_{\mathrm{A}} \boldsymbol{\nabla} \mathrm{A} - k\mathrm{AB} \tag{42}$$

and

$$\frac{\partial \mathrm{B}}{\partial t} + \mathbf{U} \cdot \boldsymbol{\nabla} \mathrm{B} = \boldsymbol{\nabla} \cdot \Gamma_{\mathrm{B}} \boldsymbol{\nabla} \mathrm{B} - rk\mathrm{AB} \tag{43}$$

where Γ denotes the molecular-diffusion coefficient. Note that if we multiply Eq. (42) by r and then subtract Eq. (43), we can eliminate the chemical source term as follows:

$$\frac{\partial (r\mathrm{A} - \mathrm{B})}{\partial t} + \mathbf{U} \cdot \boldsymbol{\nabla} (r\mathrm{A} - \mathrm{B}) = \nabla^2 (\Gamma_{\mathrm{A}} r\mathrm{A} - \Gamma_{\mathrm{B}} \mathrm{B}) \tag{44}$$

However, the diffusion term is now more complicated and cannot be closed unless A and B are known separately.

As discussed for the general case in Fox (2003), to proceed further we must assume that $\Gamma_{\mathrm{A}} \approx \Gamma_{\mathrm{B}}$ so that Eq. (44) can be written as

$$\frac{\partial (r\mathrm{A} - \mathrm{B})}{\partial t} + \mathbf{U} \cdot \boldsymbol{\nabla} (r\mathrm{A} - \mathrm{B}) = \Gamma \nabla^2 (r\mathrm{A} - \mathrm{B}) \tag{45}$$

The applicability of this approximation depends on the relative importance of the convection and the diffusion terms, and it becomes more accurate for cases dominated by convection (i.e., at large Reynolds numbers).

As discussed earlier, acid–base reactions are always nonpremixed. For example, a semi-batch reactor could initially be filled with base at concentration B_0 and acid is added with concentration A_0. Likewise, a continuous reactor could be run with two feed streams: one for acid and one for base. For both of these examples, the degree of mixing between the acid stream and the rest of the reactor contents can be quantified by introducing the mixture fraction ξ, which obeys

$$\frac{\partial \xi}{\partial t} + \mathbf{U} \cdot \boldsymbol{\nabla} \xi = \Gamma \nabla^2 \xi \tag{46}$$

with boundary conditions $\xi = 1$ in the acid inlet stream and $\xi = 0$ in the base inlet stream (and inside the reactor at $t = 0$). For reactors with more than two inlet streams, it is possible to define a mixture-fraction vector $\boldsymbol{\xi}$ (Fox, 2003), which obeys Eq. (46) and has N components with the properties $0 \leq \xi_n \leq 1$ and $\Sigma_{n=1}^{N} \xi_n = 1$. The modeling approaches discussed below for a single mixture fraction component ξ can thus be extended to $\boldsymbol{\xi}$ to treat more complex flow configurations (Fox, 2003).

The mixture fraction as defined above describes turbulent mixing in the reactor and does not depend on the chemistry. However, by comparing Eqs. (45) and (46), we can note that they have exactly the same form. Thus, for the acid–base reaction, the mixture fraction is related to $r\mathrm{A}-\mathrm{B}$ by

$$\xi = \frac{r\mathrm{A} - \mathrm{B} + \mathrm{B}_0}{r\mathrm{A}_0 - \mathrm{B}_0} \tag{47}$$

and the stoichiometric mixture fraction is given by

$$\xi_{\mathrm{st}} = \frac{\mathrm{B}_0}{r\mathrm{A}_0 + \mathrm{B}_0} \tag{48}$$

Using the fact that A and B cannot coexist at the same spatial location, we then find

$$A = \begin{cases} (\xi - \xi_{\mathrm{st}})\left(\mathrm{A}_0 + \mathrm{B}_0/r\right) & \text{if } \xi > \xi_{\mathrm{st}} \\ 0 & \text{otherwise} \end{cases} \tag{49}$$

and

$$B = \begin{cases} 0 & \text{if } \xi > \xi_{\mathrm{st}} \\ (\xi_{\mathrm{st}} - \xi)(r\mathrm{A}_0 + \mathrm{B}_0) & \text{otherwise} \end{cases} \tag{50}$$

Thus, the CFD simulation need to only treat the turbulent mixing problem for the mixture fraction. Once ξ (or its statistics) are known, the acid and base concentrations can be found from Eqs. (49) and (50), respectively.

The acid–base reaction is a simple example of using the mixture fraction to express the reactant concentrations in the limit where the chemistry is much faster than the mixing time scales. This idea can be easily generalized to the case of multiple fast reactions, which is known as the equilibrium-chemistry limit. If we denote the vector of reactant concentrations by $\boldsymbol{\phi}$ and assume that it obeys a transport equation of the form

$$\frac{\partial \boldsymbol{\phi}}{\partial t} + \mathbf{U} \cdot \boldsymbol{\nabla} \boldsymbol{\phi} = \Gamma \nabla^2 \boldsymbol{\phi} + \mathbf{S}(\boldsymbol{\phi}) \tag{51}$$

then in the equilibrium limit we need to only consider the solution to a simpler equation that includes only the chemical source term as follows:

$$\frac{\mathrm{d}\boldsymbol{\phi}}{\mathrm{d}t} = \mathbf{S}(\boldsymbol{\phi}) \tag{52}$$

In fact, we are only interested in the value of $\boldsymbol{\phi}$ for $t = \infty$ subject to initial conditions that depend on the mixture fraction as follows:

$$\boldsymbol{\phi}_0(\xi) = \xi \boldsymbol{\phi}_1 + (1 - \xi)\boldsymbol{\phi}_2 \tag{53}$$

where $\boldsymbol{\phi}_1$ is the reactant concentration vector in the first inlet stream (defined by $\xi = 1$) and $\boldsymbol{\phi}_2$ is the reactant concentration vector in the second inlet stream.

When formulating the equilibrium-chemistry approximation we implicitly assume that the solution to Eq. (52) for large t depends only on the mixture fraction, and not on the mixing history of the fluid element. For some mixing-sensitive reactions (see Section III.B below), this assumption does not hold and the equilibrium-chemistry approximation is not applicable. These reactions are typically irreversible and the final product distribution depends on the mixing path in concentration phase space traversed by the fluid particle. In general, the equilibrium-chemistry approximation should only be used for systems of fast *reversible* reactions. For this case, $\boldsymbol{\phi}_\infty(\xi)$ found from solving Eq. (52) will depend only on ξ. Note that adding a reverse reaction to the acid–base reaction (Eq. 41) discussed above will not change the basic conclusion that A and B can be determined from ξ. Only the final formulae (Eqs. 49 and 50) will change, and these can be found using the methods described in Fox (2003).

In a turbulent flow, the local value (i.e., at a point in space) of the mixture fraction will behave as a random variable. If we denote the probability density function (PDF) of ξ by $f_\xi(\zeta)$ where $0 \leq \zeta \leq 1$, the integer moments of the mixture fraction can be found by integration:

$$\langle \xi^n \rangle = \int_0^1 \zeta^n f_\xi(\zeta)\, \mathrm{d}\zeta \tag{54}$$

In most applications, the moments of principal interest are the mean $\langle \xi \rangle$ and variance $\langle \xi'^2 \rangle = \langle \xi^2 \rangle - \langle \xi \rangle^2$. The most widely used approach for approximating

f_ξ is the presumed PDF method wherein the PDF depends only on a small set of moments. For example, the beta PDF can be used and has the functional form

$$f_\xi(\zeta) = \frac{(a+b-1)!}{(a-1)!(b-1)!}\zeta^{a-1}(1-\zeta)^{b-1} \tag{55}$$

where a and b depend on the mean and variance as follows:

$$a = \langle\xi\rangle\left(\frac{\langle\xi\rangle(1-\langle\xi\rangle)}{\langle\xi'^2\rangle} - 1\right) \quad \text{and} \quad b = \frac{1-\langle\xi\rangle}{\langle\xi\rangle}a \tag{56}$$

The spatial dependencies of $\langle\xi\rangle$ and $\langle\xi'^2\rangle$ are found by solving Eqs. (28) and (29), respectively.

A typical CFD model for acid–base and equilibrium chemistry solves Eqs. (25)–(29), and then uses Eq. (55) to approximate f_ξ. Once f_ξ is known, the expected values of the reactant concentrations are computed by numerical quadrature from the formula

$$\langle\boldsymbol{\phi}\rangle = \int_0^1 \boldsymbol{\phi}_\infty(\zeta) f_\xi(\zeta)\,\mathrm{d}\zeta \tag{57}$$

For example, $\langle\mathrm{A}\rangle$ and $\langle\mathrm{B}\rangle$ can be computed using Eqs. (49) and (50), respectively. Note that instead of Eq. (55), we could use the simpler expression for f_ξ given by Eq. (33), which avoids the need for numerical quadrature. In both cases, the mean and variance of the mixture fraction are identical (and thus both models account for finite-rate mixing effects.) In practical applications, the differences in the predicted values of $\langle\boldsymbol{\phi}\rangle$ can often be small (Wang and Fox, 2004).

B. Consecutive-Competitive and Parallel Reactions

To go beyond the equilibrium-chemistry limit to consider cases where some of the reaction rates are finite compared to the flow time scales, we need an efficient method to solve for chemical species with chemical-source terms. The straightforward approach for doing this is to simply solve a transport equation for each chemical species with its corresponding chemical-source term. However, it is often the case that one or more of the reaction steps is very fast compared to the flow time scales, leading to numerical difficulties or poor convergence. An elegant method for avoiding this problem is to rewrite the transport equations in terms of the mixture fraction and a set of reaction-progress variables (Fox, 2003).

Some typical examples of the reactions that can be treated in this manner are consecutive–competitive reactions:

$$\begin{aligned} \mathrm{A} + \mathrm{B} &\xrightarrow{k_1} \mathrm{R} \\ \mathrm{A} + \mathrm{R} &\xrightarrow{k_2} \mathrm{S} \end{aligned} \tag{58}$$

and parallel reactions as follows:

$$\begin{aligned} \mathrm{A} + \mathrm{B} &\xrightarrow{k_1} \mathrm{P}_1 \\ \mathrm{A} + \mathrm{C} &\xrightarrow{k_2} \mathrm{P}_2 \end{aligned} \tag{59}$$

In most applications, the first reaction in each set is an acid–base reaction so that k_1 is very large. For Eq. (59), B and C are premixed and added to A under conditions such that B is in stoichiometric excess to A. Likewise, for Eq. (58), B is reacted in stoichiometric excess with A to produce the desired product R. Under these conditions, the first reaction in each set is favored. However, if mixing occurs with the same time scale as the second reaction, the undesired by-product (S in Eq. (58) and P_2 in Eq. (59)) will be produced. Thus, the amount of by-product produced is a sensitive measure of the quality of mixing in the chemical reactor.

The description of Eqs. (58) and (59) in terms of the mixture fraction and reaction-progress variables is described in detail by Fox (2003). Here we will consider a variation of Eq. (59) wherein the acid acts as a catalyst in the second reaction (Baldyga *et al.*, 1998):

$$\begin{aligned} \mathrm{A} + \mathrm{B} &\xrightarrow{k_1} \mathrm{P}_1 \\ \mathrm{A} + \mathrm{C} &\xrightarrow{k_2} \mathrm{A} + \mathrm{P}_2 \end{aligned} \tag{60}$$

This parallel reaction set was used, for example, by Johnson and Prud'homme (2003a) to investigate the quality of mixing in a confined impinging-jets reactor.

Following the steps outline in Fox (2003), the reactant concentrations in Eq. (60) can be written in terms of the mixture fraction ξ and two reaction-progress variables Y_1 and Y_2 as

$$c_{\mathrm{A}} = \mathrm{A}_0[1 - \xi - (1 - \xi_{s1})Y_1] \tag{61}$$

$$c_{\mathrm{B}} = \mathrm{B}_0(\xi - \xi_{s1}Y_1) \tag{62}$$

and

$$c_{\mathrm{C}} = \mathrm{C}_0(\xi - \xi_{s2}Y_2) \tag{63}$$

where the two stoichiometric mixture fractions are

$$\xi_{s1} = \frac{\mathrm{A}_0}{\mathrm{A}_0 + \mathrm{B}_0} \quad \text{and} \quad \xi_{s2} = \frac{\mathrm{A}_0}{\mathrm{A}_0 + \mathrm{C}_0} \tag{64}$$

and A_0, B_0, and C_0 are the inlet concentrations of reactants A, B, and C, respectively. Note that in the absence of chemical reactions, the reaction-progress variables are defined such that $Y_1 = Y_2 = 0$.

The microscopic transport equations for the reaction-progress variables can be found from the chemical species transport equations by generalizing the procedure used above for the acid–base reactions (Fox, 2003). If we assume that $\Gamma_A \approx \Gamma_B \approx \Gamma_C$, then the transport equations are given by

$$\frac{\partial Y_\alpha}{\partial t} + \mathbf{U} \cdot \boldsymbol{\nabla} Y_\alpha = \Gamma \nabla^2 Y_\alpha + S_\alpha(\xi, Y_1, Y_2) \quad \text{for } \alpha = 1, 2 \tag{65}$$

where the chemical-source terms are

$$S_1(\xi, Y_1, Y_2) = \frac{k_1}{B_0 \xi_{s1}} c_A c_B = B_0 \xi_{s1} k_1 \left(\frac{1 - \xi}{1 - \xi_{s1}} - Y_1 \right) \left(\frac{\xi}{\xi_{s1}} - Y_1 \right) \tag{66}$$

and

$$S_2(\xi, Y_1, Y_2) = \frac{k_2}{C_0 \xi_{s2}} c_A c_C = B_0 \xi_{s1} k_2 \left(\frac{1 - \xi}{1 - \xi_{s1}} - Y_1 \right) \left(\frac{\xi}{\xi_{s2}} - Y_2 \right) \tag{67}$$

Note that since the reaction rates must always be nonnegative, the chemically accessible values of the reaction-progress variables will depend on the value of the mixture fraction. We will discuss this point further by looking next at the limiting case where the rate constant k_1 is very large and k_2 is finite.

In many applications, due to the large value of k_1, the first reaction is essentially instantaneous compared to the characteristic flow time scales. Thus, if the transport equation is used to solve for Y_1, the chemical-source term S_1 will make the CFD code converge slowly. To avoid this problem, Y_1 can be written in terms of ξ by setting the corresponding reaction-rate expression (S_1) equal to zero as follows:

$$Y_{1\infty} = \min \left(\frac{\xi}{\xi_{s1}}, \frac{1 - \xi}{1 - \xi_{s1}} \right) \tag{68}$$

It is then no longer necessary to solve a transport equation for Y_1 and the numerical difficulties associated with treating the first reaction with a finite-rate chemistry solver are thereby avoided.

As with the acid–base reaction, Eq. (68) implies that A and B cannot coexist at any point in the flow. Using this infinite-rate approximation, we need only solve transport equations for ξ and Y_2, where the source term for Y_2 is now

$$S_{2\infty}(\xi, Y_2) = B_0 \xi_{s1} k_2 \left(\frac{1 - \xi}{1 - \xi_{s1}} - Y_{1\infty} \right) \left(\frac{\xi}{\xi_{s2}} - Y_2 \right) \tag{69}$$

Note that $S_{2\infty}$ must be nonnegative, and thus the expression above only holds for ξ and Y_2 values that satisfy this condition. For all other values, $S_{2\infty}$ is null.

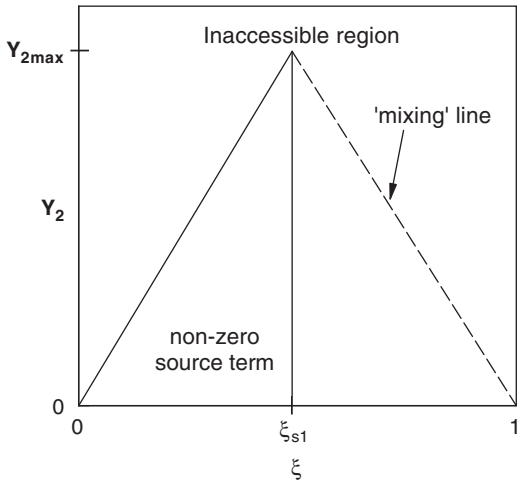

FIG. 5. Region in ξ–Y_2 phase space with non-zero chemical source term and the mixing line.

Applying Eq. (68), we find that when $S_{2\infty}$ is nonzero, it equals

$$S_{2\infty}(\xi, Y_2) = \mathrm{A}_0 k_2 \left(1 - \frac{\xi}{\xi_{s1}}\right)\left(\frac{\xi}{\xi_{s2}} - Y_2\right) \quad \text{if } 0 \le \xi \le \xi_{s1} \text{ and } 0 \le Y_2 \le \xi/\xi_{s2} \tag{70}$$

The region in ξ–Y_2 composition space where this chemical source term is non-zero is shown in Fig. 5. Note that the maximum conversion of C occurs when $\xi = \xi_{s1}$ and corresponds to $Y_{2\max} = \xi_{sl}/\xi_{s2}$ or (using Eq. 63) to $c_C = 0$ (i.e., complete conversion).

As mentioned earlier, in applications of Eq. (60) the reactor is operated with excess B so that $\xi_{s1} < 1/2$. If the mixing in the reactor is good, the mixture fraction in all fluid particles at the exit of the reactor will be equal to the mean ($\xi = \langle\xi\rangle > 1/2$). Thus, if mixing were much faster than the characteristic reaction time of Eq. (70) ($(\mathrm{A}_0 k_2)^{-1}$), then the chemical-source term in Eq. (70) would be zero and no reaction would occur so that $Y_2 = 0$ at the exit. In contrast, any local deviations from perfect mixing can lead to zones in the reactor where $\xi \le \xi_{s1}$ and hence to the production of the by-product Y_2. In the opposite limit where k_2 is large compared to the mixing rates, the maximum attainable value for Y_2 when $\xi_{s1} \le \xi \le 1$ is the mixing line (Fox, 2003), defined by

$$Y_{2\mathrm{mix}}(\xi) = Y_{2\max}\left(\frac{1-\xi}{1-\xi_{s1}}\right) \quad \text{for } \xi_{s1} \le \xi \le 1 \tag{71}$$

and shown as a dashed line in Fig. 5. Using this expression, we find that the maximum attainable conversion is

$$X_{\max} = \frac{\xi_{s1}(1-\bar{\xi})}{\bar{\xi}(1-\xi_{s1})} \quad \text{for} \quad \xi_{s1} \le \bar{\xi} \le 1 \tag{72}$$

The accessible region in $\xi - Y_2$ phase space for the reaction given in Eq. (60) is represented by the triangular region in Fig. 5 found by connecting the feed points and the maximum conversion point. Phase-space trajectories begin at the two feed streams [stream 1: (0; 0) and stream 2: (1; 0)]. If ξ_{s1} is less than the outlet value of the mixture fraction, then the amount of by-product formed is determined by the amount of time spent in the region with nonzero source term (t_{mix}) and the characteristic time of the second reaction (t_{r}). If t_{r} is large compared to t_{mix}, then the by-product concentration will be near zero. If the inverse is true, then the by-product concentration will be near $X_{\max}$.

The CFD model for the reaction given in Eq. (60) in the limit where the first reaction is very fast must account for fluctuations in ξ and Y_2 due to turbulent mixing. In general, this is done by solving for their joint PDF (Fox, 2003), denoted here by $f(\zeta, y)$. There are several ways this can be accomplished:

1. Solve the joint PDF transport equation.
2. Assume a functional form for the joint PDF.
3. Assume a functional form for the conditional PDF of Y_2 given ξ and use a presumed PDF for f_{ξ}.

Method 1 will be discussed in Section III.C. Method 3 can be implemented in several different forms (Baldyga, 1994; Klimenko and Bilger, 1999; Fox and Raman, 2004), but the lowest order approximation requires a model for the conditional expected value of Y_2 given that $\xi = \zeta$ (denoted by $\langle Y_2|\zeta\rangle$) where $\langle Y_2|0\rangle = \langle Y_2|1\rangle = 0$. By definition, $\langle Y_2|\zeta\rangle$ will be a single-valued function of mixture fraction and will lie in the triangular region in Fig. 5. The simplest such model is the one proposed by Baldyga (1994), which uses a linear-interpolation procedure to find the conditional moment from the unconditional moment $\langle Y_2\rangle$ (Fox, 2003). Here we will look at a multi-environment model that is based on method 2.

The multi-environment model for the joint PDF generalizes Eq. (33) by writing

$$f(\zeta, y; \mathbf{x}, t) = \sum_{n=1}^{N} p_n(\mathbf{x}, t)\, \delta(\zeta - \xi_n(\mathbf{x}, t))\, \delta(y - Y_{2n}(\mathbf{x}, t)) \tag{73}$$

where Y_{2n} is the value of Y_2 corresponding to environment n. Here we will consider only the two-environment model ($N = 2$) where the CFD models for

p_1, ξ_1 and ξ_2 are given by Eqs. (36), (37), and (38), respectively. Similarly, the CFD models for the reaction-progress variable in the two environments are

$$\frac{\partial \rho p_1 Y_{21}}{\partial t} + \boldsymbol{\nabla} \cdot \left(\rho \langle \mathbf{U} \rangle p_1 Y_{21}\right) = \boldsymbol{\nabla} \cdot (D + D_{\mathrm{T}}) \boldsymbol{\nabla} p_1 Y_{21} + \rho p_1 S_{2\infty}(\xi_1, Y_{21}) + \rho \gamma p_1 p_2 (Y_{22} - Y_{21}) + \frac{D_{\mathrm{T}}}{Y_{21} - Y_{22}} \left(p_1 |\boldsymbol{\nabla} Y_{21}|^2 + p_2 |\boldsymbol{\nabla} Y_{22}|^2\right) \tag{74}$$

and

$$\frac{\partial \rho p_2 Y_{22}}{\partial t} + \boldsymbol{\nabla} \cdot \left(\rho \langle \mathbf{U} \rangle p_2 Y_{22}\right) = \boldsymbol{\nabla} \cdot (D + D_{\mathrm{T}}) \boldsymbol{\nabla} p_2 Y_{22} + \rho p_2 S_{2\infty}(\xi_2, Y_{22}) + \rho \gamma p_1 p_2 (Y_{21} - Y_{22}) + \frac{D_{\mathrm{T}}}{Y_{22} - Y_{21}} \left(p_1 |\boldsymbol{\nabla} Y_{21}|^2 + p_2 |\boldsymbol{\nabla} Y_{22}|^2\right) \tag{75}$$

Except for the chemical source term, these equations have the same form as those used for the mixture fraction. Note that the chemical source term ($S_{2\infty}$) is evaluated using the mixture fraction and reaction-progress variable in the particular environment. The average chemical source term $\langle S_{2\infty}(\xi, Y_2) \rangle$ will thus not be equal to $S_{2\infty}$ ($\langle \xi \rangle, \langle Y_2 \rangle$) unless micromixing occurs much faster than the second reaction.

The CFD model for the reaction given in Eq. (60) with $k_1 = \infty$ has state variables

$$\tilde{\Phi} \in \left[\langle \mathbf{U} \rangle, k, \varepsilon, p_1, \xi_1, \xi_2, Y_{21}, Y_{22}\right]$$

By definition of the reaction-progress variables, Y_{21} and Y_{22} are zero for the inlet streams, and nonnegative inside the reactor due to the chemical source term. Once the CFD model has been solved, the reactant concentrations in each environment n are found from

$$c_{\mathrm{A}n} = \mathrm{A}_0[1 - \xi_n - (1 - \xi_{\mathrm{s}1}) Y_{1n}] \tag{76}$$

$$c_{\mathrm{B}n} = \mathrm{B}_0[\xi_n - \xi_{\mathrm{s}1} Y_{1n}] \tag{77}$$

and

$$c_{\mathrm{C}n} = \mathrm{C}_0(\xi_n - \xi_{\mathrm{s}2} Y_{2n}) \tag{78}$$

where

$$Y_{1n} = \min\left(\frac{\xi_n}{\xi_{\mathrm{s}1}}, \frac{1 - \xi_n}{1 - \xi_{\mathrm{s}1}}\right) \tag{79}$$

The mean reactant concentrations are then defined by ($p_2 = 1 - p_1$)

$$\langle c_{\mathrm{A}} \rangle = p_1 c_{\mathrm{A}1} + p_2 c_{\mathrm{A}2} \tag{80}$$

$$\langle c_{\mathrm{B}} \rangle = p_1 c_{\mathrm{B}1} + p_2 c_{\mathrm{B}2} \tag{81}$$

and

$$\langle c_C \rangle = p_1 c_{C1} + p_2 c_{C2} \tag{82}$$

The overall conversion of C, denoted by X, is computed using

$$X = 1 - \frac{\langle c_C \rangle}{C_0 \langle \xi \rangle} \tag{83}$$

The value of X at the reactor outlet is a sensitive measure of the degree of mixing in the reactor. If $X \ll 1$, then mixing in the reactor is rapid compared to the second reaction in Eq. (60). In contrast, if $X \approx 1$, then mixing is slow.

The CFD model described above has been used by Liu and Fox (2006) to simulate the experiments of Johnson and Prud'homme (2003a) in a confined impinging-jets reactor. In these experiments, two coaxial impinging jets with equal flow rates are used to introduce the two reactant-streams. The jet Reynolds number Re_j determines the fluid dynamics in the reactor. Typical CFD results are shown in Fig. 6–9 for a jet Reynolds number of $Re_j = 400$ and a reaction time of $t_r = 4.8$ msec. The latter is controlled by fixing the inlet concentrations of the reactants. Further, details on the reactor geometry and the CFD model can be found in Liu and Fox (2006).

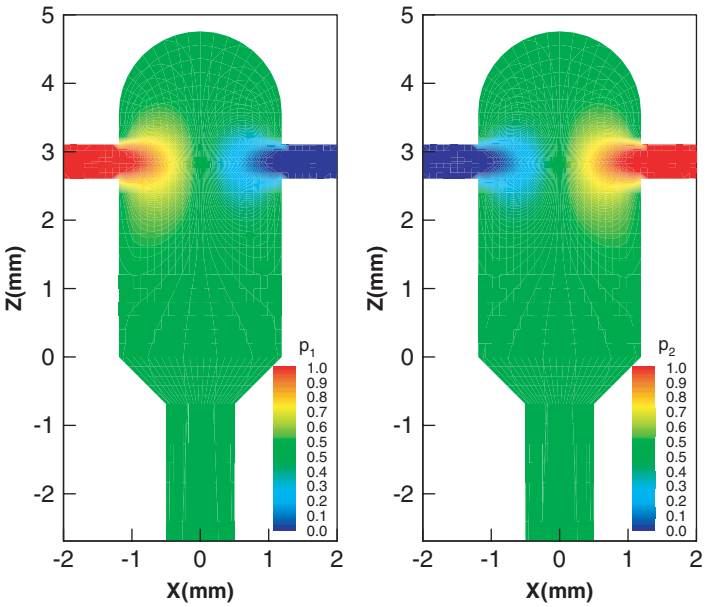

FIG. 6. Volume fractions p_1 and p_2 in the cross-section of the confined impinging-jets reactor.

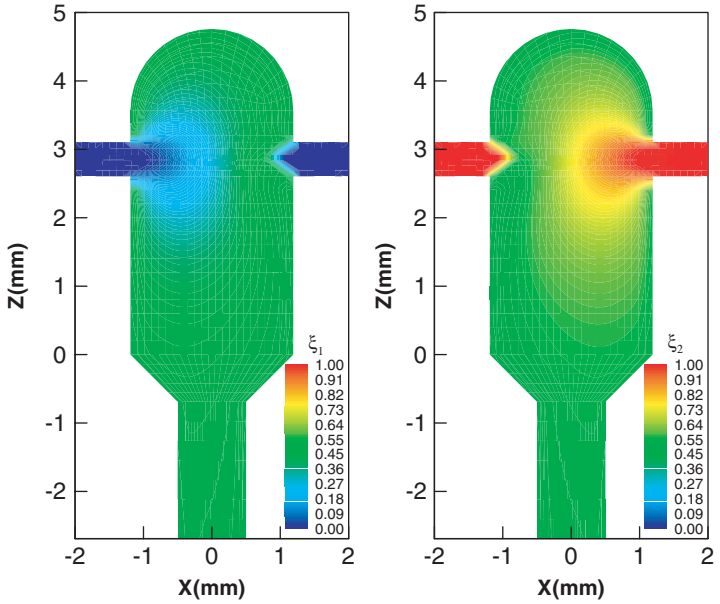

FIG. 7. Mixture fractions ξ_1 and ξ_2 in the cross-section of the confined impinging-jets reactor.

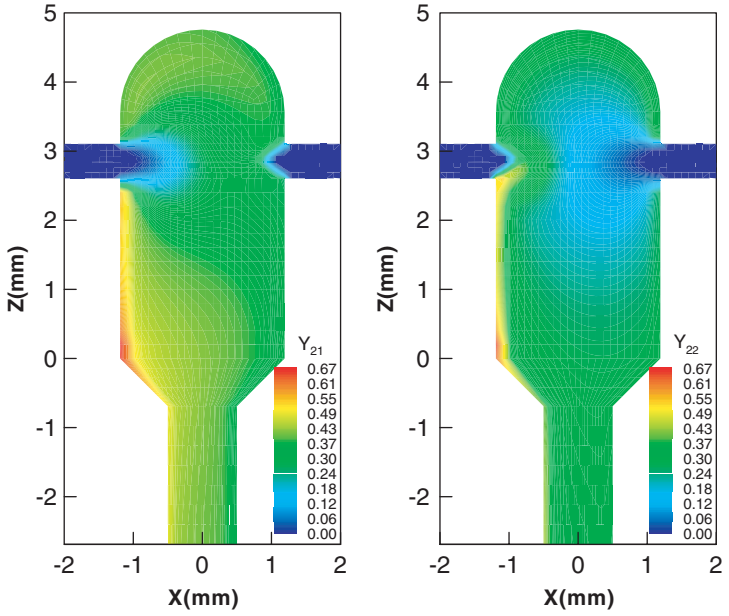

FIG. 8. Reaction-progress variables Y_{21} and Y_{22} in the cross-section of the confined impinging-jets reactor.

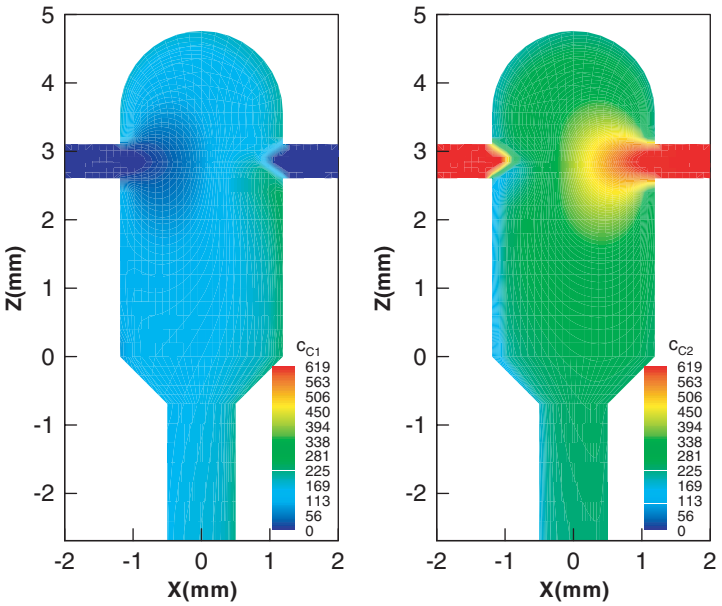

FIG. 9. Reactant concentrations c_{C1} and c_{C2} in the cross-section of the confined impinging-jets reactor.

In Fig. 6, the volume fractions for each environment p_1 and p_2 are shown in a cross-section of the reactor, which includes the inlet jets and the outlet tube. Note that because $p_2 = 1–p_1$ and the inlet flow rates are equal, the contour plots are symmetric about the vertical axis. For the same reason, $p_1 = p_2 = 1/2$ on the vertical axis. In the left-hand inlet stream $p_1 = 1$, corresponding to reactant A. In the right-hand inlet stream $p_2 = 1$, corresponding to reactants B and C. On the outlet cross-section mixing is nearly complete so that $p_1 \approx p_2$. Finally, note that since Eq. (36) does not contain a term for micromixing, the distribution of p_1 and its deviation from 1/2 measures the degree of macromixing at any point in the reactor. We can therefore conclude the reactor is fairly well macromixed everywhere except in the region near the inlet jets.

In Fig. 7, the mixture fractions in each environment ξ_1 and ξ_2 are shown. By definition of the inlet conditions, in the inlet tubes $\xi_1 = 0$ and $\xi_2 = 1$. The variations away from the inlet values represent the effect of micromixing. For example, if we set $\gamma = 0$ in Eqs. (36) and (37) to eliminate micromixing, then ξ_1 and ξ_2 would remain at their inlet values at all points in the reactor. Note that the spatial distributions of ξ_1 and ξ_2 are antisymmetric with respect to the vertical axis (as would be expected from the initial conditions.) In the outlet tube, ξ_1 and ξ_2 are very near the perfectly micromixed value of 1/2. Finally, by comparing Fig. 6 and Fig. 7, we can observe that macromixing occurs slightly faster than micromixing in this reactor (i.e., p_n are closer to their outlet values than are ξ_n.)

The results shown in Figs. 6 and 7 can be combined to compute the mean mixture fraction $\langle \xi \rangle$ and its variance $\langle \xi''^2 \rangle$ from Eqs. (34) and (35), respectively. Example plots are shown in Liu and Fox (2006) and, as expected, they agree with the solution found by solving the moment transport equations directly (Eqs. 28 and 29).

In Fig. 8, the reaction-progress variables in each environment Y_{21} and Y_{22} are shown. By definition of the inlet conditions, in the inlet tubes $Y_{21} = Y_{22} = 0$. Recall that Y_2 is produced by the second (finite-rate) reaction in Eq. (60). Thus, as observed in the plots, it is largest in zones in the reactor where A is in excess. The largest values are found near the left wall of the reactor where the convective velocity is low and A is in slight stoichiometric excess. The residence time for fluid particles in this region is relatively long compared to the reaction time. In general, Y_{21} is larger than Y_{22}, which is easily explained by the fact that A enters the reactor in environment one. Finally, note that at the reactor outlet Y_2 is not uniformly mixed across the tube. Thus, despite the high energy dissipation in the reactor (as measured by the pressure drop), the macromixing at the outlet is not complete (Liu and Fox, 2006).

In Fig. 9, the distribution of reactant C is shown in each environment. As c_C is a linear combination of ξ and Y_2 (Eq. 78), we can distinguish features of both Fig. 7 and Fig. 8 in the plots in Fig. 9. In particular, because C is injected in the right-hand inlet stream, c_{C2} and ξ_2 appear to be quite similar. Finally, as shown in Liu and Fox (2006), the CFD predictions for the outlet conversion X are in excellent agreement with the experimental data of Johnson and Prud'homme (2003a). For this reactor, the local turbulent Reynolds number Re_L is relatively small. The good agreement with experiment is thus only possible if the effects of the Reynolds and Schmidt numbers are accounted for using the correlation for R shown in Fig. 4. Further details on the simulations and analysis of the CFD results can be found in Liu and Fox (2006).

The example reactions considered in this section all have the property that the number of reactions is less than or equal to the number of chemical species. Thus, they are examples of so-called "simple chemistry" (Fox, 2003) for which it is always possible to rewrite the transport equations in terms of the mixture fraction and a set of reaction-progress variables *where each reaction-progress variable*reaction-progress variable –> *depends on only one reaction*. For chemical mechanisms where the number of reactions is larger than the number of species, it is still possible to decompose the concentration vector into three subspaces: (i) conserved-constant scalars (whose values are null everywhere), (ii) a mixture-fraction vector, and (iii) a reaction-progress vector. Nevertheless, most commercial CFD codes do not use such decompositions and, instead, solve directly for the mass fractions of the chemical species. We will thus look next at methods for treating detailed chemistry expressed in terms of a set of "elementary" reaction steps, a thermodynamic database for the species, and chemical rate expressions for each reaction step (Fox, 2003).

C. Detailed Chemistry

In a CFD model with detailed chemistry, the user must provide a chemical mechanism involving K chemical species A_β of the form (Fox, 2003)

$$\sum_{\beta=1}^{K} \upsilon_{\beta i}^{f} \mathrm{A}_\beta \underset{k_i^r}{\overset{k_i^f}{\rightleftharpoons}} \sum_{\beta=1}^{K} \upsilon_{\beta i}^{r} \mathrm{A}_\beta \quad \text{for } i \in 1, \ldots, I \text{ reactions} \tag{84}$$

The rate constants (k_i^f and k_i^r) and the stoichiometric coefficients ($\upsilon_{\beta i}^f$ and $\upsilon_{\beta i}^r$) are all assumed to be known. Likewise, the reaction rate functions R_i for each reaction step, the equation of state for the density ρ, the specific enthalpies for the chemical species H_k, as well as the expression for the specific heat of the fluid c_p must be provided. In most commercial CFD codes, user interfaces are available to simplify the input of these data. For example, for a combusting system with gas-phase chemistry, chemical databases such as *Chemkin-II* greatly simplify the process of supplying the detailed chemistry to a CFD code.

The reaction rates R_i will be functions of the state variables defining the chemical system. While several choices are available, the most common choice of state variables is the set of species mass fractions Y_β and the temperature T. In the literature on reacting flows, the set of state variables is referred to as the *composition vector* $\boldsymbol{\phi}$:

$$\boldsymbol{\phi} = [Y_1, \ldots Y_K, T]^{\mathrm{T}}$$

where the mass fractions sum to unity: $Y_1 + \cdots + Y_K = 1$. The microscopic balance equation for the composition vector has the form of Eq. (1) (Bird *et al.*, 2002). For a turbulent reacting flow, the CFD transport equation will thus have the form of Eq. (3) after averaging.

With detailed chemistry, the most difficult term to close in the CFD transport equation will be the averaged chemical source term $\widetilde{\mathbf{S}(\boldsymbol{\phi})}$. As described in detail in Fox (2003), the chemical source term depends on the reaction rates R_i, which can be highly nonlinear in the composition vector $\boldsymbol{\phi}$. For this reason, simple closures that neglect correlations between components of the composition vector are usually inaccurate. Nevertheless, the default closure for detailed chemistry in most commercial CFD is the so-called laminar-chemistry approximation: $\widetilde{\mathbf{S}(\boldsymbol{\phi})} = \mathbf{S}(\tilde{\boldsymbol{\phi}})$. In words, this closure approximates the average chemical source term by its value evaluated at the average composition vector. In general, the laminar-chemistry approximation overpredicts the reaction rate of the principal reactants, which in reality will be reduced by finite-rate turbulent mixing (Fox, 2003). The simplest example is the reaction rate for the acid–base reaction $\widetilde{S} = -k\widetilde{\mathrm{AB}} = 0$, which is null because acid and base do not coexist. The laminar-chemistry approximation for this case is $\widetilde{S} = -k\tilde{\mathrm{A}}\tilde{\mathrm{B}}$ which forces either $\widetilde{\mathrm{A}}$ or $\widetilde{\mathrm{B}}$ to be null for large k. In reality, this is usually not the case in a turbulent flow unless $\langle \xi'^2 \rangle = 0$.

To represent correlations between the components of $\boldsymbol{\phi}$, we can introduce the joint composition PDF denoted by $f_{\boldsymbol{\phi}}(\boldsymbol{\psi})$, where $\boldsymbol{\psi}$ is the sample-space composition vector (Fox, 2003). Starting from the microscopic transport equation for $\boldsymbol{\phi}$, it is possible to derive a CFD transport equation for $f_{\boldsymbol{\phi}}$ $(\boldsymbol{\psi}; \mathbf{x}, t)$, in which the chemical source term appears in closed form. This CFD transport equation is the starting point for *transported PDF methods*. In transported PDF methods, closures are required for turbulent dispersion and molecular mixing. However, once such closures are introduced into the CFD transport equation, we are still faced with the computational challenge of dealing with a large number of independent variables $(\boldsymbol{\psi}; \mathbf{x}, t)$. One method for overcoming this difficulty is to use Monte–Carlo simulation techniques wherein $f_{\boldsymbol{\phi}}$ is represented by a finite number of so-called notional particles (Fox, 2003). Typically, 50–100 notional particles are needed for each CFD grid cell to accurately capture the correlations between the components of $\boldsymbol{\phi}$ and to control statistical errors. For comparison, the laminar-chemistry approximation uses in effect one notional particle per grid cell. The transported PDF method will therefore be more computationally demanding, but represents the state of the art for treating detailed chemistry coupled to turbulent mixing. Reader interested in further details on PDF methods and the corresponding simulation codes are advised to consult Fox (2003). There are many reported applications of transported PDF methods to combusting systems (see, for example, results for a turbulent diffusion flame in Raman *et al.* (2004), and Fox (2003) for other references). Applications to chemical process systems are rarer, but some recent examples are Raman *et al.* (2003) and Liu *et al.* (2004).

The relatively high cost of transported PDF methods has led us to explore lower-cost methods for approximating the CFD transport equation for $f_{\boldsymbol{\phi}}$ (Wang and Fox, 2004). In principle, transported PDF simulations can be made cheaper by using only a small number of notional particles N. However, the random fluctuations introduced by the simulation method lead to statistical errors that scale like $1/\sqrt{N}$. Thus, when N is small the statistical error is quite significant. Ideally, we would like to have an acceptably accurate method that works for N as small as one, and whose accuracy increases for larger N in a well-defined deterministic manner. Our method for accomplishing this task is called the direct quadrature method of moments (DQMOM) (Fox, 2003; Wang and Fox, 2004; Marchisio and Fox, 2005). We briefly describe the resulting CFD model below. Readers interested in more details should consult the references given above.

The application of DQMOM to the *closed* composition PDF transport equation is described in detail by Fox (2003). If the IEM model is used to describe micromixing and a gradient-diffusivity model is used to describe the turbulent fluxes, the CFD model will have the form

$$\frac{\partial \rho p_n}{\partial t} + \boldsymbol{\nabla} \cdot \left(\rho \langle \mathbf{U} \rangle p_n\right) = \boldsymbol{\nabla} \cdot (D + D_{\mathrm{T}}) \boldsymbol{\nabla} p_n \qquad \text{for } n = 1, \ldots, N \tag{85}$$

and

$$\frac{\partial \rho p_n \phi_{\alpha n}}{\partial t} + \boldsymbol{\nabla} \cdot \left(\rho \langle \mathbf{U} \rangle p_n \phi_{\alpha n}\right) = \boldsymbol{\nabla} \cdot (D + D_{\mathrm{T}}) \boldsymbol{\nabla} p_n \phi_{\alpha n} + \rho p_n S_\alpha(\boldsymbol{\phi}_n) + \rho p_n \gamma \left(\langle \phi_\alpha \rangle - \phi_{\alpha n}\right) + \rho b^*_{\alpha n} \tag{86}$$

where the subscript n denotes the environment and the subscript α denotes the component of the composition vector. Thus, p_n is the mass fraction of environment n, and $\boldsymbol{\phi}_n$ is the composition vector in environment n. The reader will recognize these equations as an N-environment generalization of the two-environment model introduced earlier. Note that, as in transported PDF simulations, the chemical source term $S_\alpha(\boldsymbol{\phi}_n)$ appears in closed form in Eq. (86).

By definition, the sum of the mass fractions is unity: $p_1 + \cdots + p_N = 1$. Thus, one of the equations for p_n in Eq. (85) is redundant. In Eq. (86), $\phi_{\alpha n}$ is one of the $K+1$ components of the composition vector in environment n. The mean composition $\langle \phi_\alpha \rangle$ appearing in the micromixing model is defined by

$$\langle \phi_\alpha \rangle = \sum_{n=1}^{N} p_n \phi_{\alpha n} \tag{87}$$

Note that if the mass fractions are used to define the composition vector, then by definition

$$\sum_{\alpha=1}^{K} \phi_{\alpha n} = 1 \tag{88}$$

where the sum is over all the K chemical species. This implies that the sum of Eq. (86) over all species must yield Eq. (85), and thus that one of the chemical species equations is redundant. Redundancy can be avoided in the CFD model by solving Eq. (85) only for $n = 1,\ldots, N-1$, and Eq. (86) for $n = 1,\ldots, N$ but with only $K-1$ mass fractions. To avoid numerical errors, the mass fraction of the species not solved for should be relatively large and, preferably, correspond to a chemically inert species. The composition vector will then have K (including temperature) components, and a total of $N(K+1)-1$ transport equations must be solved to represent the model in the CFD code. Alternatively, since the sum of the chemical source term in Eq. (86) over all chemical species is null, the CFD model can solve only Eq. (86) for $\alpha = 1,\ldots, K+1$ and not use Eq. (85). This leads to $N(K+1)$ equations (i.e., one more than required[1]), but has the benefit that all of the transport equations have the same form.

The final term in Eq. (86) is the correction term $b^*_{\alpha n}$, which comes from applying DQMOM to the transport equation for the composition PDF (Fox,

[1]The "extra" equation is the mass continuity equation for ρ.

2003). This term is computed by solving a linear system of equations defined for each $\alpha = 1,\ldots, K+1$ by

$$\sum_{n=1}^{N} \phi_{\alpha n}^{m-1} b_{\alpha n}^{*} = \sum_{n=1}^{N} (m-1) p_n \phi_{\alpha n}^{m-2} D_{\mathrm{T}} |\nabla \phi_{\alpha n}|^2 \quad \text{for } m = 1,\ldots,N \tag{89}$$

This expression results from forcing the transport equations for the first N moments of ϕ_α, denoted by $\langle \phi_\alpha^m \rangle$, to agree with the composition PDF transport equation (Fox, 2003). For example, with $N = 2$ the linear system in Eq. (89) can be written in matrix form as

$$\begin{bmatrix} 1 & 1 \\ \phi_{\alpha 1} & \phi_{\alpha 2} \end{bmatrix} \begin{bmatrix} b_{\alpha 1}^{*} \\ b_{\alpha 2}^{*} \end{bmatrix} = \begin{bmatrix} 0 \\ p_1 D_T |\nabla \phi_{a1}|^2 + p_2 D_T |\nabla \phi_{a2}|^2 \end{bmatrix} \tag{90}$$

Solving for $b_{\alpha n}^{*}$ yields

$$b_{\alpha 1}^{*} = \frac{D_{\mathrm{T}}}{\phi_{\alpha 2} - \phi_{\alpha 1}} \left(p_1 |\nabla \phi_{\alpha 1}|^2 + p_2 |\nabla \phi_{\alpha 2}|^2 \right) \tag{91}$$

and

$$b_{\alpha 2}^{*} = \frac{D_{\mathrm{T}}}{\phi_{\alpha 2} - \phi_{\alpha 1}} \left(p_1 |\nabla \phi_{\alpha 1}|^2 + p_2 |\nabla \phi_{\alpha 2}|^2 \right) \tag{92}$$

The reader will recognize these terms as having of the same form as the correction terms in the two-environment model discussed earlier. With $N = 1$, $b_{\alpha 1}^{*} = 0$ and the model reduces to the laminar-chemistry approximation. With $N = 2$, additional information is obtained concerning the second-order moments of the composition vector. Likewise, by using a larger N, the Nth-order moments are controlled by the DQMOM correction terms found from Eq. (89).

As noted earlier, the sum of the mass fractions is unity and thus Eq. (86) will be consistent with Eq. (85) only if the sum of the correction term $b_{\alpha n}^{*}$ over all chemical species $\alpha = 1,\ldots, K$ is null. In general, this will not be the case if Eq. (89) is used. Another difficulty that can arise is that the mass fractions in two environments may be equal, e.g., $\phi_{\alpha 1} = \phi_{\alpha 2}$, and thus the coefficient matrix in Eq. (89) will be singular. This can occur, for example, in the equilibrium-chemistry limit where the compositions depend only on the mixture fraction, i.e., $\boldsymbol{\phi} = \boldsymbol{\phi}_\infty(\xi)$. For chemical species that are not present in the feed streams, the equilibrium values for $\xi = 0$ and $\xi = 1$ are zero, but for intermediate values of the mixture fraction, the equilibrium values are positive. This implies that the equilibrium values will be the same for at least two values of the mixture fraction in the range $0 < \xi < 1$. Thus, in the equilibrium limit it is inevitable that two environments will have equal mass fractions for certain species at some point in the flow field. Since singularity implies an underlying correlation between

components of the composition vector, in most cases these difficulties can be overcome by computing the correction terms using a set of moments that is different than $\langle \phi_\alpha^m \rangle$ (i.e., one can include cross moments $\langle \phi_\alpha^{m-p} \phi_\beta^p \rangle$. For example, one possible choice of moments that also ensures that the sum of the correction terms is null is to use the cumulative mass fractions. We will describe this choice next, but the reader should keep in mind that other choices may be required if the coefficient matrix in Eq. (89) becomes singular.

Let Y_α denote the mass fractions of the K chemical species describing the reacting flow. By definition, $\sum_{\alpha=1}^{K} K\ Y_\alpha = 1$. Assuming that the chemical species are numbered such that the major species (e.g., reactants) appear first,[2] followed by the minor species (e.g., products), we can define a linear transformation by

$$X_\beta = \sum_{\alpha=1}^{\beta} Y_\alpha \quad \text{for } \beta = 1, \ldots, K \tag{93}$$

Note that by definition $X_K = 1$ and thus X_β is the cumulative mass fraction of the first β species. The inverse transformation corresponding to Eq. (93) is

$$Y_1 = X_1 \quad \text{and} \quad Y_\alpha = X_\alpha - X_{\alpha-1} \quad \text{for } \alpha \geq 2 \tag{94}$$

The correction terms can be computed using either Y_α or X_α. However, it is clear that the correction terms will depend on which choice is used since the moments controlled by DQMOM are different (i.e., $\langle Y_\alpha^m \rangle$ vs. $\langle X_\alpha^m \rangle$). Thus, for example, with fixed N one set of moments may lead to singular correction terms, but not the other. In general, we can continue to solve for the mass fractions in the CFD model, but with the correction terms computed using the cumulative mass fractions as follows.

1. Given the mass fractions in each environment $Y_{\alpha n}$, use Eq. (93) to compute the cumulative mass fractions $X_{\alpha n}$.
2. Use the integer moments of X_α to compute the correction terms as follows:

$$\sum_{n=1}^{N} X_{\alpha n}^{m-1} b_{\alpha n}^{+} = \sum_{n=1}^{N} (m-1) p_n X_{\alpha n}^{m-2} D_{\mathrm{T}} |\nabla X_{\alpha n}|^2 \quad \text{for } m = 1, \ldots, N \tag{95}$$

3. Compute the correction terms for the mass fractions $b_{\alpha n}^{*}$ using Eq. (94) as follows:

$$b_{1n}^{*} = b_{1n}^{+} \quad \text{and} \quad b_{\alpha n}^{*} = b_{\alpha n}^{+} - b_{\alpha-1 n}^{+} \quad \text{for } \alpha \geq 2 \tag{96}$$

[2] In the computer code, a sorting algorithm can be used to put the mean mass fractions $\langle Y_\alpha \rangle$ in descending order before defining X_β. By keeping track of the order of the indices, one can easily define the inverse transformation needed to compute Y_α from X_β.

Note that since $X_{Kn} = 1$, Eq. (95) leads to the degenerate case where $b^+_{Kn} = 0$, and thus the sum of the correction terms over all species is null. Also, if one of the mass fractions is null[3] (say $Y_\gamma = 0$) then $X_\gamma = X_{\gamma-1}$ and thus the correction term for such mass fractions will be null due to Eq. (96).

As discussed in detail in Wang and Fox (2004), on the one hand, for non-reacting systems the DQMOM approach with N environments will exactly reproduce the moment equations for each chemical species up to order N. However, N cannot be chosen to be too large because the coefficient matrix in Eq. (89) can become poorly conditioned. In contrast, the moments estimated from the transported PDF simulations will have statistical fluctuations that can only be reduced by time/ensemble averaging. In this sense, DQMOM is preferable. On the other hand, for reacting systems the moments of chemical species obey transport equations that contain unclosed averages involving the nonlinear chemical source term. In both approaches, these averages are approximated by

$$\left\langle \phi_\alpha^{m-1} S_\alpha(\boldsymbol{\phi}) \right\rangle = \int \psi_\alpha^{m-1} S_\alpha(\boldsymbol{\psi}) f_{\boldsymbol{\phi}} \mathrm{d}\boldsymbol{\psi} \approx \sum_{n=1}^{N} p_n \phi_{\alpha n}^{m-1} S_\alpha\left(\boldsymbol{\phi}_n\right) \tag{97}$$

where in a transported PDF code p_n is the particle weight and $\boldsymbol{\phi}_n$ is the particle composition vector (Fox, 2003). The integral in Eq. (97) is just the definition of the expected value. It can be seen that the integral is replaced by a finite sum over a set of N "quadrature" points. Thus, the accuracy of the moments will depend on the degree of nonlinearity of $\mathbf{S}(\boldsymbol{\phi})$. For a weakly nonlinear source term, a low-order quadrature method may be adequate and DQMOM would be preferred. Such cases have been successfully investigated by Wang and Fox (2004). In contrast, for strong nonlinearities (e.g., typical of combusting systems), a large value of N may be needed to approximate the integral in Eq. (97) and transported PDF simulations would be preferred.

In practice, it may be difficult to determine in advance which method is best to use for a particular application. For example, the CFD results may be more sensitive to large-scale inhomogeneities in the flow field than to the chemical source term closure. A rational approach to determine whether a more detailed SGS model is needed might be to start with $N = 1$ (laminar-chemistry approximation) and compare the predicted mean chemical species fields to the two-environment model ($N = 2$). If the differences are small, then the simpler model is adequate. However, if the differences are large, then the CFD simulation can be repeated with $N = 3$ and the results compared to $N = 2$. Naturally, once this procedure has "converged," it will still be necessary to validate the CFD results with experimental data whenever possible. Indeed, it may be necessary to

[3]If the mass fractions are sorted in descending order, then all of the null mass fractions will be grouped together at the end of the array. The procedure can thus be simplified by using only the non-zero mass fractions to define X_β. In practice, one can define a lower limit for Y_α and set the correction term to zero for mass fractions below this limit.

improve the turbulent transport and micromixing models before satisfactory agreement is obtained even with the state-of-the-art transported PDF method.

IV. Production of Fine Particles

The CFD models discussed in the previous section considered mass balances for a finite number of chemical species. In this section, we will extend these models to include systems wherein a second phase is produced. Such systems include aerosols (Friedlander, 2000; Wright *et al.*, 2001), reactive precipitation (Pohorecki and Baldyga, 1983; Garside and Tavare, 1985; Pohorecki and Baldyga, 1988; Villermaux and David, 1988; Marcant and David, 1991; Mahajan and Kirwan, 1993; David and Marcant, 1994; Seckler *et al.*, 1995; Mahajan and Kirwan, 1996; Aoun *et al.*, 1999; Johnson and Prud'homme, 2003b,c), colloids (Oles, 1992; Sandkühler *et al.*, 2003, 2005; Waldner *et al.*, 2005), and flame synthesis of nanoparticles (Kodas *et al.*, 1987; Akhtar *et al.*, 1991; Xiong and Pratsinis, 1991; Kruis *et al.*, 1993; Pratsinis *et al.*, 1996; Zhu and Pratsinis, 1997; Briesen *et al.*, 1998; Pratsinis, 1998; Kammler and Pratsinis, 1999, 2000; Kammler *et al.*, 2001; Mueller *et al.*, 2004a,b; Tani *et al.*, 2004a,b) (to name just a few examples). We will limit the discussion to systems wherein the particles are "not too large," in other words, to particles that on average follow the local fluid velocity (Davies, 1949). Systems with larger particles will be considered in Section V. In terms of the CFD model, the primary difference between "fine" and "large" particles is that the former can be treated as pseudo species by extending the mass balances and chemical kinetic expressions that we have already considered (Piton *et al.*, 2000; Johannessen *et al.*, 2000, 2001). In contrast, for larger particles, a separate momentum balance is required for each phase (Fan *et al.*, 2004), which significantly complicates the solution procedure used to solve the CFD model.

The definition of a "fine" particle can be made more quantitative by introducing the article Stokes number St, which measures the particle-to-fluid response-time ratio to changes in the velocity (Fuchs, 1964):

$$\mathrm{St} = \frac{\gamma \rho_s d_s^2}{12 \rho_f \nu_f} \tag{98}$$

In this definition, ρ_s and ρ_f are the solid and fluid densities, respectively. The characteristic diameter of the particles is d_s (which is used in calculating the projected cross-sectional area of particle in the direction of the flow in the drag law). The kinematic viscosity of the fluid is ν_f and γ is a characteristic strain rate for the flow. In a turbulent flow, γ can be approximated by $1/\tau_\eta$ when d_s is smaller than the Kolmogorov length scale η. (Unless the turbulence is extremely intense, this will usually be the case for fine particles.) Based on the Stokes

number, we can neglect the momentum equation for the solid phase when $\mathrm{St} < 0.14$ (Dring, 1982). Note that for systems with growing or aggregating particles, the characteristic diameter of the largest particles should be used to compute the Stokes number. Thus, as a general rule of thumb, in a liquid-phase turbulent flow solid particles (with $\rho_s \approx \rho_f$) will follow the fluid if $d_s \leq \eta$. Since typical minimum values for the Kolmogorov length scale in practical systems are in the range 10–100 μm, nucleation and growth of nanoparticles and crystals, and colloidal aggregation can all be treated as systems involving fine particles.

A fundamental modeling challenge that arises when dealing with particulate systems is the need to describe the particle size distribution (PSD). Depending on the application (Randolph and Larson, 1988; Ramkrishna, 2000), this is done by defining a population balance equation (PBE) governing a number density function (NDF) $n(l; \mathbf{x}, t)$. The latter is defined by an "internal coordinate" l, which may correspond to mass, volume, or (as done here) length.[4] In words, $n(l; \boldsymbol{x}; t$, is the number concentration of particles with lengths in the range $[l, l + \mathrm{d}l]$) and thus it has units of (number)/(volume × length).

The NDF is very similar to the PDFs introduced in the previous section to describe turbulent reacting flows. However, the reader should not confuse them and must keep in mind that they are introduced for very different reasons. The NDF is in fact an extension of the finite-dimensional composition vector $\boldsymbol{\phi}$ to the case of an infinite number of scalars (parameterized by $0 \leqslant l < \infty$). Thus, even in the case of laminar flow where the PDFs are not needed, the NDF still introduces an extra dimension (l) to the problem description. The choice of the state variables in the CFD model used to solve the PBE will depend on how the internal coordinate is "discretized." Roughly speaking (see Ramkrishna (2000) for a more complete discussion), there are two approaches that can be employed:

1. Sectional methods that represent the NDF by a "histogram" (Kumar and Ramkrischna, 1996).
2. Quadrature methods that approximate integral constraints (e.g., moments) of the NDF (McGraw, 1997).

For cases with only one internal coordinate, either approach can be implemented in a CFD code (but the computational cost for the same accuracy can be very different). However, for cases with more than one internal coordinate, only the quadrature methods are computationally tractable on current computers. Thus, in the examples below, we will describe only CFD models based on the

[4]The preferred choice of internal coordinates is discipline dependent. Nevertheless, the conservation of solid mass will imply constraints on particular moments of the PSD. In general, given the relationship between the various choices of coordinates, it is possible (although not always practical) to rewrite the PBE in terms of any choice of internal coordinate.

quadrature approach. Details on particular applications of this approach can be found in our recent publications (Marchisio *et al.*, 2001a,b, 2003a,b; Wang and Fox, 2003; Wang *et al.*, 2005a).

A. Mixing-Dependent Nucleation and Growth

As a first example of a CFD model for fine-particle production, we will consider a turbulent reacting flow that can be described by a species concentration vector **c**. The microscopic transport equation for the concentrations is assumed to have the "standard" form as follows:

$$\frac{\partial \mathbf{c}}{\partial t} + \boldsymbol{\nabla} \cdot (\mathbf{U}\mathbf{c}) = \boldsymbol{\nabla} \cdot (\Gamma \boldsymbol{\nabla} \mathbf{c}) + \mathbf{S}(\mathbf{c}) \tag{99}$$

All of the chemical species, except one, will be assumed to be completely soluble. The one partially insoluble species will nucleate and grow a solid phase. A typical example is $A + B \rightarrow P$ where P is a sparingly soluble compound. The rates of nucleation J and molecular surface growth G can be functions of the local concentration vector **c**, the particle size l, and the local turbulence properties. Neglecting aggregation and breakage processes, a microscopic PBE for this system can be written as follows:

$$\frac{\partial n}{\partial t} + \boldsymbol{\nabla} \cdot (\mathbf{U}n) = \boldsymbol{\nabla} \cdot (\Gamma_n \boldsymbol{\nabla} n) + J(l, \mathbf{c}) - \frac{\partial}{\partial l}[G(l, \mathbf{c})n] \tag{100}$$

Note that we have used the fluid velocity **U** to describe convection of particles, which is valid for small Stokes number. In most practical applications, J is a highly nonlinear function of **c**. Thus, in a turbulent flow the average nucleation rate will depend strongly on the local micromixing conditions. In contrast, the growth rate G is often weakly nonlinear and therefore less influenced by turbulent mixing.

The quadrature approach for treating Eq. (100) introduces a moment transformation defined by

$$m_k = \int_0^\infty l^k n(l) \mathrm{d}l \quad \text{for } k = 0, 1, \ldots, \infty \tag{101}$$

Applying this transformation to Eq. (100) yields

$$\frac{\partial m_k}{\partial t} + \boldsymbol{\nabla} \cdot (\mathbf{U}m_k) = \boldsymbol{\nabla} \cdot (\Gamma \boldsymbol{\nabla} m_k) + \overline{J}_k(\mathbf{c}) + k\overline{G}_{k-1}(\mathbf{c}) \tag{102}$$

where the moments of the nucleation function are defined by

$$\overline{J}_k(\mathbf{c}) = \int_0^\infty l^k J(l, \mathbf{c}) \, \mathrm{d}l \tag{103}$$

and the growth rates for the moments are defined by

$$\overline{G}_k(\mathbf{c}) = \int_0^\infty l^k G(l, \mathbf{c}) n(l)\, \mathrm{d}l \tag{104}$$

Note that in the special case of size-independent growth, this term can be expressed as a closed function of the moments, i.e., $\overline{G}_k(\mathbf{c}) = G(\mathbf{c}) m_k$. Note also that when deriving Eq. (102) we have neglected the size-dependence of Γ_n. This is justified in turbulent flows and, in any case, to do otherwise would require a micromixing model that accounts for differential diffusion (Fox, 2003).

In principle, any functional form could be used for the nucleation rate. However, to simplify the discussion, we will assume that only particles of zero size are formed by nucleation so that Eq. (103) becomes

$$\overline{J}_k(\mathbf{c}) = \delta_{0,k} J(\mathbf{c}) \tag{105}$$

where $\delta_{j,k}$ is the Kronecker delta and $J(\mathbf{c})$ contains the dependence of the nucleation rate on the local composition vector. Note that under this assumption nucleation only appears in the equation for the moment of order $k = 0$.

Due to the presence of the unknown NDF inside the integral in Eq. (104), the growth term is not closed (i.e., it cannot be computed exactly in terms of the moments unless G is independent of l). In the quadrature method of moments (QMOM), the integral is approximated by a sum over a set of M weights (w_m) and M abscissas (l_m):

$$\overline{G}_k(\mathbf{c}) = \sum_{m=1}^{M} w_m l_m^k G(l_m, \mathbf{c}) \tag{106}$$

The weights and abscissas are determined in QMOM by forcing them to agree with the quadrature approximation of the first $2M$ moments:

$$m_k = \sum_{m=1}^{M} w_m l_m^k \quad \text{for } k = 0, 1, \ldots, 2M-1 \tag{107}$$

This system of $2M$ nonlinear equations is ill-conditioned for large M, but can be efficiently solved using the product-difference (PD) algorithm introduced by McGraw (1997). Thus, given the set of $2M$ moments on the left-hand side of Eq. (107), the PD algorithm returns w_m and l_m for $m = 1, \ldots, M$. The closed microscopic transport equation for the moments can then be written for $k = 0, \ldots, 2M-1$ as

$$\frac{\partial m_k}{\partial t} + \nabla \cdot (\mathbf{U} m_k) = \nabla \cdot (\Gamma \nabla m_k) + \delta_{0,k} J(\mathbf{c}) + k \sum_{m=1}^{M} w_m l_m^{k-1} G(l_m, \mathbf{c}) \tag{108}$$

To proceed further, this expression and Eq. (99) must be averaged to find the CFD transport equations for the species concentrations and the moments.

By defining the composition vector to include the species concentrations and the moments as follows:

$$\boldsymbol{\phi} = [c_1, \ldots, c_K, m_0, \ldots, m_{2M-1}]^{\mathrm{T}}$$

we can observe that the microscopic transport equations have the same form as those used for detailed chemistry in Section III.C. Thus, any turbulent reacting flow model that can be used for detailed chemistry can also be used as a CFD model for fine-particle production. For example, using the DQMOM approach to treat the composition PDF leads to Eqs. (85) and (86) with source terms for the moments given by the last two terms in Eq. (108) as follows:

$$S_k(\boldsymbol{\phi}) = \delta_{0,k} J(\mathbf{c}) + k \sum_{m=1}^{M} w_m l_m^{k-1} G(l_m, \mathbf{c}) \tag{109}$$

Note that each environment in the micromixing model will have its own set of concentrations $c_{\alpha n}$ and moments m_{kn}, reflecting the fact that the PSD is coupled to the chemistry and will thus be different at every SGS point in the flow. The PD algorithm is applied separately in each environment to compute the weights (w_{mn}) and abscissa (l_{mn}) from the quadrature formula as follows:

$$m_{kn} = \sum_{m=1}^{M} w_{mn} l_{mn}^{k} \quad \text{for } k = 0, 1, \ldots, 2M-1 \tag{110}$$

Thus, the source terms for each environment $S(\mathbf{c})$ and $S_k(\boldsymbol{\phi})$ will be closed. Of particular interest are the local nucleation rates $J(\mathbf{c}_n)$. As discussed in Wang and Fox (2004), due to poor micromixing the local nucleation rates can be much larger than those predicted by the average concentrations $J(\langle \mathbf{c} \rangle)$. This results in a rapid increase in the local particle number density m_{0n} due to the creation of a very large number of nuclei. As discussed below, this will have significant consequences on the local rate of aggregation.

The CFD model for nucleation and growth can now be solved to determine the average species concentrations $\langle \mathbf{c} \rangle$ and the average moments of the NDF $\langle m_k \rangle$. However, to properly interpret the computational results, care must be taken in defining the averages for terms involving the moments. Starting from the definition of the moments from the microscopic NDF (Eq. 101), the average moments are defined by

$$\langle m_k \rangle = \int_0^\infty l^k \langle n(l) \rangle \, \mathrm{d}l \tag{111}$$

where $\langle n(l)\rangle$ is the Reynolds-average NDF. For the multi-environment model, the Reynolds-average quantities are defined by

$$\langle m_k\rangle = \sum_{n=1}^{N} p_n m_{kn} \quad \text{and} \quad \langle n(l)\rangle = \sum_{n=1}^{N} p_n n_n(l) \tag{112}$$

where $n_n(l)$ is the NDF in environment n. Using the definition of the weights and abscissas (Eq. 110), the average moments can be expressed as follows:

$$\langle m_k\rangle = \sum_{n=1}^{N} p_n \sum_{m=1}^{M} w_{mn} l_{mn}^k = \sum_{m=1}^{M} \langle w_m l_m^k\rangle \neq \sum_{m=1}^{M} \langle w_m\rangle \langle l_m\rangle^k \tag{113}$$

Thus the weights and abscissas for the average NDF cannot be found to be averaging those for the NDF in each environment. Due to the nonlinear relationship between the moments and weights and abscissas, this result is not surprising.[5] However, it does illustrate that $\langle w_m\rangle$ and $\langle l_m\rangle$ are not the relevant quantities needed to reconstruct $\langle m_k\rangle$.

B. Brownian and Shear-Induced Aggregation and Breakage

As mentioned above, when local nucleation rates are high, the local number density of particles will be large and aggregation will be favored. For very small particles (e.g., submicron), the dominant aggregation mechanism is Brownian motion (Einstein, 1905). Physically, the particles move by random walks driven by momentum exchange with solvent molecules. When two particles collide, they will stick together with a probability p_B to form a doublet. By this mechanism, larger clusters are eventually formed with a fractal dimension d_f (Meakin, 1988; Sorensen, 2001; Lattuada *et al.*, 2003a,b). If the volume fraction of particles is high enough, the clusters can reach "infinite" size in a finite time

[5] If we interpret the weights and abscissas as a delta-function representation of the NDF:

$$n_n(l) = \sum_{m=1}^{M} w_{mn}\delta(l - l_{mn})$$

then the average NDF is represented by $N+M$ delta functions:

$$\langle n(l)\rangle = \sum_{n=1}^{N}\sum_{m=1}^{M} p_n w_{mn}\delta(l - l_{mn})$$

By using the PD algorithm, this set of $N \times M$ delta functions is reduced to a set of only M delta functions, but with the same values for the first $2M$ moments $\langle m_k\rangle$ as the original set. It should be obvious that this cannot be accomplished by simply averaging the weights and abscissas.

span through a process called gelation (Sandkühler *et al.*, 2005). However, if the clusters are growing in a turbulent flow field, once their characteristic size is greater than approximately one micron other shear-driven processes become dominant (Oles, 1992). These are typically classified as shear-induced growth, breakage and restructuring. As in the case of chemical kinetics, aggregation and breakage models are required to describe these phenomena. From the perspective of developing CFD models, we can assume that such "kinetic expressions" are available. Thus, our focus here will be on how to implement the PBE in a CFD simulation to predict the moments of the PSD.

The simplest aggregation and breakage models can be formulated in terms of the NDF $n(\upsilon)$, which uses volume as the independent variable.[6] The microscopic transport equation for the NDF has the form (Wang *et al.*, 2005a,b)

$$\frac{\partial n}{\partial t} + \nabla \cdot (\mathbf{U}n) = \nabla \cdot (\Gamma_n \nabla n) + J(\upsilon, \mathbf{c}) - \frac{\partial}{\partial \upsilon}[G(\upsilon, \mathbf{c})n] + A(\upsilon) + B(\upsilon) \tag{114}$$

where $A(\upsilon)$ and $B(\upsilon)$ are the aggregation and breakage terms, respectively. Although we do not do so here, these terms can be assumed to be dependent on the species concentrations $\mathbf{c}$ without changing the form of the CFD model. For binary aggregation and breakage, the aggregation term can be expressed as follows (Ramkrishna, 2000):

$$A(\upsilon) = \frac{1}{2}\int_0^{\upsilon} \beta(\upsilon - s, s)n(\upsilon - s)n(s)\,\mathrm{d}s - n(\upsilon)\int_0^{\infty} \beta(\upsilon, s)n(s)\mathrm{d}s \tag{115}$$

where β is the aggregation kernel. A typical breakage term has the form

$$B(\upsilon) = \int_{\upsilon}^{\infty} b(\upsilon|s)a(s)n(s)\mathrm{d}s - a(\upsilon)n(\upsilon) \tag{116}$$

where b is the daughter-size distribution and a is the breakage kernel.

For Brownian aggregation, the aggregation kernel can be written as follows (Elimelech *et al.*, 1995; Sandkühler *et al.*, 2003):

$$\beta(\upsilon, s) = \frac{2p_{\mathrm{B}}k_{\mathrm{B}}T}{3\mu}\left(\upsilon^{1/d_{\mathrm{f}}} + s^{1/d_{\mathrm{f}}}\right)\left(\upsilon^{-1/d_{\mathrm{f}}} + s^{-1/d_{\mathrm{f}}}\right) \tag{117}$$

[6]It is also possible to use length as the independent variable as described in Wang *et al.* (2005b).

while for shear-induced aggregation it has the form (Oles, 1992; Elimelech *et al.*, 1995) as follows:

$$\beta(v,s) = \gamma\alpha(v,s)\left(v^{1/d_f} + s^{1/d_f}\right)^3 \tag{118}$$

A general expression can be found by combining these two cases (Melis *et al.*, 1999). In these expressions, k_B is the Boltzmann constant, T is the fluid temperature (Kelvin), μ is the fluid viscosity, γ is the local shear rate, and α is an efficiency factor. For shear-induced breakage, the kernel is usually fit to experimental data (Wang *et al.*, 2005a,b). A typical form is (Pandya and Spielman, 1983) as follows:

$$a(v) = c_1\gamma^{c_2}v^{c_3/d_f} \tag{119}$$

where $c_1 - c_3$ are empirical fitting parameters. A typical daughter-size distribution is

$$b(v|s) = \delta(v - fs) + \delta(v - (1-f)s) \tag{120}$$

where $f = 1/2$ corresponds to equal-size daughters and $f \ll 1$ corresponds to erosion (i.e., a very small and a very large daughter).

At this point, we should step back and make a few comments concerning Eq. (114). First, it should be obvious to the reader that many modeling assumptions have already been invoked to arrive at forms for the aggregation and breakage terms and the rate functions needed to define them. Therefore, we should keep in mind that, just as when working with chemical kinetics, the CFD predictions can be no better than the basic physical/chemical models used to describe the source terms. By their nature, aggregation and breakage terms are much more difficult to formulate accurately than gas-phase chemical mechanisms. Thus, we should expect a greater degree of mismatch with experimental data for CFD solutions for aggregation-breakage systems than we are accustomed to with, for example, combustion systems (Raman *et al.*, 2004). Due to the uncertainties in the "kinetics" for aggregation and (especially) breakage, the use of a highly sophisticated SGS model for turbulent mixing (e.g., transported PDF or CMC models) is likely unwarranted for most systems of interest. In fact, at present the greatest need in this domain is carefully designed experiments to accurately measure the rate constants appearing in the aggregation and breakage expressions.

A second general observation can be made by comparing the aggregation terms (Eq. 115) to the breakage terms (Eq. 116): The former is second order in $n(v)$ and the latter is first order. This implies that when $n(v)$ is very large (e.g., due to high local nucleation), aggregation will be favored. In fact, in shear-dominated systems gelation is prevented only by virtue of the fact that the aggregation efficiency α drops off rapidly for large clusters. Thus, in systems

with nucleation, growth, aggregation, and breakage (e.g., aggregating nanoparticles), the PSD can be nonzero over a very wide range of cluster volumes (i.e., 3–4 orders of magnitude is not uncommon). If sectional methods are used to approximate $n(v)$, such systems typically require a relatively large number of sections (e.g., 25–100) for reasonable accuracy (Marchisio *et al.*, 2003b). For this reason, when used in a CFD model, sectional methods require an unfavorable trade-off between reasonable computational cost and accuracy. Quadrature methods, which have lower cost for equivalent accuracy (Marchisio *et al.*, 2003b), are thus a better choice for combining with CFD to describe these complex systems.

A final observation concerns the shear rate γ appearing in both the aggregation and breakage kernels. Since from the outset we have assumed that the clusters are small compared to the Kolmogorov length scale, the local shear rate seen by a cluster is the instantaneous shear $(\varepsilon/v)^{1/2}$, where ε is the fluctuating dissipation rate (Fox, 2003). The fluctuating dissipation is very different than the average dissipation ε computed by the turbulence model (Fox and Yeung, 2003). On average $\langle\varepsilon\rangle = \varepsilon$, but $\varepsilon(t)$ fluctuates strongly on a characteristic time scale proportional to the Kolmogorov time scale τ_η. Whether these fluctuations must be accounted for in the CFD model depends on the characteristic aggregation time. Marchisio *et al.* (2006) estimate that when the local solid volume fraction exceeds 10^{-3}, the fluctuations must be included in the CFD model. Otherwise, γ can be set equal to $(\varepsilon/v)^{1/2}$. In any case, we see from this discussion that γ scales with the local turbulent Reynolds number like $\gamma \sim \mathrm{Re}_\mathrm{L}^{1/2}$. Thus, shear-induced aggregation and breakage will be important phenomena in turbulent flows and their importance will increase with increasing Reynolds number.

We now turn to the question of developing a CFD model for fine-particle production that includes nucleation, growth, aggregation, and breakage. Applying QMOM to Eq. (114) leads to a closed set of moment equations as follows:

$$\frac{\partial m_k}{\partial t} + \nabla \cdot (\mathbf{U} m_k) = \nabla \cdot (\Gamma \nabla m_k) + S_k(\boldsymbol{\phi}) \tag{121}$$

where the moment source term is given by (Marchisio *et al.*, 2003a)

$$S_k(\boldsymbol{\phi}) = \delta_{0,k} J(\mathbf{c}) + k \sum_{m=1}^{M} w_m v_m^{k-1} G(v_m, \mathbf{c}) + \sum_{m=1}^{M} w_m a(v_m)\left(b_m^{(k)} - v_m^k\right) + \frac{1}{2} \sum_{m=1}^{M} \sum_{p=1}^{M} w_m w_p \left[(v_m + v_p)^k - v_m^k - v_p^k\right] \beta(v_m, v_p) \tag{122}$$

and

$$b_m^{(k)} = \int_0^\infty v^k b(v|v_m) \mathrm{d}v \tag{123}$$

Thus, just as we saw with Eq. (109), the moment source term has the form found with detailed chemistry (i.e., the right-hand side of Eq. (122) depends only on $\boldsymbol{\phi}$).[7] The CFD transport equation can therefore be developed along the same lines that we discussed earlier for nucleation and growth. In other words, the DQMOM model can be used to describe micromixing of the moments of the PSD at the sub-grid scale, along with turbulent transport models to describe macromixing. One new factor that can arise when dealing with aggregation is that the moment source terms can be "stiff." To handle this problem in CFD simulations, Wang and Fox (2003) successfully implemented a tabulation method originally designed for combustion chemistry.

C. Multivariate Population Balances

The CFD model described above is adequate for particle clusters with a constant fractal dimension. In most systems with fluid flow, clusters exposed to shear will restructure without changing their mass (or volume). Typically restructuring will reduce the surface area of the cluster and the fractal dimension will grow toward $d_f = 3$, corresponding to a sphere. To describe restructuring, the NDF must be extended to (at least) two internal coordinates (Selomulya *et al.*, 2003; Zucca *et al.*, 2006). For example, the joint surface, volume NDF can be denoted by $n(s, \upsilon; \mathbf{x}, t)$ and obeys a bivariate PBE.

With two (or more) internal coordinates, numerical approaches for the PBE using sectional methods become intractable in the context of CFD. A practical alternative is to use a finite number of samples to approximate the NDF in terms of delta functions as follows:

$$n(s,\upsilon) = \sum_{m=1}^{M} w_m \delta(s - s_m)\delta(\upsilon - \upsilon_m) \tag{124}$$

The weights w_m and abscissas s_m and υ_m are related to the bivariate moments by

$$m_{k_1 k_2} = \iint s^{k_1}\upsilon^{k_2} n(s,\upsilon)\mathrm{d}s\mathrm{d}\upsilon = \sum_{m=1}^{M} w_m s_m^{k_1}\upsilon_m^{k_2} \tag{125}$$

Thus, it would be natural to attempt to extend the QMOM approach to handle a bivariate NDF. Unfortunately, the PD algorithm needed to solve the weights and abscissas given the moments cannot be extended to more than one variable. Other methods for inverting Eq. (125) such as nonlinear equation solvers can be used (Wright *et al.*, 2001; Rosner and Pykkonen, 2002), but in practice are computationally expensive and can suffer from problems due to ill-conditioning.

[7]There are, however, important differences. For example, in detailed chemistry the source terms do not depend on the flow quantities. In contrast, all of the rate functions for particulate systems can potentially depend on the local flow quantities such as the instantaneous shear rate.

To overcome the difficulty of inverting the moment equations, Marchisio and Fox (2005) introduced the direct quadrature method of moments (DQMOM). With this approach, transport equations are derived for the weights and abscissas directly, thereby avoiding the need to invert the moment equations during the course of the CFD simulation. As shown in Marchisio and Fox (2005), the NDF for one variable with moment equations given by Eq. (121) yields two microscopic transport equations of the form

$$\frac{\partial w_m}{\partial t} + \boldsymbol{\nabla} \cdot (\mathbf{U} w_m) = \boldsymbol{\nabla} \cdot (\Gamma \boldsymbol{\nabla} w_m) + a_m + a_m^* \tag{126}$$

and

$$\frac{\partial w_m \upsilon_m}{\partial t} + \boldsymbol{\nabla} \cdot (\mathbf{U} w_m \upsilon_m) = \boldsymbol{\nabla} \cdot (\Gamma \boldsymbol{\nabla} w_m \upsilon_m) + b_m + b_m^* \tag{127}$$

where the source terms a_m and b_m are found from the moment source terms S_k, and a_m^* and b_m^* are "correction" terms that depend on $\Gamma |\nabla \upsilon_m|^2$. The role of the correction terms is to ensure that Eqs. (126) and (127) are mathematically equivalent to Eq. (121), and they result from the diffusion terms during the nonlinear change of variables (Eq. 107). Thus, they will be null in the absence of molecular diffusion and their forms do not depend on the moment source terms.

The extension of DQMOM to bivariate systems is straightforward and, for the surface, volume NDF, simply adds another microscopic transport equation as follows:

$$\frac{\partial w_m s_m}{\partial t} + \boldsymbol{\nabla} \cdot (\mathbf{U} w_m s_m) = \boldsymbol{\nabla} \cdot (\Gamma \boldsymbol{\nabla} w_m s_m) + c_m + c_m^* \tag{128}$$

Example calculations for a bivariate system can be found in Marchisio and Fox (2006) and Zucca *et al.* (2006). We should note that for multivariate systems the choice of the moments used to compute the source terms is more problematic than in the univariate case. For example, in the bivariate case a total of $3M$ moments must be chosen to determine a_m, b_m and c_m. In most applications, acceptable accuracy can be obtained with $3 \leq M \leq 5$. Thus, the maximum number of moments that will be required is 15, and one might decide to use bivariate moments up to order four as shown below:

$m_{0,0}$,
$m_{1,0}$, $m_{0,1}$,
$m_{2,0}$, $m_{1,1}$, $m_{0,2}$,
$m_{3,0}$, $m_{2,1}$, $m_{1,2}$, $m_{0,3}$,
$m_{4,0}$, $m_{3,1}$, $m_{2,2}$, $m_{1,3}$, $m_{0,4}$.

However, there is no guarantee that this set of moments will be linearly independent. Even if they do work, we can note that compared to the univariate case where the ten moments m_0–m_9 would be employed, the accuracy (as measured

by the highest-order moment used) decreases as the number of internal coordinates increases. Thus, the only way to obtain equivalent accuracy would be to increase M.

Leaving aside the question of determining which moments to use, we also need a consistent method for deriving a CFD transport equation for turbulent reacting flows from the microscopic transport equations for the weights and abscissas. In particular, since the moments have a nonlinear dependence on the weights and abscissas, the definition of the micromixing model in terms of the weights and abscissas must be consistent with that used for the moments.[8] The development of a consistent model is most easily done by proceeding in three independent steps as follows:

1. Find the multi-environment model for the case where the moment source terms are null and there is no micromixing: $a_m = a_m^* = b_m = b_m^* = c_m = c_m^* = 0$.
2. Extend the model to include micromixing, but no moment source terms: $a_m = b_m = c_m = 0$.
3. Extend the model to include the moment source terms due to nucleation, growth, etc.

We will now briefly illustrate how these steps are carried out.

The multi-environment model for turbulent transport of the bi-variate moments in the absence of moment source terms has the form

$$\frac{\partial p_n}{\partial t} + \boldsymbol{\nabla} \cdot (\mathbf{U} p_n) = \boldsymbol{\nabla} \cdot (\Gamma_{\mathrm{T}} \boldsymbol{\nabla} p_n) \tag{129}$$

and, for arbitrary values of k_1 and k_2

$$\frac{\partial p_n m_{k_1 k_2 n}}{\partial t} + \boldsymbol{\nabla} \cdot (\mathbf{U} p_n m_{k_1 k_2 n}) = \boldsymbol{\nabla} \cdot (\Gamma_{\mathrm{T}} \boldsymbol{\nabla} p_n m_{k_1 k_2 n}) + b^*_{k_1 k_2 n} \tag{130}$$

where the bi-variate moments in environment n are given in terms of the weights and abscissas by

$$m_{k_1 k_2 n} = \sum_{m=1}^{M} w_{mn} v_{mn}^{k_1} s_{mn}^{k_2} \tag{131}$$

As discussed earlier with other transported scalars, the correction term appearing on the right-hand side of Eqs. (130) is found by solving a linear system defined by

$$\sum_{n=1}^{N} m_{k_1 k_2 n}^{k-1} b^*_{k_1 k_2 n} = \sum_{n=1}^{N} (k-1) p_n m_{k_1 k_2 n}^{k-2} \Gamma_{\mathrm{T}} \left| \boldsymbol{\nabla} m_{k_1 k_2 n} \right|^2 \quad \text{for } k = 1, \ldots, N \tag{132}$$

[8] We develop the CFD equations using the DQMOM model for micromixing. Nevertheless, care must also be taken when using other micromixing models, including transported PDF methods.

Note that in this expression k is unrelated to k_1 and k_2, which are determined by the choice of moment $m_{k_1k_2n}$. Equation (132) defines the correction term $b^*_{k_1k_2n}$ for a fixed set of indices (k_1, k_2, n). In other words, given the weights and abscissas we can use Eq. (131) to compute the bi-variate moments, which can then be used in Eq. (132) to solve for $b^*_{k_1k_2n}$.

The multi-environment model for the weights and abscissas has the form

$$\frac{\partial p_n w_{mn}}{\partial t} + \boldsymbol{\nabla} \cdot (\mathbf{U} p_n w_{mn}) = \boldsymbol{\nabla} \cdot (\Gamma_{\mathrm{T}} \boldsymbol{\nabla} p_n w_{mn}) + A_{mn} + A^*_{mn} \tag{133}$$

$$\frac{\partial p_n w_{mn} \upsilon_{mn}}{\partial t} + \boldsymbol{\nabla} \cdot (\mathbf{U} p_n w_{mn} \upsilon_{mn}) = \boldsymbol{\nabla} \cdot (\Gamma_{\mathrm{T}} \boldsymbol{\nabla} p_n w_{mn} \upsilon_{mn}) + B_{mn} + B^*_{mn} \tag{134}$$

and

$$\frac{\partial p_n w_{mn} s_{mn}}{\partial t} + \boldsymbol{\nabla} \cdot (\mathbf{U} p_n w_{mn} s_{mn}) = \boldsymbol{\nabla} \cdot (\Gamma_{\mathrm{T}} \boldsymbol{\nabla} p_n w_{mn} s_{mn}) + C_{mn} + C^*_{mn} \tag{135}$$

where the final two terms on the right-hand sides are null in the absence of micromixing and moment source terms. The correction terms A^*_{mn}, B^*_{mn} and C^*_{mn} are determined such that they are equivalent to the correction term $b^*_{k_1k_2n}$ in Eq. (130). In other words, if we use Eq. (131) to replace $m_{k_1k_2n}$ in Eq. (130), then Eqs. (133)–(135) will be equivalent to Eq. (130) when the correction terms satisfy the following linear system:

$$\begin{aligned}
&(1 - k_1 - k_2) \sum_{m=1}^{M} \upsilon_{mn}^{k_1} s_{mn}^{k_2} A^*_{mn} + k_1 \sum_{m=1}^{M} \upsilon_{mn}^{k_1 - 1} s_{mn}^{k_2} B^*_{mn} + k_2 \sum_{m=1}^{M} \upsilon_{mn}^{k_1} s_{mn}^{k_2 - 1} C^*_{mn} \\
&= b^*_{k_1k_2n} + k_1(k_1 - 1) p_n \sum_{m=1}^{M} w_{mn} \upsilon_{mn}^{k_1 - 2} s_{mn}^{k_2} \Gamma_{\mathrm{T}} |\boldsymbol{\nabla} \upsilon_{mn}|^2 \\
&+ k_1 k_2 p_n \sum_{m=1}^{M} w_{mn} \upsilon_{mn}^{k_1 - 1} s_{mn}^{k_2 - 1} \Gamma_{\mathrm{T}} (\boldsymbol{\nabla} \upsilon_{mn} \cdot \boldsymbol{\nabla} s_{mn})^2 \\
&+ k_2(k_2 - 1) p_n \sum_{m=1}^{M} w_{mn} \upsilon_{mn}^{k_1} s_{mn}^{k_2 - 2} \Gamma_{\mathrm{T}} |\boldsymbol{\nabla} s_{mn}|^2
\end{aligned} \tag{136}$$

Note that the correction terms are proportional to Γ_{T} and result from turbulent velocity fluctuations (represented by a gradient-diffusion model). For the multi-environment model the composition vector is defined by

$$\boldsymbol{\phi} = [w_1, \ldots, w_M,\ w_1 \upsilon_1, \ldots, w_M \upsilon_M,\ w_1 s_1, \ldots, w_M s_M]^{\mathrm{T}}$$

Thus, a total of $3M$ variables are needed to describe the evolution of the bi-variate NDF in a turbulent flow. The first step in the construction of the CFD model is now complete.

In the second step we must add the micromixing terms from the DQMOM model to Eqs. (133)–(135). However, as we discussed earlier, we need to keep in mind that micromixing conserves the moments of the NDF, and not the weights and abscissas (see Eq. 113). The micromixing model in environment n for the bi-variate moments has the form

$$M_{k_1k_2n} = \gamma\left(\langle m_{k_1k_2}\rangle - m_{k_1k_2n}\right) \tag{137}$$

where the moments in environment n are given by Eq. (131) and the average moments are found by averaging over all N environments:

$$\langle m_{k_1k_2}\rangle = \sum_{n=1}^{N} p_n m_{k_1k_2n} \tag{138}$$

Thus, given the weights and abscissas, the micromixing term for the moments is closed. Applying DQMOM, the micromixing source terms (which are added to the right-hand sides of Eqs. (133)–(135)) can be shown to obey for each $n = 1,\ldots, N$ the linear system defined by

$$(1-k_1-k_2)\sum_{m=1}^{M} v_{mn}^{k_1} s_{mn}^{k_2} A_{mn} + k_1 \sum_{m=1}^{M} v_{mn}^{k_1-1} s_{mn}^{k_2} B_{mn} + k_2 \sum_{m=1}^{M} v_{mn}^{k_1} s_{mn}^{k_2-1} C_{mn} = p_n M_{k_1k_2n} \tag{139}$$

Note that the right-hand side of this expression contains the closed micromixing term for the moments (Eq. 137). To find the $3M$ micromixing source terms (A_{mn}, B_{mn}, C_{mn}) from this expression, we must choose a set of $3M$ bi-variate moments. Note that because the moment equations are closed when only micromixing is considered, the chosen moments will be reproduced exactly. A convenient choice is to use the uncoupled moments m_{k0} and m_{0k}. (Note that this same choice should then be used in Eq. (136).) This yields the linear system

$$(1-k)\sum_{m=1}^{M} v_{mn}^{k} A_{mn} + k \sum_{m=1}^{M} v_{mn}^{k-1} B_{mn} = p_n M_{k0n} \quad \text{for } k = 0,\ldots,2M-1 \tag{140}$$

which can be solved to find A_{mn} and B_{mn} for each $n = 1,\ldots, N$, and the linear system

$$k\sum_{m=1}^{M} s_{mn}^{k-1} C_{mn} = p_n M_{0kn} + (k-1)\sum_{m=1}^{M} s_{mn}^{k} A_{mn} \quad \text{for } k = 1,\ldots,M \tag{141}$$

which can be solved to find C_{mn}. The second step in the construction of the CFD model is now complete.

The third step is to add the moment source terms due to nucleation, growth, aggregation, and restructuring. The exact form of these terms will depend on the models used to describe these processes (see for example Eq. 122). However, if we denote the source term for the bi-variate moments as $S_{k_1k_2}(\boldsymbol{\phi})$, where $\boldsymbol{\phi}$ is the composition vector including all variables needed to describe the kinetics, then the source terms (including micromixing) in the CFD model (A_{mn}, B_{mn}, C_{mn}) can be found by simply adding $p_n S_{k_1k_2}(\boldsymbol{\phi}_n)$ to the right-hand side of Eq. (139). The extension of DQMOM to multi-variate systems with more than two internal coordinates is discussed in Marchisio and Fox (2005). As far as the CFD model equations are concerned, no additional complications arise for higher-dimensional systems. Nevertheless, from a practical point of view the reader should keep in mind that going to higher dimensions will necessarily diminish the accuracy of the method as compared to the uni-variate case.

We end here with our discussion of CFD models for fine-particle production. The reader hopefully has a good feel for the issues involved and at least a cursory understanding of the available models. The current status of the field is such that the CFD tools available for the analysis of fine-particle systems are adequate for most applications. Currently, the weakest link in the modeling process is description of physical processes such as aggregation and breakage, and their coupling to the flow field. As mentioned earlier, there is a need for carefully designed experiments with *local* measurements of the PSD and turbulence fields that can be used for CFD validation. As in the field of turbulent mixing, the ideal experiment would be spatially homogeneous, or a most one-dimensional, to focus on the source terms for the chemical reactions and the moments. It would also be useful to conduct a few "idealized experiments" using direct numerical simulations (DNS) for homogeneous fine-particle systems undergoing nucleation, growth, aggregation, and breakage. Although such "experiments" cannot be directly compared to real systems, they would still be useful for calibrating CFD models used for micromixing and shear-induced aggregation and breakage.

V. Multiphase Reacting Systems

The CFD models considered up to this point are, as far as the momentum equation is concerned, designed for single-phase flows. In practice, many of the chemical reactors used in industry are truly multiphase, and must be described in the context of CFD by multiple momentum equations. There are, in fact, several levels of description that might be attempted. At the most detailed level, direct numerical simulation of the transport equations for all phases with fully resolved interfaces between phases is possible for only the simplest systems. For

example, for fluid-particle systems the Navier–Stokes equation must be solved for the fluid phase between the particles with enough detail to capture momentum transport at the particle surfaces (Nguyen and Ladd, 2005). At the same time, Newtonian equations for the particle positions and momenta must be solved simultaneously to account for fluid surface forces and particle–particle collisions. Obviously, such a detailed model could not be used to describe a large chemical reactor such as a fluidized bed. Less costly methods have thus been developed and are described in other chapters of this issue. In general, the methods available in commercial CFD codes are based on the so-called "multifluid" model (Drew and Passman, 1999) that makes no attempt to capture the details at the interfaces between phases. Instead, the fluid at the subgrid scale is described by the volume or mass fractions for each phase much in the same way that environments are used to describe micromixing in single-phase flows). We will thus look briefly at the structure of multifluid models and describe some of the modeling assumptions that are required for multiphase reacting flows.

A. Multifluid CFD Models

In this section, we will look briefly at multifluid CFD models. Our primary objective is to understand the modeling issues that arise and how they are dealt with in CFD codes. To fix ideas, we will look at a gas–solid system (e.g., a fluidized bed) wherein the solid particles undergo growth, aggregation, and breakage. Unlike in Section IV, we will assume here that the particle Stokes number (St) can be larger than 0.14. Thus, it will be necessary to account for particle momentum separately from the gas phase (or at least to account for the effect of the second phase in the momentum balance). Nevertheless, the particle size distribution (PSD) can be accounted for using DQMOM (Fan *et al.*, 2004). For simplicity, we will assume that the particle density ρ_s is constant and independent of particle size, and that the gas density ρ_g is constant. At the subgrid scale, the two phases are described by the volume fractions α_g and α_s for the gas and solid phases, respectively. By definition, $\alpha_g + \alpha_s = 1$. In addition, the DQMOM representation of the solid phase will introduce a volume fraction for each abscissa α_{sm} for $m = 1, \ldots, M$. By definition, $\alpha_{\mathrm{s}1} + \cdots + \alpha_{\mathrm{s}M} = \alpha_\mathrm{s}$. (See Fan *et al.* (2004) for details.)

The multifluid CFD model at its most basic level consists of mass and momentum balances for each "phase." For the present example, the mass balance for the gas phase can be written as follows:

$$\frac{\partial \rho_\mathrm{g} \alpha_\mathrm{g}}{\partial t} + \boldsymbol{\nabla} \cdot (\rho_\mathrm{g} \alpha_\mathrm{g} \mathbf{U}_\mathrm{g}) = -\sum_{m=1}^{M} M_{\mathrm{g}m} \tag{142}$$

where M_{gm} is the mass-transfer rate from the gas to the solid phases. As we will discuss later (Section V.B), a model must be provided to close the mass-transfer

term. In words, $\rho_g\alpha_g$ is the mass of gas per unit volume of the multiphase mixture (i.e., gas and solid phases), whereas ρ_g is the mass of gas per unit volume of gas. The gas velocity $\mathbf{U}_g$ appears in the convection term for the gas phase, and is normally not equal to the solids velocities.

The mass balance for the solid phases ($m+1,\ldots, M$) can be written as follows:

$$\frac{\partial \rho_s \alpha_{sm}}{\partial t} + \nabla \cdot (\rho_s \alpha_{sm} \mathbf{U}_{sm}) = M_{gm} + 3k_v \rho_s l_m^2 b_m - 2k_v \rho_s a_m \tag{143}$$

The solid velocities $\mathbf{U}_{sm}$ (one for each abscissa l_m) appear in the convection term. The source terms a_m and b_m are found from the DQMOM representation of aggregation and breakage of the solid particles (Fan *et al.*, 2004). Each particle phase is represented by its volume fraction (instead of its weight w_m) and its characteristic length l_m. Note that growth of solid particles (with constant density ρ_s) requires mass transfer from the gas phase, represented by M_{gm}. In the absence of growth the total solids volume fraction α_s does not change. Thus, the aggregation and breakage terms will cancel as follows:

$$\sum_{m=1}^{M} \left(3l_m^2 b_m - 2a_m\right) = 0 \tag{144}$$

This property will result from applying DQMOM to the aggregation and breakage terms in the PBE (Fan *et al.*, 2004).

While the mass balances given above are relatively straightforward (assuming that a suitable closure can be derived for the mass-transfer terms), the momentum balances are significantly more complicated. In their simplest forms, they can be written as follows:

$$\frac{\partial \rho_g \alpha_g \mathbf{U}_g}{\partial t} + \nabla \cdot (\rho_g \alpha_g \mathbf{U}_g \mathbf{U}_g) = -\alpha_g \nabla p + \nabla \cdot \boldsymbol{\sigma}_g + \sum_{m=1}^{M} \mathbf{f}_{gm} + \rho_g \alpha_g \mathbf{g} \tag{145}$$

and

$$\frac{\partial \rho_s \alpha_{sm} \mathbf{U}_{sm}}{\partial t} + \nabla \cdot (\rho_s \alpha_{sm} \mathbf{U}_{sm} \mathbf{U}_{sm}) = -\alpha_{sm} \nabla p + \nabla \cdot \boldsymbol{\sigma}_{sm} - \mathbf{f}_{gm} + \sum_{n=1}^{M} \mathbf{f}_{smn} + \rho_s \alpha_{sm} \mathbf{g} \tag{146}$$

for the gas and solid phases, respectively. The two terms of the left-hand sides of the momentum balances correspond to accumulation and convection. Note that the conserved quantities (for example $\rho_g \alpha_g \mathbf{U}_g$) are the momentum of a given phase per unit volume of the mixture (hence the appearance of α_g, etc.), and that

each phase has its own characteristic convection velocity (e.g., $\mathbf{U}_g$). The terms on the left-hand side of Eqs. (145) and (146) account for changes in momentum of each phase. Obviously, since momentum is exchanged between phases at the interfaces and we are not resolving the interfaces, such phase-interaction terms will require models. In contrast, body forces (i.e., gravity $\mathbf{g}$ in this example) appear in closed form.

The first term on the right-hand side of Eqs. (145) and (146) is a pressure term shared by both phases. The purpose of this term (when ρ_s and ρ_g are constant) is to ensure that the volume-average velocity, defined by

$$\mathbf{U}_{\text{vol}} = \alpha_{\text{g}}\mathbf{U}_{\text{g}} + \sum_{m=1}^{M} \alpha_{sm}\mathbf{U}_{sm} \tag{147}$$

is solenoidal in the absence of mass transfer. Indeed, dividing the mass balances (Eqs. 142 and 143) by the densities and neglecting the mass-transfer terms lead to

$$\boldsymbol{\nabla} \cdot \mathbf{U}_{\text{vol}} = 0 \tag{148}$$

Thus, just as for incompressible single-phase flow, the pressure p constrains the velocity fields to ensure (in the case of multiphase flows) that the sum of the phase volume fractions equals unity. In the presence of mass transfer, the right-hand side of Eq. (148) is nonzero; nevertheless, the role of the pressure is still the same. Finally, we should note that in gas–solid flows the maximum volume fraction of the solid phase is less than unity due to physical constraints (i.e., when particles are close packed there is still room for the gas phase so that $0 < \alpha_{\text{g}}$). To accommodate this constraint, it is common to introduce a "solid-pressure" term p_{s} that becomes extremely large when α_{g} approaches its minimum value (e.g., $\alpha_g^* = 0.4$).

The second term on the right-hand side of Eqs. (145) and (146) contains the viscous-stress models σ_g and σ_{sm}. Even for laminar flow, suitable forms for these models are difficult to determine a priori. Typical models used in CFD introduce an effective viscosity μ_{eff} for each phase, and describe the viscous stresses as follows.

$$\boldsymbol{\sigma}_x = \mu_{\text{eff},x}\left[\nabla\mathbf{U}_x + (\nabla\mathbf{U}_x)^{\text{T}}\right] \quad x = \text{g},\ sm \tag{149}$$

Leaving aside the difficult question of whether this model holds for multiphase flows, we still have the problem of determining $\mu_{\text{eff},x}$ in terms of the computed properties of the flow. The reader should appreciate that choosing an effective viscosity for a multiphase flow is much more complicated than just adding a turbulence model as done in single-phase turbulent flows. Indeed, even for a case involving two fluids (e.g., two immiscible liquids) for which the molecular viscosities are constant, the choice of the effective viscosities is not obvious. For example, even if the mass-average velocity defined by

$$\mathbf{U}_{\text{mass}} = \frac{\rho_{\text{g}}\alpha_{\text{g}}\mathbf{U}_{\text{g}} + \sum_{m=1}^{M}\rho_{\text{s}}\alpha_{sm}\mathbf{U}_{sm}}{\rho_{\text{g}}\alpha_{\text{g}} + \rho_{\text{s}}\alpha_{\text{s}}} \tag{150}$$

were laminar, the flow around individual particles could be turbulent (as measured by the particle Reynolds number defined below) and the effective viscosity should reflect this fact. The simplest models account for "particle-scale" turbulence using an expression of the form

$$\mu_{\text{eff,g}} = \mu_{\text{g}}(1 + C_{\text{s}}\alpha_{\text{s}}\text{Re}_{\text{s}}) \tag{151}$$

where μ_{g} is the molecular viscosity of the gas phase and Re_{s} is a particle Reynolds number defined by

$$\text{Re}_{\text{s}} = \frac{\rho_{\text{g}} d_{\text{s}} \, |\mathbf{U}_{\text{s}} - \mathbf{U}_{\text{g}}|}{\mu_{\text{g}}} \tag{152}$$

and d_{s} is the characteristic diameter of the particles. The model constant C_s is order unity, but must be fit to experimental data. The effective viscosity in Eq. (151) has the desired behavior in the limits where α_{s} or Re_{s} are very small; however, it is unlikely to be accurate when the product of these terms is large.

The situation for cases where $\mathbf{U}_{\text{mass}}$ is also turbulent is even more complicated. First, such "large-scale" turbulence can be due to a variety of physical phenomena, and thus have different characteristics. For example, large-scale turbulence can (as in single-phase flows) be introduced through the boundary conditions (e.g., turbulent jets) or by using mixing devices (e.g., stirred tanks). For such cases, it may be possible to make suitable modifications to single-phase turbulence models to arrive at useful expressions for the effective viscosity. In contrast, large-scale turbulence that arises due to internal properties of a multiphase flow (e.g., density differences between phases) is more difficult to describe by simple modifications of standard turbulence models.

Second, due to the difficulty of accessing multiphase flows with laser-based flow diagnostics, there is very little experimental data available for validating multiphase turbulence models to the same degree as done in single-phase turbulent flows. For example, thanks to detailed experimental measurements of turbulence statistics, there are many cases for which the single-phase k-$\boldsymbol{\varepsilon}$ model is known to yield poor predictions. Nevertheless, in many CFD codes a multiphase k-ε model is used to supply multiphase turbulence statistics that cannot be measured experimentally. Thus, even if a particular multiphase turbulent flow could be adequately described using an effective viscosity, in most cases it is impossible to know whether the multiphase turbulence model predicts reasonable values for μ_{eff}.

Third, many of the multiphase flows of interest to chemical engineers are in regimes where both particle-scale and large-scale turbulence are significant. For example, in gas–liquid bubble columns the particle Reynolds number (based on the bubble rise velocity) is typically large. Thus, even for low gas-flow rates, particle-scale turbulence will be significant. However, at low gas-flow rates and with uniform sparging, a bubble column will have no large-scale turbulence (i.e., the flow regime will be "homogeneous") (Garnier *et al.*, 2002; Harteveld *et al.*, 2003), and thus only the effective viscosity of individual "particles" should be

included in the model. As the gas flow rate is increased to a critical value of the gas holdup (which can be as high as $\alpha_g = 0.55$ (Mudde, 2005)), the flow will become unstable and large-scale turbulence will be generated. Although it has been attempted in the literature (Thorat and Joshi, 2004), it is unlikely that a two-fluid k-ε turbulence model has the necessary mathematical structure to correctly predict flow transitions or even the "turbulence" levels observed in homogeneous bubbly flows. In contrast, a two-fluid model using only a "particle-scale" effective viscosity and appropriate force models can predict flow transitions (Monahan *et al.*, 2005) in reasonable agreement with experiments (Harteveld *et al.*, 2003). Nevertheless, it is likely that different CFD models will be required for different flow regimes (e.g., homogeneous vs. churn turbulent) and the user must be careful not to extend a particular model beyond its range of applicability.

Returning to the momentum equations, the third term on the right-hand side of Eqs. (145) and (146) contains the gas–solid momentum-exchange models $\mathbf{f}_{gm}$. Likewise, the fourth term on the right-hand side of Eqs. (146) contains the solid–solid momentum-exchange model $\mathbf{f}_{smn}$. Note that because solid–solid interactions conserve momentum, the latter must be defined such that

$$\sum_{m=1}^{M}\sum_{n=1}^{M}\mathbf{f}_{smn} = 0 \tag{153}$$

Determination of accurate models for $\mathbf{f}_{gm}$ and $\mathbf{f}_{smn}$ is nontrivial (Drew and Passman, 1999), and no consensus exists on the exact forms needed to describe particular flows. Nevertheless, it is generally acknowledged that the momentum-exchange model must include "drag" terms with forms similar to

$$\mathbf{f}_{gm} = \alpha_g \alpha_{sm} C_D(\mathrm{Re}_s)\frac{3\mu_g Re_s}{4d_s^2}(\mathbf{U}_{sm} - \mathbf{U}_g) \tag{154}$$

where $C_D(\mathrm{Re}_s)$ is a drag coefficient, and

$$\mathbf{f}_{smn} = \alpha_{sm}\alpha_{sn}C_{mn}\,(\mathbf{U}_{sn} - \mathbf{U}_{sm}) \tag{155}$$

where C_{mn} depends on the properties of the solid phases (Gao *et al.*, 2006). Note that the drag models depend on the velocity difference between two phases, and thus can be nonzero even for cases where the velocity fields are uniform in time and space. Other forces that can be included depend on gradients (temporal or spatial) of the velocities or volume fractions (Drew and Passman, 1999), and thus are only significant for inhomogeneous flows. However, as can be shown using linear stability analysis (Batchelor, 1988; Lammers and Biesheuvel, 1996; Minev *et al.*, 1999; Jackson, 2000; Johri and Glasser, 2002; Sankaranarayanan and Sundaresan, 2002), spatially uniform solutions to the multifluid model are usually unstable, implying that the stationary, homogeneous solution to the multifluid model is not representative of the flow. Thus, even when simulating "homogeneous" flows, it is important to include all relevant forces when

comparing numerical simulations with experiments (Monahan *et al.*, 2005). Moreover, the computational requirements in terms of gird size needed to attain grid-independent solutions are relatively high for the "laminar" two-fluid model (Monahan *et al.*, 2005). In the context of modeling chemical reactors, it will be necessary to develop CFD models for the unresolved scales when applying multifluid models to real reactors. Although procedures for developing such models are still being actively investigated and no clear consensus has yet to emerge (Sundaresan, 2000), here we will limit ourselves to a brief discussion of the relevant issues.

To simplify the presentation, let us consider the transport equation for $\boldsymbol{U}_{\text{mass}}$ found by summing together Eqs. (145) and (146):

$$\frac{\partial \hat{\rho}\mathbf{U}_{\text{mass}}}{\partial t} + \boldsymbol{\nabla}\cdot(\hat{\rho}\mathbf{U}_{\text{mass}}\mathbf{U}_{\text{mass}}) + \boldsymbol{\nabla}\cdot(\hat{\rho}\widehat{\mathbf{u}_{\text{d}}\mathbf{u}_{\text{d}}}) = -\boldsymbol{\nabla}p + \boldsymbol{\nabla}\cdot\hat{\boldsymbol{\sigma}} + \hat{\rho}\mathbf{g} \tag{156}$$

where the phase-average density, defined by $\hat{\rho} = \rho_{\text{g}}\alpha_{\text{g}} + \rho_{\text{s}}\alpha_{\text{s}}$, obeys

$$\frac{\partial \hat{\rho}}{\partial t} + \boldsymbol{\nabla}\cdot(\hat{\rho}\mathbf{U}_{\text{mass}}) = 0 \tag{157}$$

Note that these expressions (Eqs. 156 and 157) appear deceptively simple (i.e., as if the problem can be reduced to modeling a variable-density, single-phase flow) because we have hidden the "difficult" terms in the definition of some new symbols! First, the phase-average stress $\boldsymbol{\sigma}$ is defined by

$$\hat{\boldsymbol{\sigma}} = \boldsymbol{\sigma}_{\text{g}} + \sum_{m=1}^{M} \boldsymbol{\sigma}_{\text{s}m} \tag{158}$$

and (based on the model in Eq. (149)) it is not a simple function of $\boldsymbol{U}_{\text{mass}}$. Second, a new "multiphase" stress term $\widehat{\mathbf{u}_{\text{d}}\mathbf{u}_{\text{d}}}$ has be introduced and is defined by

$$\hat{\rho}\widehat{\mathbf{u}_{\text{d}}\mathbf{u}_{\text{d}}} = \rho_{\text{g}}\alpha_{\text{g}}\mathbf{u}_{\text{g}}\mathbf{u}_{\text{g}} + \rho_{\text{s}m}\alpha_{\text{s}m}\sum_{m=1}^{M}\mathbf{u}_{\text{s}m}\mathbf{u}_{\text{s}m} \tag{159}$$

where $\mathbf{u}_{\text{g}} = \mathbf{U}_{\text{g}} - \mathbf{U}_{\text{mass}}$ and $\mathbf{u}_{\text{s}m} = \mathbf{U}_{\text{s}m} - \mathbf{U}_{\text{mass}}$ are the differences between the phase velocities and the mass-average velocity. We can note that for a constant-density, two-phase system with $\rho_{\text{g}} \neq \rho_{\text{s}}$, $\mathbf{U}_{\text{g}}$ and $\mathbf{U}_{\text{s}}$ are related to $\mathbf{U}_{\text{mass}}$ and $\mathbf{U}_{\text{vol}}$ by

$$\begin{aligned}
\mathbf{U}_{\text{g}} &= \frac{\rho_{\text{s}}}{\alpha_{\text{g}}(\rho_{\text{s}} - \rho_{\text{g}})}\mathbf{U}_{\text{vol}} - \frac{\hat{\rho}}{\alpha_{\text{g}}(\rho_{\text{s}} - \rho_{\text{g}})}\mathbf{U}_{\text{mass}} \\
\mathbf{U}_{\text{s}} &= \frac{\rho_{\text{g}}}{\alpha_{\text{s}}(\rho_{\text{s}} - \rho_{\text{g}})}\mathbf{U}_{\text{vol}} + \frac{\hat{\rho}}{\alpha_{\text{s}}(\rho_{\text{s}} - \rho_{\text{g}})}\mathbf{U}_{\text{mass}}
\end{aligned} \tag{160}$$

Thus the two-fluid model can be formulated in terms of any two velocities chosen from the set $\mathbf{U}_{\text{g}}$, $\mathbf{U}_{\text{s}}$, $\mathbf{U}_{\text{mass}}$ and $\mathbf{U}_{\text{vol}}$, which might be useful, for example, to

examine the limiting case where $\rho_g \ll \rho_s$. The closures for shear stresses $\hat{\boldsymbol{\sigma}}$ and convection due to differences in the phase velocities $\widehat{\mathbf{u}_d\mathbf{u}_d}$ in Eq. (156) are necessarily flow dependent. Nevertheless, the simplest closures might use Eq. (149) with $\mathbf{U}_{mass}$ and an effective viscosity depending on $\hat{\rho}$ and assume that the slip velocity between phases $\mathbf{u}_d$ is a known constant (e.g., depending on density difference and bubble size). We should also note that it is possible to write the model in terms of the volume-average velocity $\mathbf{U}_{vol}$ (Eq. 147). However, the resulting expressions are more complicated than Eqs. (156) and (157).

Up to this point we have not introduced any modeling concepts to deal with "large-scale" turbulence. However, if the Reynolds number corresponding to Eq. (156) is large enough, the velocity field $\mathbf{U}_{mass}$ will become turbulent. In this case, the computational resources needed to resolve all of the relevant flow scales will increase drastically, and the multifluid CFD model will no longer be tractable for analyzing chemical reactors. To deal with this difficulty, we can introduce a multiphase turbulence model based on Reynolds averaging Eq. (156). Because $\hat{\rho}$ is not constant, we will in fact use the Favre average. For example, if the Reynolds-average velocity is denoted by $\langle \mathbf{U}_{mass} \rangle$, then the Favre-average velocity is defined by

$$\widetilde{\mathbf{U}}_{mass} = \frac{\langle \hat{\rho}\mathbf{U}_{mass} \rangle}{\langle \hat{\rho} \rangle} \tag{161}$$

Note that we have also introduced the Reynolds-average, phase-average density $\langle \hat{\rho} \rangle$. Applying the Favre average to Eq. (157) yields a closed expression for the mass balance as follows:

$$\frac{\partial \langle \hat{\rho} \rangle}{\partial t} + \boldsymbol{\nabla} \cdot (\langle \hat{\rho} \rangle \, \widetilde{\mathbf{U}}_{mass}) = 0 \tag{162}$$

Applying the same process to Eq. (156) yields

$$\frac{\partial \langle \hat{\rho} \rangle \widetilde{\mathbf{U}}_{mass}}{\partial t} + \boldsymbol{\nabla} \cdot (\langle \hat{\rho} \rangle \widetilde{\mathbf{U}}_{mass} \widetilde{\mathbf{U}}_{mass}) + \boldsymbol{\nabla} \cdot (\langle \hat{\rho} \rangle \widetilde{\mathbf{u}_{mass}\mathbf{u}_{mass}}) + \boldsymbol{\nabla} \cdot (\langle \hat{\rho} \rangle \widetilde{\widehat{\mathbf{u}_d\mathbf{u}_d}}) = -\boldsymbol{\nabla} \langle p \rangle + \boldsymbol{\nabla} \cdot \langle \hat{\boldsymbol{\sigma}} \rangle + \langle \hat{\rho} \rangle \mathbf{g} \tag{163}$$

where the velocity fluctuations due to large-scale turbulence are denoted by $\mathbf{u}_{mass} = \mathbf{U}_{mass} - \tilde{\mathbf{U}}_{mass}$. The most important unclosed terms in Eq. (163) are the turbulence stresses $\widetilde{\mathbf{u}_{mass}\mathbf{u}_{mass}}$ and the Favre-average multiphase stresses $\widetilde{\widehat{\mathbf{u}_d\mathbf{u}_d}}$. The first of these is usually closed by introducing a multiphase turbulence model with appropriate modifications to include the effect of interfacial momentum exchange on production (dissipation) of large-scale turbulence. The second term $\widetilde{\widehat{\mathbf{u}_d\mathbf{u}_d}}$ is not directly related to turbulent velocity fluctuations. Instead, it will depend on correlations between the phase-average density $\hat{\rho}$ and the velocity difference $\boldsymbol{u}_d$. For example, if the bubble rise velocity U_r were constant and independent of the gas volume fraction, then $\widetilde{\widehat{\mathbf{u}_d\mathbf{u}_d}} \approx U_r^2 \mathbf{e}_v \mathbf{e}_v$where $\mathbf{e}_v = -\mathbf{g}/|\mathbf{g}|$is

the unit vector in the vertical direction. More generally, the turbulent two-fluid model for gas–liquid flow should have properties similar to turbulence generated by buoyancy in single-phase flows (Riley and DeBruynKops, 2003). Likewise, in gas–solid flows $\mathbf{u}_d$ will depend on the Favre-average drag term, and thus on the particle Stokes number through correlations between gas- and solid-phase velocity fluctuations (Fan and Zhu, 1998). Although computationally expensive using present-day computers (Agrawal *et al.*, 2001; Zhang and VanderHeyden, 2002), it might be instructive to use direct simulations of the laminar two-fluid model (i.e., before Favre averaging) to parameterize multiphase turbulence models as has been done for stably stratified flows (Shih *et al.*, 2005). This possibility is especially attractive because it offers access to flow statistics that cannot be measured experimentally. At the very least, it might allow us to distinguish between the adequacy of the various multiphase turbulence models available in the literature (Mudde, 2005).

The goal of the discussion above was obviously not to describe multiphase turbulence models, but rather to point out the difficulties encountered when trying to derive a consistent set of transport equations. Although it is usually not done, it is worthwhile to think of the averaging process used to arrive at Eqs. (162) and (163) in two distinct steps: (1) ensemble averages over different phase configurations to derive the "laminar" multifluid model (i.e., Eq. 146) that can be used to describe multiphase flows without large-scale turbulence, and (2) Reynolds or Favre averages (or even LES) to describe turbulent multiphase flows. Ideally, direct numerical simulations (DNS) of two-phase flows with resolved interfaces could be used to develop two-fluid models for laminar multiphase flows. For example, the recent work of Nguyen and Ladd (2005) uses DNS to understand the sedimentation of mono- and poly-disperse hard-sphere suspensions when the large-scale flow is laminar, and the work of Bunner and Tryggvason (2003) uses DNS to investigate bubbly flows. If a two-fluid model (which does not resolve the interfaces) could be derived that adequately reproduces these DNS data, then it could be used to investigate the effects of large-scale turbulence that arises, for example, when the system is subjected to shear (Lakehal *et al.*, 2002). The results from direct simulations of the two-fluid model in the turbulent regime could then be used to develop and validate multiphase turbulence models along the lines suggested by Sundaresan (2000). Fortunately, with the continuing advances in computer power, steady advances in DNS of two-phase systems can be expected. There is thus reason to be optimistic that more powerful multiphase turbulence models will eventually be available for modeling practical systems such as chemical reactors.

In the current state of the art, almost all multiphase CFD models available in commercial codes use some type of turbulence model based on extending models originally developed for single-phase flows. Such CFD models are thus meant to describe fully turbulent flows (as opposed to laminar or transitional flows). Nevertheless, many of these models have not been validated

experimentally in the context of dense multiphase flows for the reasons discussed earlier, and thus should be used with caution even for turbulent multiphase flows. In any case, there is still considerable room for improvement of multiphase CFD models through comparison with carefully designed experiments for canonical flows. Even more so than for single-phase turbulence, it can be expected that particular models will have limited ranges of applicability and will have to be "tuned" for multiphase flows with different physics. For example, a two-fluid model for a solid–liquid slurry in an agitated reactor will require different physical models than a churn-turbulent bubble column. In the first case, large-scale turbulence is generated by the agitation system, while in the second case, it is generated by buoyancy and interfacial dynamics. However, for specific flows of interest to the chemical industry, it should be possible to develop reliable CFD models for multiphase flow dynamics that can be used to investigate scalar transport and chemical reactions needed to model chemical reactors. In the next section, we will thus look briefly at the additional models needed to describe the transport and production of chemical species and thermal energy.

B. Interphase Mass/Heat-Transfer Models

Our discussion of multiphase CFD models has thus far focused on describing the mass and momentum balances for each phase. In applications to chemical reactors, we will frequently need to include chemical species and enthalpy balances. As mentioned previously, the multifluid models do not resolve the interfaces between phases and models based on correlations will be needed to close the interphase mass- and heat-transfer terms. To keep the notation simple, we will consider only a two-phase gas–solid system with $\alpha_g + \alpha_s = 1$. If we denote the mass fractions of N_{sp} chemical species in each phase by $Y_{g\alpha}$ and $Y_{s\alpha}$, respectively, we can write the species balance equations as

$$\frac{\partial \rho_g \alpha_g Y_{g\alpha}}{\partial t} + \nabla \cdot (\rho_g \alpha_g Y_{g\alpha} \mathbf{U}_g) = \nabla \cdot \mathbf{J}_{g\alpha} - M_\alpha + R_{g\alpha}, \tag{164}$$

and

$$\frac{\partial \rho_s \alpha_s Y_{s\alpha}}{\partial t} + \nabla \cdot (\rho_s \alpha_s Y_{s\alpha} \mathbf{U}_s) = \nabla \cdot \mathbf{J}_{s\alpha} - M_\alpha + R_{s\alpha}. \tag{165}$$

The terms $\mathbf{J}_{g\alpha}$ and $\mathbf{J}_{s\alpha}$ are the diffusive fluxes of species α in the gas and solid phases, respectively. Note that in addition to molecular-scale diffusion, these terms include dispersion due to "particle-scale" turbulence. The latter is usually modeled by introducing a gradient-diffusion model with an effective diffusivity along the lines of Eqs. (149) and (151). Thus, for large particle Reynolds numbers the molecular-scale contribution will be negligible. The term M_α is the

mass-transfer rate from the gas to the solid phase for species α. By definition, the mass fractions sum to unity so that $\Sigma_{\alpha=1}^{N_{sp}} \mathbf{J}_{g\alpha} = \Sigma_{\alpha=1}^{N_{sp}} \mathbf{J}_{s\alpha} = 0$ and $M_g = \Sigma_{\alpha=1}^{N_{sp}} M_\alpha$ (see Eq. 142). The terms $R_{g\alpha}$ and $R_{s\alpha}$ are the reaction rates for species α in each phase. By definition, mass is conserved so that $\Sigma_{\alpha=1}^{N_{sp}} R_{g\alpha} = 0$ and $\Sigma_{\alpha=1}^{N_{sp}} R_{s\alpha} = 0$. Although we do not write them explicitly here, the reader can appreciate that the enthalpy balances for each phase will have a form similar to Eqs. (164) and (165), and can be used to determine the temperatures T_g and T_s of each phase. Likewise, mass transfer will lead to corresponding terms in the momentum balances (Eqs. 145 and 146) (Bird *et al.*, 2002).

CFD models for turbulent multiphase reacting flows do not solve the "laminar" two-fluid balances (Eqs. 164 and 165) directly. First, Reynolds averaging is applied to eliminate the large-scale turbulent fluctuations. Using Eq. (164) as an example, we can apply Reynolds averaging to find (with ρ_g constant)

$$\frac{\partial \rho_g \langle \alpha_g \rangle \widetilde{Y}_{g\alpha}}{\partial t} + \nabla \cdot \left(\rho_g \langle \alpha_g \rangle \widetilde{Y}_{g\alpha} \widetilde{\mathbf{U}}_g \right) + \nabla \cdot \left(\rho_g \langle \alpha_g \rangle \widetilde{Y''_{g\alpha} \mathbf{u}''_g} \right) = \nabla \cdot \langle \mathbf{J}_{g\alpha} \rangle - \langle M_\alpha \rangle + \langle R_{g\alpha} \rangle \tag{166}$$

The Reynolds-average gas volume fraction $\langle \alpha_g \rangle$ is found from

$$\frac{\partial \rho_g \langle \alpha_g \rangle}{\partial t} + \nabla \cdot \left(\rho_g \langle \alpha_g \rangle \widetilde{\mathbf{U}}_g \right) = -\langle M_g \rangle \tag{167}$$

wherein the Reynolds-average mass-transfer term $\langle M_g \rangle$ is unclosed. The Favre-average gas velocity $\widetilde{\mathbf{U}}_g$ is defined by

$$\widetilde{\mathbf{U}}_g = \frac{\langle \alpha_g \mathbf{U}_g \rangle}{\langle \alpha_g \rangle} \tag{168}$$

and its transport equation is found by Reynolds averaging Eq. (145). Although we do not write it out explicitly here, the reader should appreciate that the Reynolds-average gas-phase momentum equation has a number of unclosed terms that require models.

Returning to Eq. (166), the third term on the left-hand side involves the turbulent scalar fluxes, defined by

$$\widetilde{Y''_{g\alpha} \mathbf{u}''_g} = \frac{\langle \alpha_g Y''_{g\alpha} u''_g \rangle}{\langle \alpha_g \rangle} \tag{169}$$

where the scalar and velocity fluctuations are defined by $Y''_{g\alpha} = Y_{g\alpha} - \widetilde{Y}_{g\alpha}$ and $\mathbf{u}''_g = \mathbf{U}_{g\alpha} - \widetilde{\mathbf{U}}_g$, and respectively. The usual model for the scalar fluxes is gradient diffusion as follows:

$$\widetilde{Y''_{g\alpha} \mathbf{u}''_g} = -\Gamma_T \nabla \widetilde{Y}_{g\alpha} \tag{170}$$

where Γ_T is a turbulent diffusivity that is computed from the multiphase turbulence model. The CFD model can then be written as

$$\frac{\partial \rho_g \langle \alpha_g \rangle \widetilde{Y}_{g\alpha}}{\partial t} + \boldsymbol{\nabla} \cdot \left(\rho_g \langle \alpha_g \rangle \widetilde{Y}_{g\alpha} \widetilde{\mathbf{U}}_g \right) = \boldsymbol{\nabla} \cdot \left(\Gamma_{\text{eff}} \boldsymbol{\nabla} \tilde{Y}_{g\alpha} \right) - \langle M_\alpha \rangle + \langle R_{g\alpha} \rangle \tag{171}$$

where we have combined the (usually negligible) particle-scale diffusive flux and the turbulent fluxes into an effective-diffusion coefficient (Γ_{eff}).

As mentioned earlier, since the interfaces between phases are not resolved in the CFD model, the Reynolds-average mass-transfer terms ($\langle M_\alpha \rangle$), and the Reynolds-average reaction rates ($\langle R_{g\alpha} \rangle$) in Eq. (171) must be modeled in terms of known quantities. This situation is very much like classical reaction engineering models for multiphase reactors with the important difference that all quantities are known *locally*. Such quantities include

$$\langle \alpha_g \rangle, \quad \widetilde{Y}_{g\alpha}, \quad \widetilde{Y}_{s\alpha}, \quad \widetilde{T}_g, \quad \widetilde{T}_s, \quad \widetilde{\mathbf{U}}_g, \quad \widetilde{\mathbf{U}}_s$$

and local multiphase turbulence statistics. Note that these variables, although local, tell us nothing about the internal structure of the phases (i.e., subgrid-scale information). For example, $\widetilde{T}_s$ represents the Favre-average temperature of a solid particle consistent with the Favre-average enthalpy of a single particle.[9] If, as is often the case, the temperature varies strongly between the center and outer surface of a particle, a SGS model will be required to account for this effect on, for example, the chemical reactions. The principal advantage of using the CFD model over a classical CRE model is thus the ability to account for the effect of *local* fluid dynamics (e.g., $|\widetilde{\mathbf{U}}_g - \widetilde{\mathbf{U}}_s|$) on the mass/heat-transfer rate between phases. In CFD codes, this is typically done by using correlations for $\langle M_\alpha \rangle$ written in terms of the local Sherwood (or Nusselt) number and particle Reynolds number (modified perhaps by a function of $\langle \alpha_g \rangle$ to account for particle–particle interactions). In the case where large-scale mixing is infinitely rapid, these correlations will reduce to the classical CRE models for homogeneous multiphase reactors. However, such cases are rare (and need not be modeled using CFD), and it is more likely that large-scale mixing will be rate limiting at certain locations within the reactor. Indeed, it is exactly in such cases that CFD modeling will be of most benefit for reactor design and analysis.

[9]This discussion also applies to the original variable T_s, which represents the ensemble-average temperature of particles located at a particular point at a given time. Basically, we know the total enthalpy of each particle, but we do not know how it is distributed inside any given particle. Since the reaction rate can be very sensitive to the local temperature, we will need a SGS model to describe the coupling between intraparticle transport processes and chemical reactions.

C. Coupling with Chemistry

The species balances given above (Eqs. 164 and 165) include the reaction source terms on the right-hand sides. However, for these expressions to be useful in CFD modeling, the user must supply the reaction rate functions and the kinetic parameters. In addition, just as in single-phase turbulent reacting flows (Fox, 2003), it may be necessary to account for micromixing effects on the chemical kinetics by using SGS models in the Reynolds-average transport equations (e.g., for $\langle R_{g\alpha} \rangle$ in Eq. (171)). For example, consider the parallel reactions

$$\mathrm{A} + \mathrm{B} \rightarrow \mathrm{R}$$
$$\mathrm{A} + \mathrm{C} \rightarrow \mathrm{S}$$

with A in the gas phase and excess B and C in the liquid phase. If the first reaction is very rapid, then in the absence of micromixing effects in the liquid phase only R would be produced. However, if A cannot be rapidly mixed into the liquid phase (after mass transfer from the gas phase), then some S will be produced as an unwanted by-product. In many ways, this situation is analogous to the reaction systems discussed in Section III.B. If we define a mixture fraction ξ that is unity in the gas phase (i.e., for pure A) and initially zero in the liquid phase, then the degree of conversion of the first reaction ($Y_{1\infty}$) can be parameterized by the value of ξ in the liquid phase (see Eq. 68). However, the rate of the second reaction will depend on the local mixture fraction in a nontrivial manner (see Eq. 70). Thus, if we simply ignore SGS fluctuations in the liquid mixture fraction we will likely severely underestimate the extent of the second reaction. In theory, it is possible to write a presumed PDF transport model for the mixture fraction in the liquid phase. However, unlike in single-phase turbulence, the source term for the mixture fraction in the liquid phase is the mass-transfer term and the sink term for mixture-fraction fluctuations will depend on the rate of molecular mixing in different regions around the interphase (e.g., boundary layer, wake, far field). A similar situation is encountered in spray combustion (Revéillon *et al.*, 2004) where evaporating liquid droplets act as source terms for reactants in the gas phase. It thus may be useful to adapt SGS models for spray combustion (at least the parts modeling the mixture fraction mean and variance) to describe SGS mixing in more general settings such as gas–liquid flows. One can also use direct simulations of bubbly reacting flows (Khinast, 2001; Khinast *et al.*, 2003; Koynov and Khinast, 2004; Raffensberger *et al.*, 2005) to explore the validity of SGS models developed for two-phase reacting flows.

From the discussion above, we should keep in mind that even if no SGS micromixing model is used to describe the multiphase flow, it may often be the case that chemical reactions (and indeed micromixing) will be limited by mass/heat transfer between the phases. Because the multifluid model (see Eqs. 164 and

165) includes mass-transfer terms, the reaction rates will usually be mass transfer limited in cases where the chemical kinetics are fast. Thus, since we are already relying on correlations to calculate the mass/heat-transfer rates, it may not be fruitful to try to include a detailed description of micromixing inside each phase. Indeed, it will more likely be the case that improving the correlations (e.g., to include the effect of chemical reactions on local mass transfer) will have a greater impact on the accuracy of CFD model predictions.

Finally, to conclude our discussion on coupling with chemistry, we should note that in principle fairly complex reaction schemes can be used to define the reaction source terms. However, as in single-phase flows, adding many fast chemical reactions can lead to slow convergence in CFD simulations, and the user is advised to attempt to eliminate instantaneous reaction steps whenever possible. The question of determining the rate constants (and their dependence on temperature) is also an important consideration. Ideally, this should be done under laboratory conditions for which the mass/heat-transfer rates are all faster than those likely to occur in the production-scale reactor. Note that it is not necessary to completely eliminate mass/heat-transfer limitations to determine usable rate parameters. Indeed, as long as the rate parameters found in the lab are reliable under well-mixed (vs. perfect-mixed) conditions, the actual mass/heat-transfer rates in the reactor will be lower, leading to accurate predictions of chemical species under mass/heat-transfer-limited conditions.

VI. Conclusions and Future Perspectives

From the brief overview of CFD models presented in this work, the reader will hopefully have gained an initial appreciation of the utility and power of CFD tools for chemical reactor analysis and design. In Section II we have discussed the basic formulation and specific steps needed to set up a CFD model. We have also introduced the key concept of subgrid-scale (SGS) modeling and its importance in describing unresolved phenomena in reactor-scale CFD models. However, it is worth repeating here that the development of SGS models for chemical reactions and molecular transport is a natural extension of "traditional" chemical reaction engineering modeling activities, and thus one of the key areas where chemical engineers can have a large impact on the field. In Section III we gave an example of an SGS model developed for mixing-sensitive chemical reactions. This simple model for mass-transfer-limited chemical reactions can be easily extended to other applications such as high-Schmidt-number laminar flows. In Section IV we discussed efficient methods for adding a population balance equation to a CFD code to model the production of fine particles. More generally, the ability to represent the evolution of a population of entities (e.g., particles, bubbles, drops) in the context of CFD results in a very powerful tool for describing complex reacting flows. At present, methods based on the direct quadrature method of moments

(DQMOM) are still in their initial stages of development. Nevertheless, they have already been applied with great success by a growing number of researchers to a wide variety of problems. The versatility of DQMOM was demonstrated in Section IV by applying it twice to the one modeling problem: first to model micromixing between fluid elements containing a bivariate number density function (NDF), and then to represent the bivariate NDF itself. Finally, in Section V we discussed the challenges associated with CFD models for multiphase reacting flows. Although there are still a number of open problems to be solved in multiphase flow CFD, when used with caution existing CFD models can be used for at least qualitative analysis of chemical reactors.

In my opinion, the perspective for future developments in the field of CFD modeling of chemical reactors is quite strong. On the one hand, the continued growth of computational power both through faster computers and better algorithms will make it possible to solve more and more complex problems. On the other hand, we are fortunate in this field that the basic microscopic balance equations are known, even though they lead to complex multiscale, multiphysics phenomena. The accessibility of large-scale computing facilities will allow us to explore this complexity using direct simulations for specific "academic" problems that can be used to test the SGS models needed for CFD simulations of industrial reactors. In general, advances in the development of SGS models will require collaboration between computational physicist/chemist working on direct simulation of academic problems and chemical reaction engineers developing multiphysics models. Indeed, the reader should appreciate that it is almost never the case that a reliable SGS model can be developed by simply analyzing the results from a large-scale direct simulation. Inversely, SGS model developed without validation against detailed experimental or direct simulation data are usually of limited value. Instead, the more fruitful approach is to first develop a tentative SGS model based on a preliminary understanding of the physics/chemistry of the problem, and then to design a large-scale direct simulation to test key assumptions/predictions of the model. This dialogue between model development and model validation is continued until a suitably reliable SGS model is found. SGS models developed in this manner have a strong fundamental underpinning and have a much greater chance of being applicable to a wide range of operating conditions.

In summary, my recommendation for future progress in the field is not to follow the deceptively simple path of rushing toward the application of large-scale CFD simulations to complex industrial reactor systems if the basic SGS models have not first been shown to be reliable on "academic" problems.[10] Rather, I would recommend that we proceed more cautiously with adequate attention given to the development of the fundamental physical understanding required to develop reliable CFD models. While this path will obviously require

[10]Despite this word of caution, one should not lose site of the fact that there are many industrial reactor systems that *can be accurately simulated* with existing SGS models!

patience and perseverance, in the long run it will undoubtedly be the surest way to attain the chemical reaction engineer's long-sought goal of "experiment-free" scale-up of chemical reactors.

ACKNOWLEDGMENTS

The author's work in the area of CFD analysis of chemical reactors has been supported nearly continuously for the last 15 years by the U.S. National Science Foundation. The work on gas–solid multiphase flows and population balances was funded by the U.S. Department of Energy. The author would also like to acknowledge support from several companies, including Air Products and Chemicals, BASF, BASELL, BP Chemicals, Dow Chemical, DuPont Engineering, and Univation Technologies. Last, but not least, the author wishes to acknowledge his many collaborators over the years who are many in number to name them individually.

REFERENCES

Agrawal, K., Loezos, P. N., Syamlal, M., and Sundaresan, S. J. *Fluid Mech.* **445**, 151–185 (2001).
Akhtar, M. K., Xiong, Y., and Pratsinis, S. E. *AIChE J.* **37**, 1561–1570 (1991).
Aoun, M., Plasari, E., David, R., and Villermaux, J. *Chem. Eng. Sci.* **54**, 1161–1180 (1999).
Baldyga, J. *Chem. Eng. Sci.* **49**, 1985–2003 (1994).
Baldyga, J., Bourne, J. R., and Walker, B. *Can. J. Chem. Eng.* **76**, 641–649 (1998).
Batchelor, G. K. *J. Fluid Mech.* **193**, 75–110 (1988).
Bird, R. B., Stewart, W. E., and Lightfoot, E. N., "Transport Phenomena". 2nd edn. John Wiley & Sons, New York, USA (2002).
Briesen, H., Fuhrmann, A., and Pratsinis, S. E. *Chem. Eng. Sci.* **53**, 4105–4112 (1998).
Bunner, B., and Tryggvason, G. *J. Fluid Mech.* **495**, 77–118 (2003).
Corrsin, S *AIChE J.* **10**, 870–877 (1964).
David, R., and Marcant, B. *AIChE J.* **40**, 424–432 (1994).
Davies, C. N. "The sedimentation and diffusion of small particles". Proceedings of the Royal Society of London. Series A, Mathematical and Physical Sciences. **200**, 110–113 (1949).
Drew, D. A., and Passman, S. L., "Theory of Multicomponent Fluids". Springer-Verlag, Inc., New York, USA (1999).
Dring, R. P. *ASME J. Fluid Eng* **104**, 15 (1982).
Einstein, A. *Annalen der Physik* **17**, 549–560 (1905).
Elimelech, M., Gregory, J., Jia, X., and Williams, R. A., "Particle Deposition and Aggregation, Measurement, Modelling and Simulation". Butterworth-Heinemann, Woburn (1995).
Fan, L. S., and Zhu, C., "Principles of Gas-Solid Flows". Cambridge University Press, New York (1998).
Fan, R., Marchisio, D. L., and Fox, R. O. *Powder Technol.* **139**, 7–20 (2004).
Fiorina, B., Gicquel, O., Vervisch, L., Carpentier, S., and Darabiha, N. *Combust. Flame* **140**, 147–160 (2005).
Fox, R. O. *Chem. Eng. Process.* **37**, 521–535 (1998).

Fox, R. O., "Computational Models for Turbulent Reacting Flows". Cambridge University Press, Cambridge, UK (2003).
Fox, R. O., and Raman, V. *Phys. Fluids* **16**, 4551–4564 (2004).
Fox, R. O., and Yeung, P. K. *Phys. Fluids* **15**, 961–985 (2003).
Friedlander, S. K., "Smoke, Dust, and Haze". 2nd edn Oxford University Press, New York, USA (2000).
Fuchs, N. A., "The Mechanics of Aerosols". Pergamon Press, New York, USA (1964).
Gao, D., Fan, R., Subramaniam, S., Fox, R. O., and Hoffman, D. K., J, *Fluid Eng.* **128**, 62–68 (2005).
Garnier, C., Lance, M., and Marié, J. L. *Exp. Therm. Fluid Sci.* **26**, 811–815 (2002).
Garside, J., and Tavare, N. S. *Chem. Eng. Sci.* **40**, 1485–1493 (1985).
Harteveld, W. K., Mudde, R. F., and Van Den Akker, H. E. A. *Can. J. Chem. Eng.* **81**, 389–394 (2003).
Jackson, R., "The Dynamics of Fluidized Particles". Cambridge University Press, Cambridge, UK (2000).
Johannessen, T., Pratsinis, S. E., and Livbjerg, H. *Chem. Eng. Sci.* **55**, 177–191 (2000).
Johannessen, T., Pratsinis, S. E., and Livbjerg, H. *Powder Technol.* **118**, 242–250 (2001).
Johnson, B. K., and Prud'homme, R. K. *AIChE J.* **49**, 2264–2282 (2003a).
Johnson, B. K., and Prud'homme, R. K. *Aust. J. Chem.* **56**, 1021–1024 (2003b).
Johnson, B. K., and Prud'homme, R. K. *Phys. Rev. Lett.* **91**, 91 (2003c).
Johri, J., and Glasser, B. J. *AIChE J.* **48**, 1645–1664 (2002).
Kammler, H. K., Mueller, R., Senn, O., and Pratsinis, S. E. *AIChE J.* **47**, 1533–1543 (2001).
Kammler, H. K., and Pratsinis, S. E. *J. Nanopart. Res.* **1**, 467–477 (1999).
Kammler, H. K., and Pratsinis, S. E. *Chem. Eng. Process.* **39**, 219–227 (2000).
Khinast, J. G. *AIChE J.* **47**, 2304–2319 (2001).
Khinast, J. G., Koynov, A., and Leib, T. M. *Chem. Eng. Sci.* **58**, 3961–3971 (2003).
Klimenko, A. Y., and Bilger, R. W. *Prog. Energ. Combust. Sci.* **25**, 595–687 (1999).
Kodas, T. T., Friedlander, S. K., and Pratsinis, S. E. *Ind. Eng. Chem. Res.* **26**, 1999–2007 (1987).
Kolhapure, N. H., Fox, R. O., Daiss, A., and Mähling, F. -O. *AIChE J.* **51**, 585 (2005).
Koynov, A., and Khinast, J. G. *Chem. Eng. Sci.* **59**, 3907–3927 (2004).
Kruis, F. E., Kusters, K. A., Pratsinis, S. E., and Scarlett, B. *Aerosol Sci. Tech.* **19**, 514–526 (1993).
Kumar, S., and Ramkrischna, D. *AIChE J.* **51**, 1311–1332 (1996).
Lakehal, D., Smith, B. L., and Milelli, M. *J. Turbul.* **3**, 1–21 (2002).
Lammers, J. H., and Biesheuvel, A. *J. Fluid Mech.* **328**, 67–93 (1996).
Lattuada, M., Wu, H., and Morbidelli, M. *J. Colloid Interf. Sci.* **268**, 96–105 (2003a).
Lattuada, M., Wu, H., and Morbidelli, M. *J. Colloid Interf. Sci.* **268**, 106–120 (2003b).
Liu, Y., and Fox, R. O. *AIChE J.* **52**, 731–734 (2006).
Liu, Y., Raman, V., Fox, R. O., and Harvey, A. D. *Chem. Eng. Sci.* **59**, 5167–5176 (2004).
Mahajan, A. J., and Kirwan, D. J. *J. Phys. D – Appl. Phys.* **26**, B176–B180 (1993).
Mahajan, A. J., and Kirwan, D. J. *AIChE J.* **42**, 1801–1814 (1996).
Marcant, B., and David, R. *AIChE J.* **37**, 1698–1710 (1991).
Marchisio, D. L., and Fox, R. O. *J. Aerosol Sci.* **36**, 43–73 (2005).
Marchisio, D. L., Fox, R. O., and Barresi, A. A. *AIChE J.* **47**, 664–676 (2001a).
Marchisio, D. L., Fox, R. O., Barresi, A. A., and Baldi, G. *Ind. Eng. Chem. Res.* **40**, 5132–5139 (2001b).
Marchisio, D. L., Pikturna, J. T., Fox, R. O., Vigil, R. D., and Barresi, A. A. *AIChE J.* **49**, 1266–1276 (2003a).
Marchisio, D. L., Soos, M., Sefcik, J., and Morbidelli, M. *AIChE J.* **52**, 158–173 (2006).
Marchisio, D. L., Vigil, R. D., and Fox, R. O. *J. Colloid Interf. Sci.* **258**, 322–334 (2003b).
McGraw, R. *Aerosol Sci. Tech.* **27**, 255–265 (1997).
Meakin, P. *Adv. Colloid Interfac. Sci.* **28**, 249–331 (1988).
Melis, S., Verduyn, M., Storti, G., Morbidelli, M., and Baldyga, J. *AIChE J.* **45**, 1383–1393 (1999).

Minev, P. D., Lange, U., and Nandakumar, K. *J. Fluid Mech.* **394**, 73–96 (1999).
Minier, J. -P., and Peirano, E. *Phys. Rep.* **352**, 1–214 (2001).
Monahan, S. M., Vitankar, V. S., and Fox, R. O. *AIChE J.* **51**, 1897–1923 (2005).
Mudde, R. F. "Toward modeling and simulations of industrial bubbly flows", in "11th Workshop on Two-Phase Flow Predictions", Institut für Verfahrenstechnik, Martin-Luther-Universität, Halle-Wittenberg, Germany (2005).
Mueller, R., Jossen, R., Kammler, H. K., Pratsinis, S. E., and Akhtar, M. K. *AIChE J.* **50**, 3085–3094 (2004a).
Mueller, R., Jossen, R., Pratsinis, S. E., Watson, M., and Akhtar, M. K. *J. Am. Ceram. Soc.* **87**, 197–202 (2004b).
Nguyen, N. -Q., and Ladd, A. J. C. *J. Fluid Mech.* **525**, 73–104 (2005).
Oles, V. *J. Colloid Interf. Sci.* **154**, 351–358 (1992).
Pandya, J. D., and Spielman, L. A. *Chem. Eng. Sci.* **38**, 1983–1992 (1983).
Peters, N., "Turbulent Combustion". Cambridge University Press, Cambridge, UK (2000).
Piton, D., Fox, R. O., and Marcant, B. *Can. J. Chem. Eng.* **78**, 983–993 (2000).
Pohorecki, R., and Baldyga, J. *Chem. Eng. Sci.* **38**, 79–83 (1983).
Pohorecki, R., and Baldyga, J. *Chem. Eng. Sci.* **43**, 1949–1954 (1988).
Poinsot, T., and Veynante, D., "Theoretical and Numerical Combustion". R. T. Edwards, Philadelphia, USA (2001).
Pope, S. B., "Turbulent Flows". Cambridge University Press, Cambridge, UK (2000).
Pratsinis, S. E. *Prog. Energ. Combust. Sci.* **24**, 197–219 (1998).
Pratsinis, S. E., Zhu, W., and Vemury, S. *Powder Technol.* **86**, 87–93 (1996).
Raffensberger, J. A., Glasser, B. J., and Khinast, J. G. *AIChE J.* **51**, 1482–1496 (2005).
Raman, V., Fox, R. O., and Harvey, A. D. *Combust. Flame* **136**, 327–350 (2004).
Raman, V., Fox, R. O., Harvey, A. D., and West, D. H. *Ind. Eng. Chem. Res.* **42**, 2544–2557 (2003).
Ramkrishna, D., "Population Balances". Academic Press, San Diego, USA (2000).
Randolph, A. D., and Larson, M. A., "Theory of Particulate Processes". 2nd edn. Academic Press, San Diego, USA (1988).
Revéillon, J., Pera, C., Massot, M., and Knikker, R. *J. Turb.* **5**, 1–27 (2004).
Riley, J. J., and DeBruynKops, S. M. *Phys. Fluids* **15**, 2047–2059 (2003).
Rosner, D. E., and Pykkonen, J. J. *AIChE J.* **48**, 476–491 (2002).
Sandkühler, P., Sefcik, J., Lattuada, M., Wu, H., and Morbidelli, M. *AIChE J.* **49**, 1542–1555 (2003).
Sandkühler, P., Sefcik, J., and Morbidelli, M. *J. Phys. Chem. B* **108**, 20105–20121 (2005).
Sankaranarayanan, K., and Sundaresan, S. *Chem. Eng. Sci.* **57**, 3521–3542 (2002).
Sanyal, J., Marchisio, D. L., Fox, R. O., and Dhanasekharan, K. *Ind. Eng. Chem. Res.* **44**, 5063–5072 (2005).
Seckler, M. M., Bruinsma, O. S. L., and Van Rosmalen, G. M. *Chem. Eng. Commun.* **135**, 113–131 (1995).
Selomulya, C., Bushell, G., Amal, R., and Waite, T. D. *Chem. Eng. Sci.* **58**, 327–338 (2003).
Shih, L. H., Koseff, J. R., Ivey, G. N., and Ferziger, J. H. *J. Fluid Mech.* **525**, 193–214 (2005).
Sorensen, C. M. *Aerosol Sci. Technol.* **35**, 648–687 (2001).
Sreenivasan, K. R. *Phys. Fluids* **8**, 189–196 (1996).
Sundaresan, S. *AIChE J.* **46**, 1102–1105 (2000).
Tani, T., Takatori, K., and Pratsinis, S. E. *J. Am. Ceram. Soc.* **87**, 523–525 (2004a).
Tani, T., Takatori, K., and Pratsinis, S. E. *J. Am. Ceram. Soc.* **87**, 365–370 (2004b).
Thorat, B. N., and Joshi, J. B. *Exp.l Therm. Fluid Sci.* **28**, 423–430 (2004).
Veynante, D., and Vervisch, L. *Prog. Energ. Combust. Sci.* **28**, 193–266 (2002).
Villermaux, J., and David, R. *Journal de la Chimie Physique* **85**, 273 (1988).
Waldner, M. H., Sefcik, J., Soos, M., and Morbidelli, M. *Powder Technol.* **156**, 226–234 (2005).
Wang, L., and Fox, R. O. *Chem. Eng. Sci.* **58**, 4387–4401 (2003).
Wang, L., and Fox, R. O. *AIChE J.* **50**, 2217–2232 (2004).

Wang, L., Marchisio, D. L., Vigil, R. D., and Fox, R. O. *J. Colloid Interf. Sci.* **282**, 380–396 (2005a).
Wang, L., Vigil, R. D., and Fox, R. O. *J. Colloid Interf. Sci.* **285**, 167–178 (2005b).
Watanabe, T., and Gotoh, T. *New J. Phys.* **6**, 40–75 (2004).
Wright, D. L., Mcgraw, R., and Rosner, D. E. *J. Colloid Interf. Sci.* **236**, 242–251 (2001).
Xiong, Y., and Pratsinis, S. E. *J. Aerosol Sci.* **22**, 637–655 (1991).
Yeung, P. K., Donzis, D. A., and Sreenivasan, K. R. *Phys. Fluids* **17**, 081703 (2005).
Zhang, D. Z., and VanderHeyden, W. B. *Int. J. Multiphas. Flow* **28**, 805–822 (2002).
Zhu, W., and Pratsinis, S. E. *AIChE J.* **43**, 2657–2664 (1997).
Zucca, A., Marchisio, D. L., Barresi, A. A., and Fox, R. O. *Chem. Eng. Sci.* **61**, 87–95 (2006).